

Direct Jet Impingement Cooling of Power Electronics

Robert Skuriat

Thesis submitted to The University of Nottingham for the degree of Doctor of Philosophy

June 2012

Abstract

The aim of the work presented in this thesis is to improve the operational reliability of a power module and increase the efficiency of its associated cooling system by integrating the design of the cooler as part of the module. Power modules are increasingly used in a variety of applications ranging from aircraft and mass transport systems, to motor control and power conversion in the home. Reliability of the power module is very important in aerospace applications where the highest levels of safety and robustness are required while keeping the volume and mass of the module as low as possible. Certain parts of the power module such as the solder layer beneath the silicon device and the substrate are prone to failure with thermal cycling. The layer of thermal grease between the baseplate of the module and the heatsink significantly increases the thermal resistance between the electronic devices and the coolant fluid. The power module can be constructed so that some of the interfaces within the module which are prone to failure are improved or completely removed from the assembly greatly reducing the thermal resistance from junction to ambient. The research identified cooling methods which are able to cope with the increasingly high heat fluxes produced by power electronic devices. Jet impingement cooling was selected for testing and further development. An initial series of tests confirmed that liquid jet impingement can be used to generate high heat transfer coefficients for the efficient cooling of power modules. Results from experimental tests showed that directly cooling the substrate tile with jet impingement resulted in the devices being cooled more effectively compared to the commonly used serpentine coldplate and a direct-baseplate cooled jet impingement system. It was postulated that more efficient cooling can be achieved by targeting the hotspots on the substrate beneath each device with a carefully designed impingement array. A test apparatus was constructed to test a variety of jet impingement arrays to confirm the hypothesis. A second test apparatus was constructed to characterise the performance of the jet arrays in more detail using a thermal imaging camera to monitor the surface temperature of a single device. An optimal jet configuration was found for the efficient cooling of a single device. The work concluded that an improvement in efficiency and reliability can be gained by constructing power modules with integrated jet impingement arrays direct-substrate cooling the hotspots beneath the devices.

Acknowledgements

The research was funded by an EPSRC bursary. Power modules and devices were supplied by Dynex Semiconductor.

I would like to express my thanks to the following people:

Professor Mark Johnson, for his support and guidance over the past few years. I have enjoyed working as part of his group where we are encouraged to explore the limits of what is technically possible. Cyril Buttay, for his experience and attention to detail in setting up experiments and test rigs. Paul Evans, who was always on hand for technical assistance and for helping me with any electrical issues with my test equipment. Pearl Agyakwa and Jianfeng Li for assistance in soldering, assembly and wirebonding of the devices. Chris Cook, Paul Moss, Kevin Last and Colin Blackburn in the workshop for the numerous hours spent machining parts for my test rigs. My loving family, Leszek, Lena and Olenka for their encouragement, support and belief in me, without whom I could not have completed this work.

Publications

Mattey, N., **Skuriat, R.**, Li, J., Agyakwa, P., Evans, P., and Johnson, C.M., “Thermal and mechanical design optimization of a pressure-mounted base-plate-less high temperature power module” Electronic System-Integration Technology Conference (ESTC), 2010, Berlin, Germany

Skuriat, R., Johnson, C.M., “Direct substrate cooling of power electronics” EPE 2009. 13th European Conference on Power Electronics, Barcelona, Spain

Skuriat, R., Johnson, C.M., Dietl, K., Vasel, J., Schmitz, G., 2009, “Thermal Management of Power Electronics in the More Electric Aircraft”, Moet forum, Barcelona, Spain

Rizvi, M. J., **Skuriat, R.**, Tilford, T., Bailey, C., Johnson, C. M., & Lu, H., “CFD Analysis of Water Jet Impingement Cooling System for Effective Cooling of IGBTs used in Power Electronics”, EuroSimE 2009, Delft, The Netherlands

Skuriat, R., Johnson, C. M., “Direct Substrate Cooling of Power Electronics” CIPS 2008, 5th International Conference on Integration of Power Electronic Systems, Nuremberg, Germany

Skuriat, R., Johnson, C.M., “Thermal Performance of Baseplate and Direct Substrate Cooled Power Modules”, 4th IET Conference on Power Electronics Power Electronics, PEMD 2008, York

Contents

Abstract	i
Acknowledgements	ii
1 Power modules and cooling	1
1.1 Introduction	1
1.2 Introduction to Power Electronics and applications	1
1.2.1 The importance of electrical energy management.....	1
1.2.2 Applications of power electronics	1
1.3 The components of a power electronic system.....	3
1.3.1 Power Modules	3
1.4 Variation in module construction methods.....	6
1.4.1 Integration of the power module and cooling system.....	6
1.4.2 Pressure mounted modules.....	7
1.4.3 Double sided cooling.....	8
1.4.4 Power module operational characteristics	9
1.5 Cooling and Reliability.....	11
1.5.1 The need for cooling	11
1.6 Cooling and thermal management.....	11
1.6.1 Passive cooling and conduction of heat	12
1.6.2 Cooling techniques for high power dissipation electronics	19
1.6.3 Summary of cooling methods	25
1.7 Structure of the thesis	27
Chapter Two.....	28
Chapter Three.....	28
Chapter Four	28
Chapter Five.....	28
1.8 Chapter summary	29
2 The heat transfer path.....	30
2.1 Introduction	30

2.2	Reliability is largely a thermal problem	30
2.2.1	Thermal expansion and layers	30
2.3	The elements of the thermal path and integration.....	31
2.4	Thermal resistance of the power module	31
2.4.1	Main contributors of thermal resistance	33
2.5	Choice of materials.....	33
2.5.1	Matching the thermal expansion coefficient	34
2.6	Reducing the number of bonded interfaces	37
2.6.1	Thermal interface materials (TIMs)	37
2.7	The need for a heat spreading baseplate	38
2.7.1	Heat spreader performance.....	39
2.7.2	Optimisation and ultimate limits	42
2.7.3	Heat spreader design choices	42
2.7.4	The impact of varying the heat transfer coefficient on the need for a baseplate heatspreader	43
2.8	Chapter summary	46
3	Liquid Cooling	47
3.1	Introduction	47
3.2	Context of the Problem.....	47
3.2.1	Reducing the thermal resistance of the stack	48
3.2.2	Reducing the number of thermal layers	49
3.3	Initial Jet Impingement study	49
3.3.1	Description of the power module used for the tests	50
3.4	The coolers	51
3.4.1	Coldplate	52
3.5	Water jet impingement	52
3.5.1	Description	52
3.5.2	Design of the direct baseplate cooler	53
3.5.3	Design of the direct substrate tile cooler	56
3.6	Experimental Testing.....	57

3.6.1	Apparatus	57
3.7	Testing Procedure	58
3.7.1	Pumping power	58
3.7.2	Heat transfer coefficient	59
3.7.3	Thermal Impedance Characteristic	60
3.8	Experimental Results	60
3.8.1	Pressure drop and flow rate	60
3.8.2	Heat Transfer Coefficient	61
3.8.3	Thermal Impedance	63
3.8.4	Power Cycling	64
3.8.5	Reducing the number of thermal interfaces	65
3.9	Summary of initial jet impingement tests	66
4	Direct Substrate Cooling with Jet Impingement	67
4.1	Introduction	67
4.2	Direct substrate cooling	67
4.3	Reducing redundancy in the cooling system	68
4.3.1	Small heat sources and heat spreading	68
4.3.2	Improving the efficiency of the impingement arrays	68
4.4	Custom substrate tile	69
4.4.1	Thickness and robustness of the ceramic substrate tile	69
4.4.2	Design of the substrate tile	70
4.5	Thermal simulation of the substrate tile	72
4.5.1	Reducing redundancy	73
4.6	Jet impingement cooling	74
4.6.1	Types of jet impingement	75
4.6.2	Heat transfer coefficient profile	77
4.6.3	Arrays of jets	79
4.6.4	Nozzle shape	80
4.6.5	Erosion of the heat transfer surface	81
4.6.6	Parameters affecting heat transfer performance	82

4.7	Heat transfer correlations	83
4.7.1	Submerged jets and pressure drop	84
4.7.2	Heat transfer correlations and power module cooling	87
4.7.3	An optimal jet array configuration	92
4.8	Experimental testing	92
4.8.1	The sprayplates and jet arrays	92
4.8.2	Jet diameter	93
4.8.3	Ratio of jet spacing to jet diameter	93
4.9	Size of the array	94
4.10	Experimental test rig	95
4.11	Test Procedure	98
4.12	Experimental Results	99
4.12.1	Performance comparison at constant water flow rate	99
4.12.2	Pumping Power Comparison	100
4.12.3	Jet diameter (d)	102
4.12.4	Ratio of jet spacing to jet diameter (r/d)	104
4.12.5	Size of the array	105
4.13	Experimental testing summary	106
4.13.1	Further Work	107
4.14	Chapter summary	107
5	Improving the jet impingement array for the cooling of a single power electronic device	109
5.1	Introduction	109
5.1.1	Finding the optimum	109
5.2	Improving the test rig	110
5.2.1	Ideal design versus practical layout	110
5.2.2	Test apparatus design and assembly	113
5.2.3	Testing regime	119
5.2.4	Variable parameters	123
5.3	Jet-to-target distance - H	123

5.3.1	Experimental results	125
5.3.2	Diode temperature rise and pumping power	127
5.3.3	Diode temperature rise at constant pumping power	128
5.4	Jet-to-jet spacing and size of the array	129
5.4.1	Varying the jet-to-jet spacing	130
5.4.2	Experimental results	131
5.5	Data reduction – friction factor, f	134
5.5.1	Friction factor, f , with variable jet-to-target distance	135
5.5.2	Friction factor, f , with variable jet-to-jet spacing	137
5.5.3	Summary of experimental tests	137
6	Conclusion	139
6.1.1	Initial experimental study	139
6.1.2	Jet impingement optimisation for power electronic devices	140
6.2	The importance of the work	141
6.3	Further work	141
7	Review	142
	Chapter One	142
	Chapter Two	142
	Chapter Three	142
	Chapter Four	143
	Chapter Five	143

Chapter 1

1 Power modules and cooling

1.1 Introduction

In this chapter an overview of the power module is presented. Typical uses and applications of power modules and their specifications are described. The construction of a typical power module is described followed by an overview of alternative design topologies showing how the arrangement of the typical power module assembly can be altered and adapted depending on the criteria of the application. A number of power module cooling methods are presented with advantages and disadvantages listed for each. A problem is identified involving the optimisation of cooling of power modules in order to improve reliability. The approach to finding a solution is outlined and the structure of the thesis is described with a brief summary of each chapter.

1.2 Introduction to Power Electronics and applications

1.2.1 The importance of electrical energy management

In 2010, *17.9 billion kWh* of electricity was consumed globally [1] with 82% generated from non-renewable sources [2]. As governments and industry create a low-carbon economy, efficient management of electrical energy becomes increasingly important. Innovative power electronic systems are central to minimising the negative environmental impact of global electricity use. Energy expenditure can be reduced by introducing efficient electrical energy conversion, power control and transmission.

1.2.2 Applications of power electronics

Power modules are capable of switching *KiloWatts* and in some cases many *MegaWatts* of electrical power at frequencies up to *100kHz* (for IGBT based modules). Power modules are used in a variety of commercial and industrial applications for: motor control, energy conversion, inverters, rectifiers, switching and pulse width modulation as shown in . Almost every electronic device contains power electronic systems of some sort. For example: DC/DC

converters are used in most mobile devices such as mobile telephones and notebook computers to maintain the voltage at a fixed value regardless of the charge level of the battery. These converters are also used for electronic isolation and power factor correction. AC/DC converters (or rectifiers) change AC to DC and can also change the voltage level as part of their operation. AC/AC converters are used to change either the voltage level or the frequency of the power supply. DC/AC converters (inverters) are used primarily in uninterruptible power supply (UPS) or emergency lighting systems. For example: when mains power is available, it will charge the DC battery; if the mains power supply fails, an inverter will be used to produce AC electricity at mains voltage from the DC battery [3].

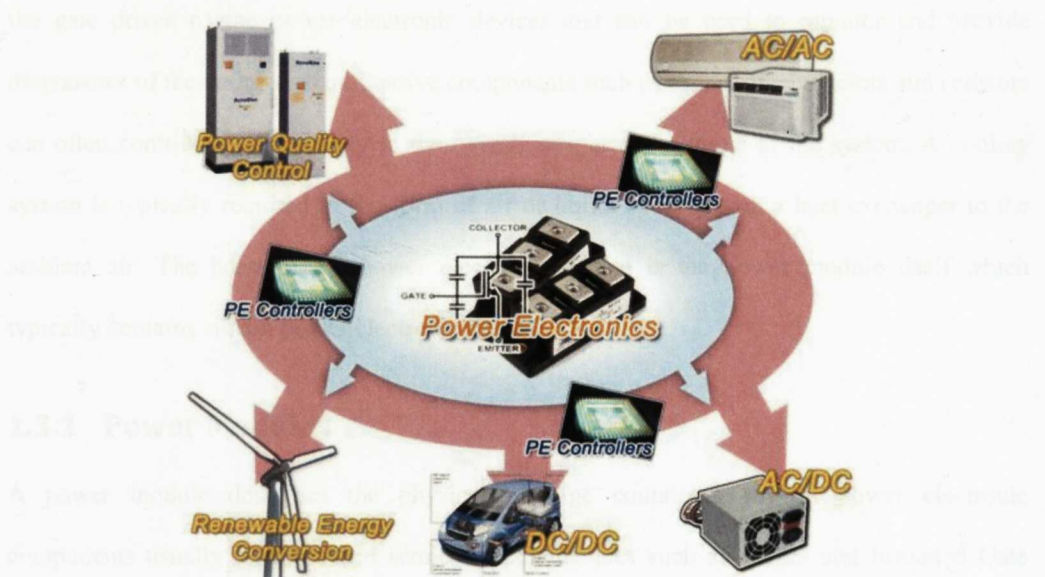


Figure 1 - Applications of power electronics include: switching, motor control, power conversion and power quality control [4].

1.2.2.1 Aerospace applications

Automotive, aerospace and military applications are the most demanding in terms of power density, weight, size and reliability performance of power modules. The aerospace and automotive industries have been the driving force in developing integrated solutions and pushing what is capable from power modules. The increased use of hybrid and electric vehicles for ground transportation has resulted in an increased demand for more power dense systems. The More Electric Concept and Rolls-Royce's More Electric Engine, MEE, endeavour to revolutionise civil aviation by replacing traditional hydraulic actuation and accompanying systems entirely with electrical actuation. Electrohydrostatic actuation for aircraft flight surfaces can generate large weight savings. The combination of higher hydraulic pressure and

the ‘more electric’ flight control architecture led to a weight reduction of approximately 1500kg for the Airbus A380 aircraft [5]. However replacing the hydraulic and mechanical systems which use well-established and tested cooling methods with electrical systems which require different types of cooling introduces active areas of research. In these applications there is a demand for increased power density and low system weight and volume while operating safely and reliably for many years.

1.3 The components of a power electronic system

A number of separate devices form a power electronic system. Microelectronic circuits control the gate drives of the power electronic devices and can be used to monitor and provide diagnostics of the entire system. Passive components such as capacitors, inductors and resistors can often contribute significantly to the overall weight and volume of the system. A cooling system is typically required in the form of air or liquid cooling with a heat exchanger to the ambient air. The heart of the power electronic system is the power module itself which typically contains silicon power electronic devices.

1.3.1 Power Modules

A power module describes the physical package containing several power electronic components usually silicon based semiconductor devices such as diodes and Insulated Gate Bipolar Transistors (IGBTs). The devices are packaged in the robust and sometimes hermetically sealed housing of the power module which provides an easy way to cool the components and connect them to the outer circuit. In Figure 2 three different Dynex Semiconductor power modules are displayed, with the cover removed from one of the modules so that the devices can be seen.

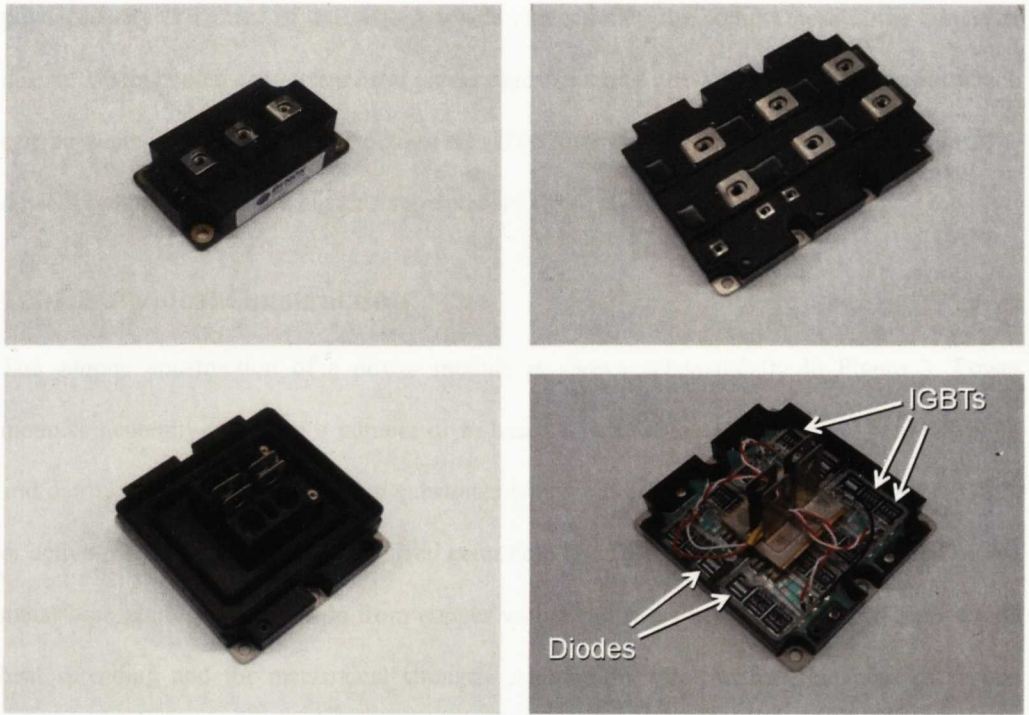


Figure 2 – Various Dynex Semiconductor power modules. In the lower right picture the cover has been removed from the power module allowing the IGBTs, diodes and gate wire connections to be seen.

Typical structures available as power modules are:

- Switch (MOSFET, IGBT), with antiparallel Diode;
- Half-bridge (inverter leg, with two switches and their corresponding diodes)
- Three-phase inverter (six switches and the corresponding diodes)

1.3.1.1 Properties of power modules

The design and construction of a power module can vary to a degree depending on the intended application. For example, power modules used in aerospace applications have specifications geared towards high power density, low package weight, low volume and reliable operation while being exposed to a range of temperatures and environmental conditions. A power module for use on an aircraft is expected to operate for 15-20 years, which is the typical life span for an avionic system. It could be exposed to temperatures ranging from -40°C to 80°C and is expected to operate safely and reliably at these temperatures. Typical power densities at the die level are $100\text{W}/\text{cm}^2$ for traditional IGBT base modules with aerospace power densities at the die level approaching $200\text{W}/\text{cm}^2$ [6]. A typical use of a power module on an aircraft would be in an AC/AC converter. The ratio of output power and converter volume is called the

power density ($kW/litre$) of the system, which characterizes the compactness of the converter design. Water cooled converters have power densities up to $10kW/litre$. Power densities which can be achieved in aerospace modules are $27kW/litre$ for Si devices or $83kW/litre$ for SiC devices (which operate at a higher temperature) [7].

1.3.1.2 Typical Construction

The general construction of a power module is shown schematically in Figure 3. Power modules generally comprise a number of Si -based power devices such as IGBTs, MOSFETs and diodes which are soldered onto substrates which are usually direct-bonded-copper (DBC) or active-metal brazed (AMB) metalized ceramics. The DBC substrate is then soldered onto a metal base plate typically made from copper with a thickness between $3mm$ and $5mm$ to aid heat spreading and for mechanical strength. Aluminium wires with a thickness of around $500\mu m$ are ultra-sonically bonded to the top of the dies. Electrical connections for the gate drives and bus-bars are soldered on. A plastic case is fitted and the module is encapsulated with dielectric gel. The copper baseplate is mounted to an air-cooled heat sink, typically machined from aluminium to save weight. When space is limited, or if air cooling is insufficient, the module is mounted onto a liquid cooled plate. Thermal grease is applied between the module's base plate and the heat sink/water-cooled plate. The substrate and bonding materials are selected with several characteristics in mind, namely: high thermal conductivity, matching coefficients of thermal expansion (CTEs), mechanical robustness and elasticity. Compromises in the design are necessary as it is not always possible to select materials which have the required dielectric or thermal properties while also having similar CTEs to the materials in the adjacent layers of the module.

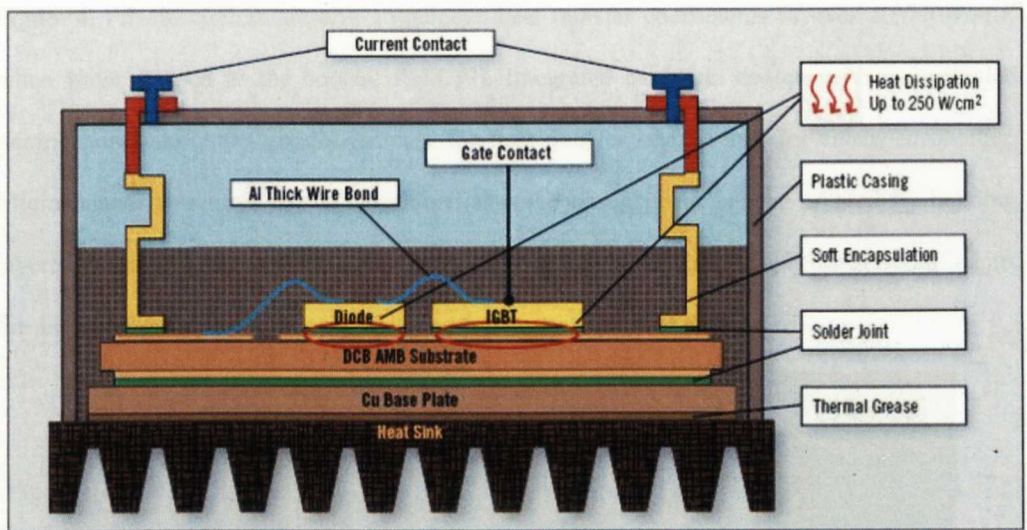


Figure 3 – A cross-section schematic diagram of the general layout of a power module with *Si* devices soldered onto a ceramic DBC substrate with air-cooled heat sink [8].

1.4 Variation in module construction methods

The construction and choice of materials in the power module can be varied somewhat depending on the criteria required by the application. To achieve lower device operating temperatures or higher power densities, a variety of solutions can be implemented for better removal of heat from the devices to the ambient. Various methods exist to cool heat-generating devices, typically there are some compromises experienced when deviating from the 'standard' module construction.

1.4.1 Integration of the power module and cooling system

More advanced and integrated solutions to the packaging and cooling of power electronic components are required in order to achieve the increased power densities and reliability demanded by aerospace applications. Direct cooling of the electronic package can reduce the number of bonded layers and interfaces in the package resulting in a more compact and lightweight system. Improved design and integration of material choices and cooling can greatly improve the performance and reliability of power modules.

1.4.1.1 Integrated baseplate coolers

The baseplate of the power module can be used as part of the cooler itself when liquid coolant is in direct contact with the baseplate material. Channels can be machined into the baseplate in patterns to enhance the heat transfer between the baseplate and the coolant fluid as shown in

Figure 4. Pin-fin coolers are able to achieve heat transfer coefficients of over $10,000 \text{ W/m}^2\text{K}$ when water is used as the coolant fluid [9]. Integrated baseplate coolers with incorporated microchannel structures greatly increase the heat transfer surface area for enhanced cooling. Microchannel structures can be machined into the baseplate or can be created by bonding layered stacks of patterned metals or composite materials. Effective heat transfer coefficients for microchannel coolers are very high and can be up to $50,000 \text{ W/m}^2\text{K}$ [10].



Figure 4 – A selection of *AlSiC* integrated baseplate pin fin coolers from CPS Technologies [11]. The shape of the pin-fins are designed to improve the heat transfer to the coolant fluid.

1.4.2 Pressure mounted modules

In pressure mounted modules some of the bonded interfaces are replaced by pressure contacts, reducing the number of bonded interfaces within the module. Electrical spring connectors are arranged in such a way as to apply a force evenly over the complete module to improve the pressure contact to the cooler. An example of this is the Semikron SkiiP range of power modules where sprung electrical connectors are used to apply a distributed force over the DBC alumina substrate tile improving the thermal connection with the cold plate (Figure 5) [12]. The main reason for constructing modules in this way is to reduce the number of bonded layers and interfaces within the module. Bonded interfaces tend to degrade and crack due to thermal cycling and can lead to failure of the power module. Although there are some potential gains in reliability due to the removal of the bonded solder interface between the DBC alumina substrate and the heat sink, the amount of heat and therefore power that the module can

dissipate is limited by the poor thermal interface to the heatsink compared to a bonded solution.

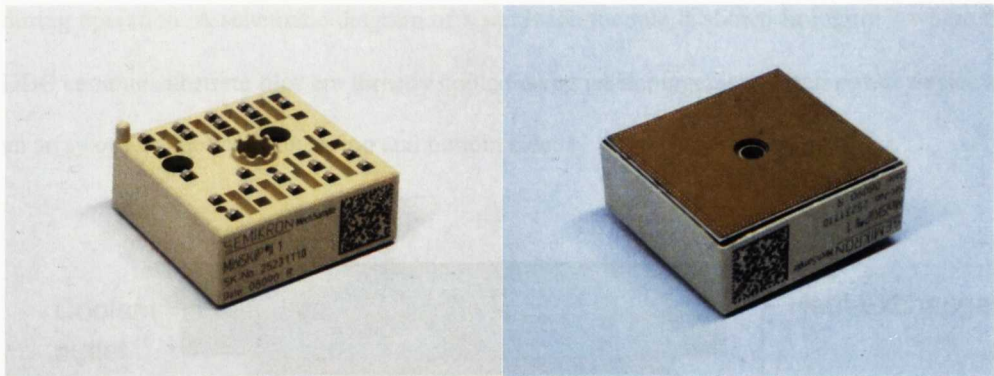


Figure 5 – A Semikron SkiiP module with sprung electrical connectors visible in the picture on the left. The picture on the right shows the DBC substrate tile which is mounted directly onto the coldplate cooler.



Figure 6 – A close-up photograph of one of the spring connectors from the Semikron SkiiP module shown in Figure 5. Over 20 connectors are held by the plastic case allowing them to flex in the vertical direction in order to apply force evenly over the module, pressure mounting it onto the cooler.

1.4.3 Double sided cooling

The silicon power electronic devices can be soldered between two DBC ceramic substrates resulting in what is often referred to as a ‘sandwich module’ [13]. These modules eliminate wirebonds from the assembly whose function is performed by a soldered interface. The resulting module is usually cooled on its top and bottom side, increasing the amount of cooling the devices receive. The sandwich module is designed without a metal heatspreader plate in the assembly further reducing the number of thermal layers between the power device and coolant fluid. A light-weight and compact module can be realised using a sandwich assembly where the DBC substrate tiles are cooled directly resulting in a very low thermal mass. A high heat

transfer coefficient direct cooling method such as jet impingement can be employed to provide the double-side cooling of the module which minimises the temperature rise of the devices during operation. A schematic diagram of a sandwich module is shown in Figure 7 where two DBC ceramic substrate tiles are directly cooled using jet impingement. Each power device has an array of jets cooling it on its top and bottom side.

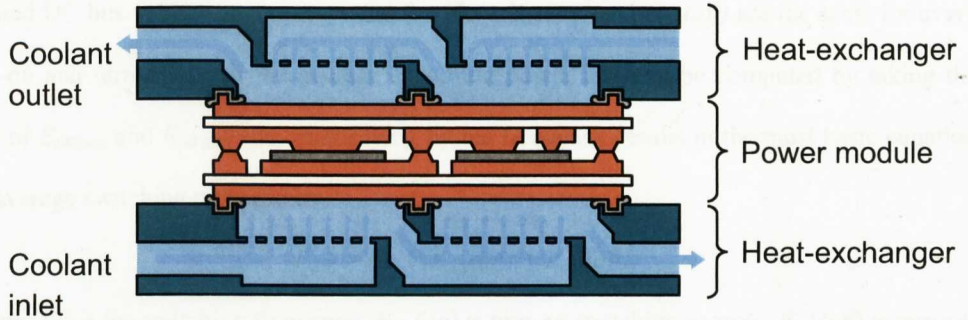


Figure 7 – A schematic diagram of a double side cooled sandwich module.

1.4.4 Power module operational characteristics

1.4.4.1 The origins of power losses and heat generation

Although power modules are very efficient some losses are still produced during operation. In power modules containing IGBTs and diodes the two most significant sources of power dissipation are conduction losses and switching losses. Conduction losses are produced while the device is on and conducting current. The total power dissipation during conduction is calculated by multiplying the on-state (saturation) voltage by the on-state current. In PWM (Pulse Width Modulation) applications the conduction loss should be multiplied by the duty cycle to obtain the average power dissipated. An approximation of conduction losses can be obtained by multiplying the IGBT's rated $V_{CE(sat)}$ by the expected average device current.

1.4.4.2 Switching loss

Switching loss is the power dissipated during the turn-on and turn-off switching transitions. In high frequency PWM switching losses can be substantial and must be considered in thermal design. The most accurate method of determining switching losses is to plot the I_C and V_{CE} waveforms during the switching transition. The product of the I_C and V_{CE} waveforms gives the instantaneous power waveform. The area under the power waveform is the switching energy

expressed in *Watt-seconds/pulse* or *J/pulse*. The standard definitions of turn-on ($E_{SW(on)}$) and turn-off ($E_{SW(off)}$) switching energy is given in Figure 8. From Figure 8 it can be observed that there are pulses of power loss at turn-on and turn-off of the IGBT. The instantaneous junction temperature rise due to these pulses is not normally a concern because of their extremely short duration. However, the sum of these power losses in an application where the device is repetitively switching on and off can be significant. In cases where the operating current and applied DC bus voltage are constant and therefore $E_{SW(on)}$ and $E_{SW(off)}$ are the same for every turn-on and turn-off event the average switching power loss can be computed by taking the sum of $E_{SW(on)}$ and $E_{SW(off)}$ and multiplying by the frequency results in the most basic equation for average switching power loss:

$$P_{SW} = f_{SW} \times (E_{SW(on)} + E_{SW(off)})$$

Where: f_{SW} is the switching frequency, $E_{SW(on)}$ is turn-on switching energy, $E_{SW(off)}$ is turn-off switching energy [14].

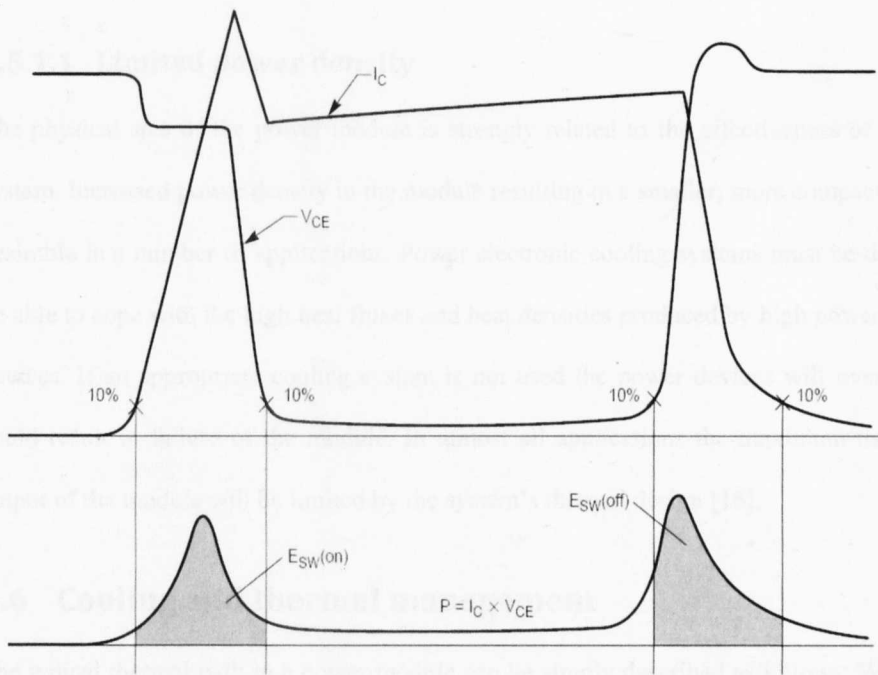


Figure 8 – An example of switching waveforms for an IGBT showing how the energy loss during turn-on and turn-off switching is calculated [14].

1.5 Cooling and Reliability

1.5.1 The need for cooling

The heat generated due to losses must be conducted away from the power devices and into the environment using a heatsink. Cooling of power modules is required in the first instance to prevent permanent damage of the *Si* devices as they will fail if operated above 125°C . High temperatures result in a degradation of electrical performance which could potentially lead to thermal runaway as resistive losses within the module increase with temperature. Additional cooling is normally required to ensure the long term reliability of the power module packaging. Failure of the power module package at bonded interfaces becomes the leading failure mechanism as the modules are power cycled [15]. Power module failure can therefore be avoided by minimising the thermally induced failure of individual components and bonded layers making up the system. Two main problems to be avoided are electronic components operating at elevated temperatures and excessive thermal cycling.

1.5.1.1 Limited power density

The physical size of the power module is strongly related to the effectiveness of the cooling system. Increased power density in the module resulting in a smaller, more compact package is desirable in a number of applications. Power electronic cooling systems must be developed to be able to cope with the high heat fluxes and heat densities produced by high power dissipating devices. If an appropriate cooling system is not used the power devices will overheat which could result in failure of the module. In almost all applications the maximum usable power output of the module will be limited by the system's thermal design [16].

1.6 Cooling and thermal management

The typical thermal path in a power module can be simply described as follows: Waste heat is generated within the power electronic devices. The heat is then conducted to the cooler through a number of layers of solid materials which make up the power module. The heat is then transferred by convection to the coolant fluid. A number of methods exist for the cooling of power electronics in commercial and aerospace applications. There is a large variation in the complexity, cost, weight and cooling efficiency of each cooling method. Some of the most

commonly used cooling methods are outlined below. In Table 1 the typical heat transfer coefficients for various power electronic cooling methods are listed.

Table 1 – Typical heat transfer coefficients for a number of commonly used power module cooling methods.

<i>Cooling Method</i>	<i>Typical heat transfer coefficient (W/m^2K)</i>
<i>Natural Convection (air)</i>	<i>3 - 25</i>
<i>Natural Convection (water)</i>	<i>15 - 1000</i>
<i>Forced Convection (air)</i>	<i>10 – 200</i>
<i>Forced Convection (water)</i>	<i>Up to 10,000</i>
<i>Condensing steam</i>	<i>5,000 – 50,000</i>
<i>Boiling Water</i>	<i>Up to 50,000</i>
<i>Microchannel</i>	<i>Up to 50,000</i>
<i>Jet Impingement</i>	<i>Up to 50,000</i>
<i>Spray cooling (water)</i>	<i>Up to 500,000</i>
<i>Ultra thin film evaporation</i>	<i>10,000 to 500,000</i>

1.6.1 Passive cooling and conduction of heat

1.6.1.1 Radiation

The heat emitted by radiation is proportional to the fourth power of the temperature difference between the device and its surroundings. In most electronic systems the proximity of equally dissipating and receiving units will result in minimal net loss of heat through radiation. Radiation is only suitable as a cooling mechanism when the electronic devices are used in isolation in an open environment where the surroundings are at a significantly lower ambient temperature compared to the device temperature, for example, on orbiting satellites.

1.6.1.2 Wick structured heat pipes

A heat pipe is a device that can efficiently transfer heat from one point to another. A heat pipe is a passive device and provides no cooling of itself as such, but is a means of removing heat from components with high heat fluxes and densities for it to be dissipated elsewhere. An external method of cooling is required at the cold end of the heat pipe. The use of a two-phase heat transfer mechanism results in a high effective thermal conductivity compared to conduction of heat through solid metals such as copper or silver. A typical value of thermal resistance for a heat pipe in an electronics cooling application is $0.4^{\circ}\text{C}/\text{W}$ [17].

A typical heat pipe is a closed cylindrical vessel with its internal walls lined with a capillary structure that is saturated with a working fluid (as shown in Figure 9). The internal pressure of the device is dictated by the vapour pressure of the working fluid at saturation conditions. Orientation of the device is a key feature of its performance as it relies on the upward convection of vapour against gravity, therefore heat should be applied at the bottom and removed at the top of the device. As heat is applied to the evaporator the working fluid is vaporised and convects upwards towards the cooler section where it condenses, giving up its latent heat of vaporisation. The working fluid in the liquid state is then returned to the hot evaporator section by capillary forces developed by the wick structure.

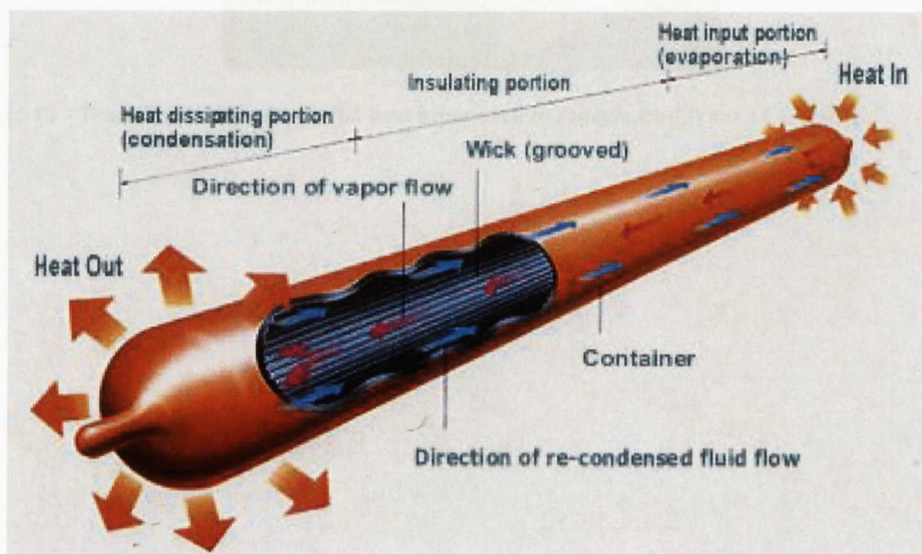


Figure 9 - Schematic diagram of a typical wick structured heat pipe [18].

Thermal transfer in heat pipes is provided through the change of phase of the working fluid and mass transfer. Heat pipes tend to have a tubular structure but are available in flat designs. Heat pipes are sensitive to orientation therefore electronic systems requiring their use have to be specifically designed to incorporate them into the layout. Heat pipes can be designed to operate over a very broad range of temperatures from cryogenic applications ($<-243^{\circ}\text{C}$) to high temperature applications ($>2000^{\circ}\text{C}$). An example of heat pipes being used to cool a CPU is shown in Figure 10 and Figure 11 where a fan is used to provide a cooling air flow at the condensing end of the device.

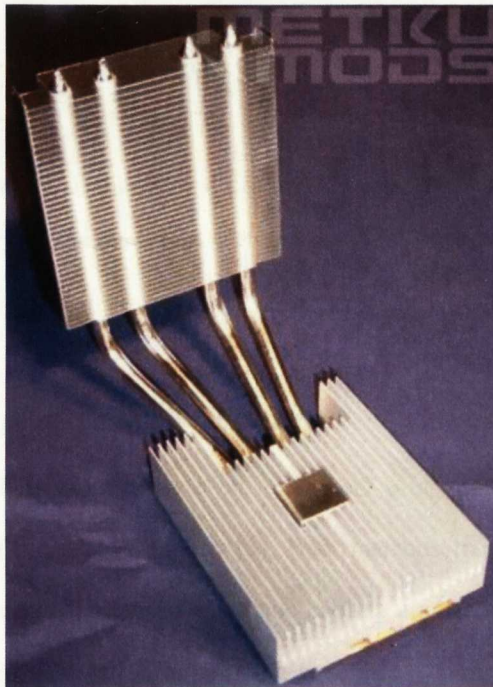


Figure 10 - Traditional wick structured heat pipes used to remove heat from a CPU [19].

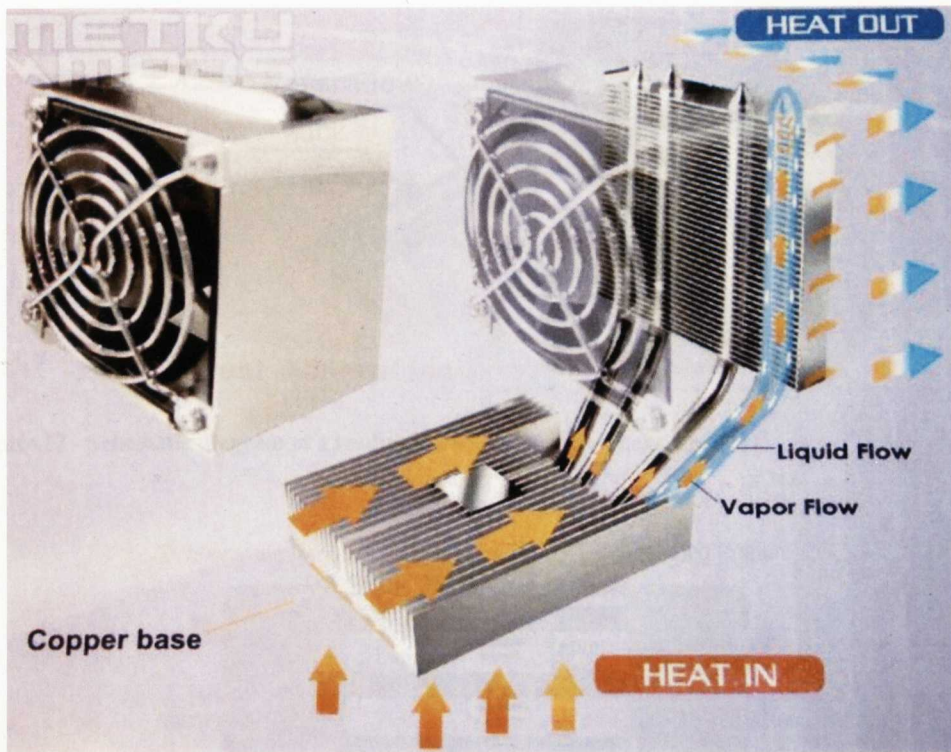


Figure 11 - Diagram showing the movement of heat from the CPU through the heat pipe to a fan driven cooling unit [20].

1.6.1.3 Closed loop pulsating heat pipes

Closed loop pulsating heat pipes operate on a different principle from conventional wick structured heat pipes (Figure 12 & Figure 13). Both methods transfer heat between a hot evaporator to a cooler condenser. In an electronic cooling application an external source of cooling is required at the cold end. Similarities between the two methods include the use of capillary action and latent heat exchange. Where a traditional heat pipe uses capillary action as a primary transport mechanism of working fluid, pulsating heat pipes utilise surface tension and capillary effects to allow operation at any orientation.

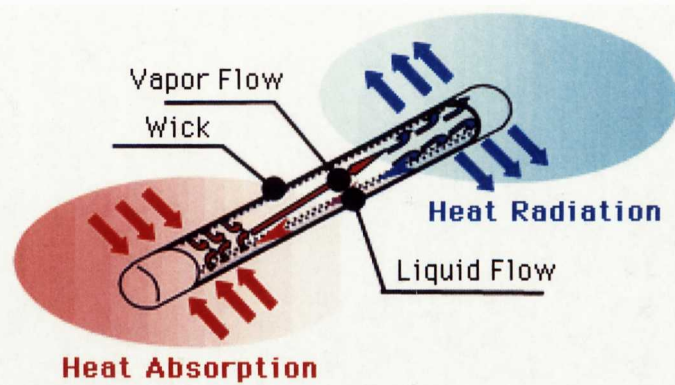


Figure 12 - Schematic diagram of a traditional wick structured heat pipe [21].

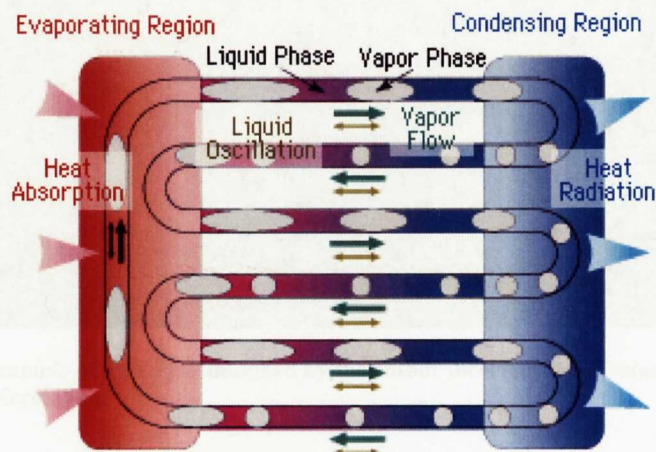


Figure 13 - Schematic diagram of a closed loop pulsating heat pipe [21].

7.6.1.3 Natural Convection

Natural convection is the air movement or motion resulting from density and is the most widely used method of cooling electronic equipment due to low cost and low complexity. The power density is increased once a thermal limit has typically been reached. Convection can be both active or passive, therefore these systems are susceptible to replacement and require regular maintenance. Due to the situation and low supply of air

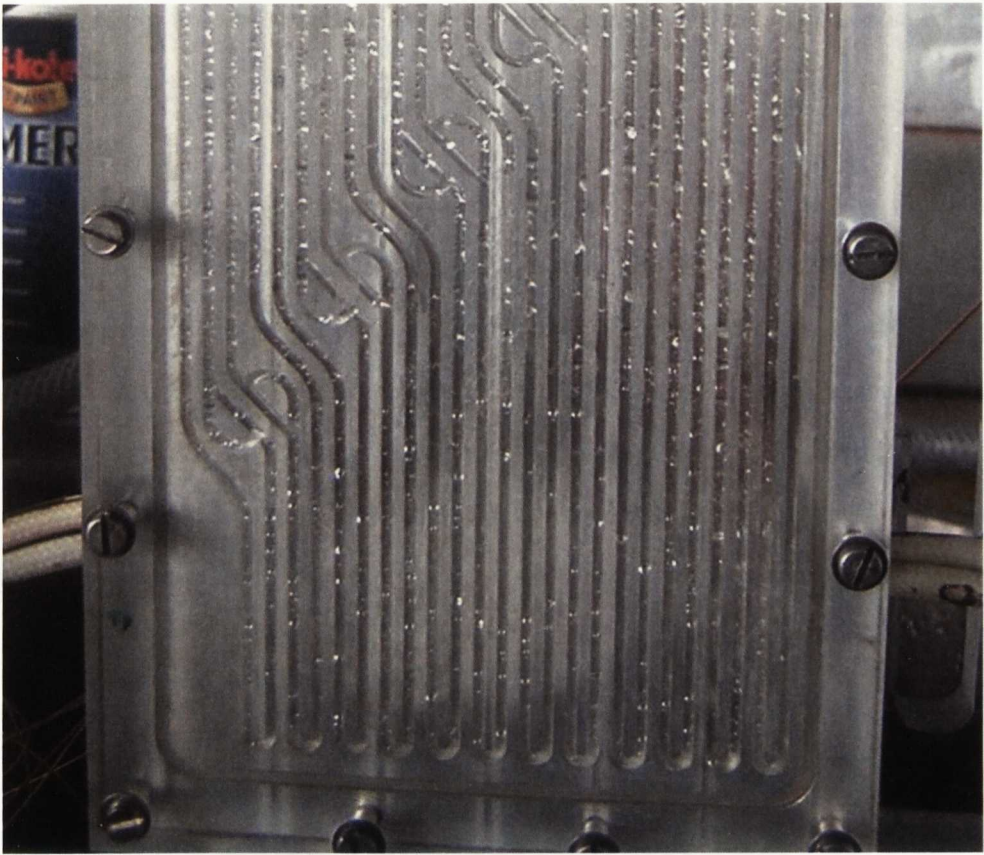


Figure 14 – An example of a CLPHP designed by the author incorporating Teslar fluidic valves to encourage fluid circulation.

Advantages of such a technology include better thermal transportation performance compared to a solid metal heat sink. Thermal conductivities (W/mK) of pulsating heat pipes are claimed to be up to 4.8 times better than silver and 5.1 times better than copper in the heat transfer direction [21]. Closed loop pulsating heat pipes are slimmer and lighter in weight compared to conventional wick structured heat pipes operating under the same conditions. The operation of pulsating heat pipes are reported to be far less sensitive to orientation compared to traditional heat pipes.

1.6.1.4 Natural Convection

Natural convection to the air requires no active pumping mechanisms and is the most widely used method of cooling conventional electronics due to low system cost and proven reliability. The power module is mounted onto a finned heat sink typically machined from aluminium. Convectors are made with no moving parts, therefore these systems are inexpensive to implement and require minimal maintenance. Due to the abundant and free supply of air a

convector can be used as part of an open loop system; once the air is used there is no need to recycle it.

One disadvantage of using natural convection to the air to cool power modules with large losses is the low heat removal capacity compared to active cooling methods. When used in an aerospace environment cooling performance suffers at high altitude due to the reduced molecular density of air and therefore heat capacity. Equipment fitted with convectors is orientation sensitive and must be configured to enhance natural flow upwards past the components that are being cooled. The system layout must be carefully arranged to prevent smaller components hindering the flow of air past components requiring the most cooling.

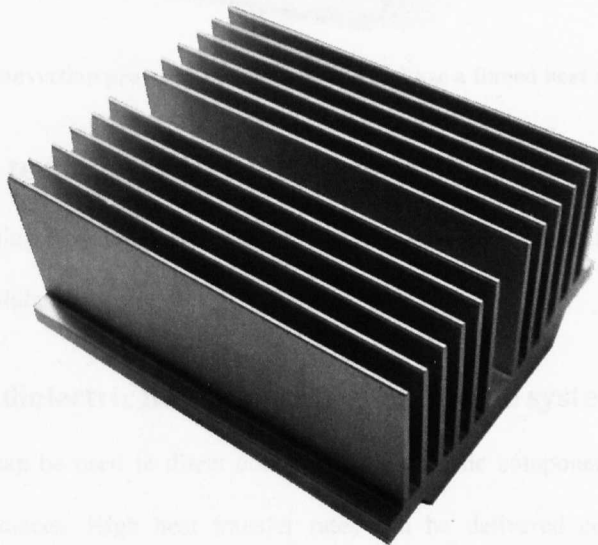


Figure 15 - A typical finned convector heat sink [22]. Finned heat sinks are typically machined from Aluminium due to its good thermal properties and low density.

1.6.1.5 Forced convection

In forced convection a fan is typically used to produce a flow of air through a finned heat sink thereby increasing the rate of heat transfer to the air compared to natural convection. In this way forced convection is much more effective in terms of heat removal to the air compared to natural convection. Forced convection can be used in open, or closed systems if the air passes through a heat exchanger or is conditioned. Disadvantages of forced air convection stem from the way a flow of air is established. If the air is bled from an aircraft engine, some conditioning such as throttling and filtering is required. Pumps and ducts increase the weight and volume of

the system. Maintenance is required and convection surfaces must be free from debris and corrosion to maintain convection coefficients. A failure in the air supply will lead to overheating and probable failure of the system.

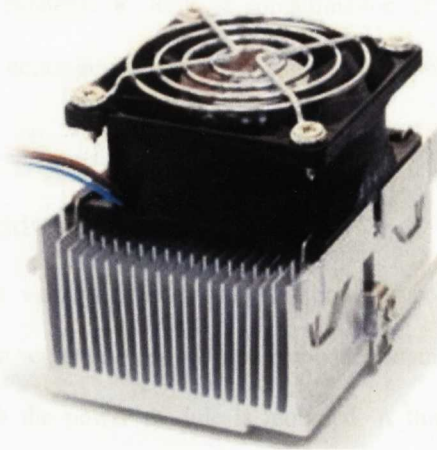


Figure 16 - Forced convection provided by a fan mounted above a finned heat sink [23].

1.6.2 Cooling techniques for high power dissipation electronics

The following cooling techniques are designed to cope with the high heat fluxes increasingly found in power modules:

1.6.2.1 Use of dielectric fluids in active and passive systems

Dielectric liquids can be used in direct contact with electronic components greatly reducing thermal path resistances. High heat transfer rates can be delivered compared to air and conduction schemes. Power modules can effectively be fully immersed in dielectric fluids such as 3M Company Fluoroinerts allowing the top of the devices to be in direct contact with the coolant fluid. The saturation temperature of the dielectric fluid can be tailored to match the operational requirements of the components, reducing the risk of elevated temperatures. When used with change of phase mechanisms dielectric liquids can maintain components at a reasonably constant temperature therefore reducing the impact of thermal cycling. Large volumes of liquid are not necessarily required which avoids excessive weight of the cooling system.

Disadvantages of using dielectric liquids is that their specific heat capacity is approximately one quarter that of water. However, water cannot be readily used as a direct contact fluid when cooling active electronic components. Some fluid reconditioning is necessary if used in a change of phase system with an additional heat exchange unit required to cool the fluid below saturation conditions to condense it. Risk of contamination of the coolant fluid and close control of the saturation conditions tends to limit the use of submerged cooling systems to stationary installations.

1.6.2.2 Forced liquid cooling: Cold plates

Liquid cold plates are a very popular cooling method for power modules. The simplest configuration consists of a serpentine copper pipe embedded in an aluminum block resulting in a flat surface onto which the power module is mounted. A thin layer of thermal grease is applied over the contact area to improve the heat transfer to the coolant by reducing the number of air-filled voids. A Water-Glycol mixture is a typical coolant fluid. An example of a serpentine coldplate is shown in Figure 17. Serpentine tubed coldplates can generate average heat transfer coefficients up to around $10,000 W/m^2K$ at the interface to the power module and do not require large amounts of pumping energy to drive the coolant fluid through them. The coldplate is a sealed unit and the coolant fluid is not in direct contact with the power module it is cooling.

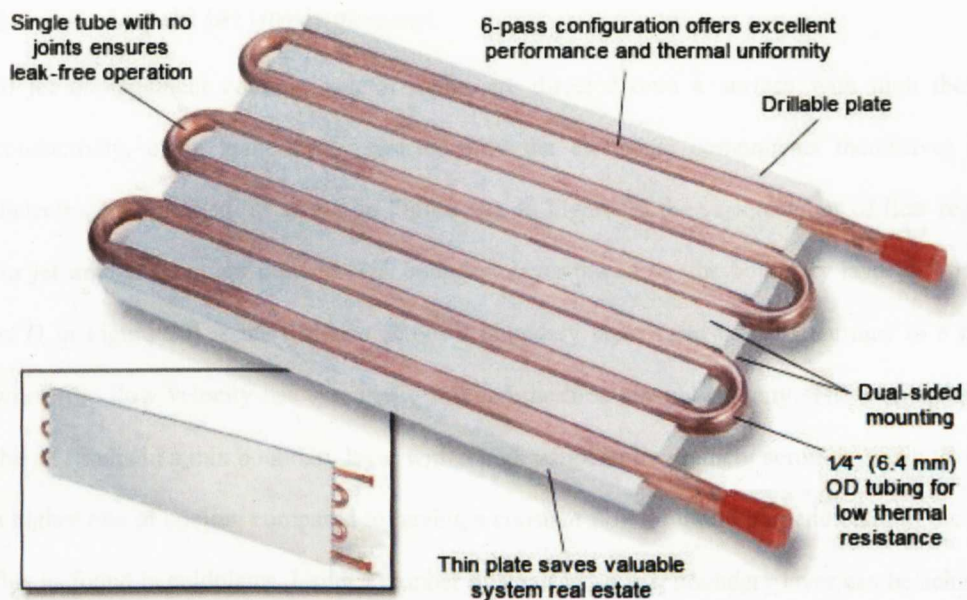


Figure 17 – An example of a typical serpentine coldplate for cooling a power module [24].

The amount of cooling can be enhanced by increasing the internal surface area using pin fins which also results in mixing of the fluid. In Figure 18 a more complicated cold plate is depicted with brazed fins inside it. The fins increase the surface area for heat transfer and can be optimized according to the specification of the power module being cooled.

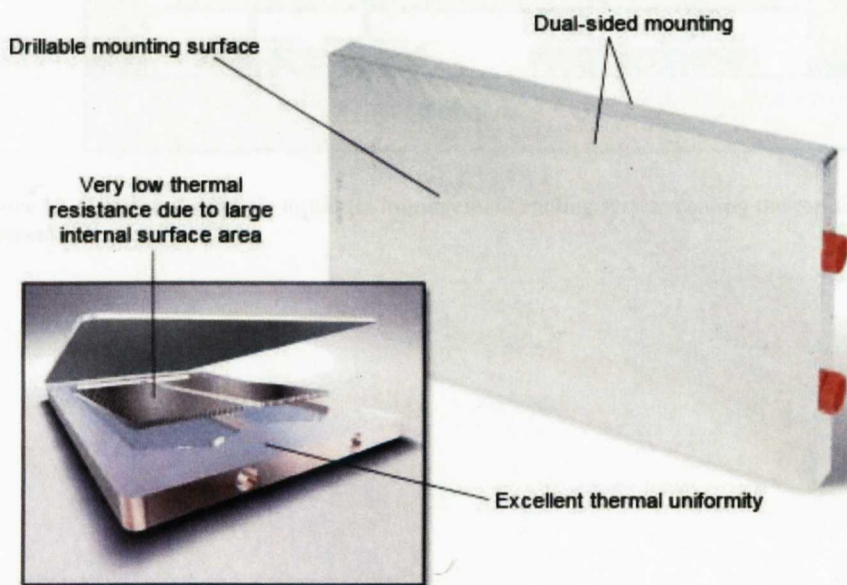


Figure 18 – Coldplate with fin enhancements to improve the heat transfer [25].

1.6.2.3 Liquid jet impingement

In jet impingement cooling, jets of liquid are directed onto a surface with high thermal conductivity, or in some cases directly onto the electronic components themselves if a dielectric fluid is used (as shown in Figure 19). In Figure 20 the various types of flow regime for jet impingement are defined. The boundary layer thickness (the boundary layer is labelled as D in Figure 20) is the distance across a boundary layer from the wall surface to a point where the flow velocity has essentially reached the 'free stream' velocity. The momentum of the jet results in a thin boundary layer with a high temperature gradient across it which leads to a higher rate of cooling compared to having a constant flow of liquid perpendicular to the heat flux as found in coldplates. Using a number of small jets a thin boundary layer can be achieved over the entire surface area of an electronic component leading to a higher temperature gradient resulting in a higher heat flux away from the component.

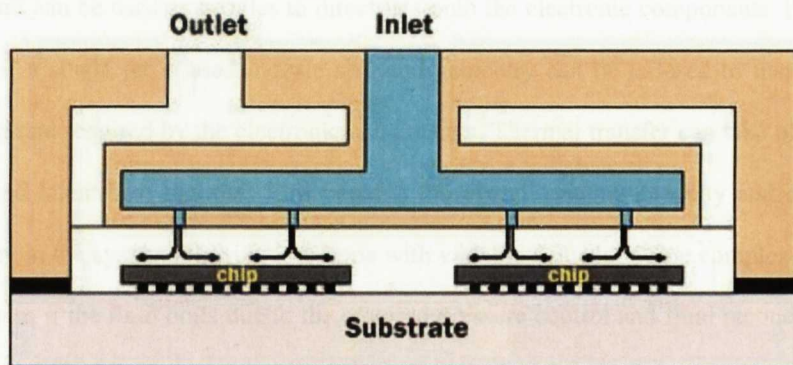


Figure 19 - Layout of a simple liquid jet impingement cooling system cooling the top side of electronic components [26].

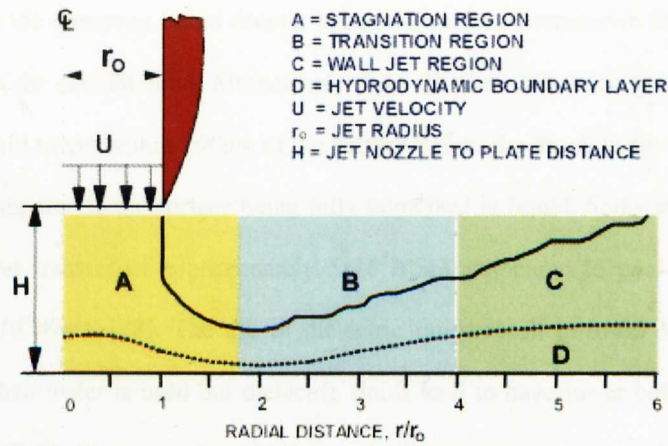


Figure 20 - Diagram representing types of flow regime resulting from jet impingement on a flat surface [27].

High heat transfer coefficients of over $30,000 \text{ W/m}^2\text{K}$ at the heat transfer surface can be achieved using jet impingement cooling. Design tolerances on nozzles are less critical compared to spray cooling. Plates with arrays of machined holes with diameters in the order of a millimetre can be used as nozzles to direct jets onto the electronic components. Flow can be localized if a single jet is used, nozzle size and geometry can be tailored to match the heat dissipation rate required by the electronic components. Thermal transfer can take place in both sensible and latent heat regimes. This benefits the overall cooling capacity and offers some redundancy in the system allowing it to cope with variable demand. Some complexity is added to the system if the fluid boils due to the required pressure control and fluid reconditioning. In this case it is necessary to condense the working fluid by cooling it below its saturation temperature. In all cases a heat exchanger and pumping mechanism incorporating filters is required. Wear of components and nozzles is of little concern compared to spray cooling where a small change in nozzle diameter will have a significant effect on the spray cone. The coolant fluid used should be filtered to prevent foreign particles from circulating around the system. The volume of working fluid required is greater than that in spray cooling resulting in a heavier system.

1.6.2.4 Spray cooling with change of phase

Dielectric fluid can be sprayed in a fine mist directly onto the surface of electronic components, water can be used if the contacting surface is electrically isolated. Heat transfer occurs by conduction and radiation through a thin film of vapour between the surface of the

component and the incoming liquid droplet hence the surface temperature is held close to the boiling point of the coolant fluid. Momentum of the droplets at a velocity of 15m/s to 20m/s allows cool liquid to get within $200\mu\text{m}$ of the surface before the droplets are vaporised. This is much closer compared to the surface being fully immersed in liquid. Spray cooling with water can achieve heat transfer of approximately $5 \times 10^5 \text{W/mK}$ compared to pool boiling of water resulting in $5 \times 10^4 \text{W/mK}$ [28]. The use of dielectric fluids result in lower heat transfer rates compared to when water is used but dielectric fluids tend to have lower boiling temperatures for example: FC-72 Fluorinert by 3M has a boiling temperature of 56°C under typical atmospheric conditions. Special machining techniques are required to manufacture spray nozzles to the precision and tolerance required to produce a fine mist. The location of nozzles is critical in order to achieve adequate cooling.

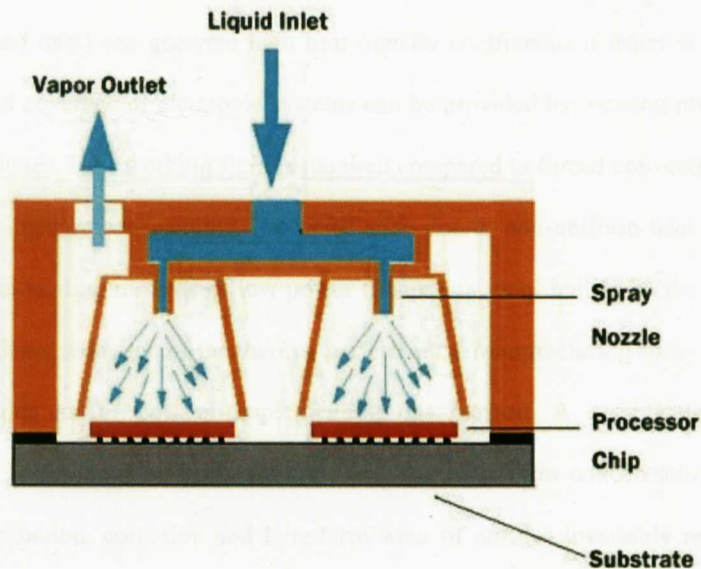


Figure 21 - Schematic diagram of a spray cooling system directly cooling the top side of an electronic device [29].

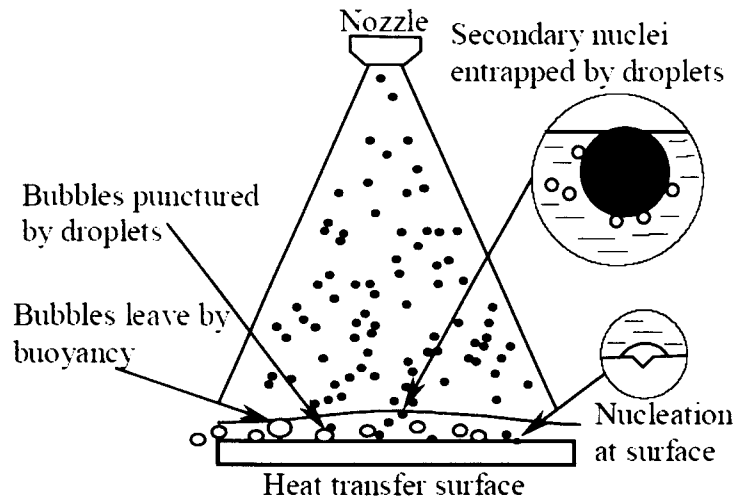


Figure 22 - Spray cooling (atomised mist) schematic diagram. Note: droplets and bubbles are not to scale [30].

Spray cooling (atomised mist) can generate high heat transfer coefficients if water is used as the coolant fluid. Good coverage of electronic systems can be provided by locating nozzles to cool the highest heat fluxes. Less working fluid is required compared to forced convection bulk flow methods and jet impingement cooling. Problems arise due to non-uniform heat sources resulting in liquid accumulating in areas of low power dissipation, pool boiling of the coolant fluid results in a significant reduction of the thermal performance. Manufacturing spray nozzles to close tolerances adds to the cost of implementing this method. A complicated fluid reconditioning system incorporating a heat exchanger is required to allow condensation of the working fluid. Contamination, corrosion and long-term wear of nozzles invariably results in poorer performance. The spray distance to components is critical in order to develop a 'spray cone'. High pressure pumping is required to create a fine spray. The velocity and momentum of the spray is critical. If it is too great it can lead to erosion of the surface and splashing away without properly wetting the component resulting in poor cooling. A spray velocity which is too small will result in insufficient cooling and the electronic component may overheat. Spray cooling must be used as a change of phase method as it has poor sensible cooling action.

1.6.3 Summary of cooling methods

In order to maintain power electronic devices at a reasonable temperature during operation it is necessary to implement a cooling method which can cope with high heat fluxes. Wick

structured heat pipes use a change of phase method to transport heat away from the source electronics and offer low thermal resistance with the added benefit of having no moving mechanical parts. This allows the heat sink to be located away from the module and is useful if the power modules are awkwardly located or difficult to access. The simplicity of heat pipes is negated by the fact that they do not produce any cooling themselves; they merely behave like a material with high thermal conductivity. When trying to dissipate hundreds of *Watts* of heat from a power module and if large, heavy systems are to be avoided, an active cooling method must be used. The design of the heat transfer path from the power electronic devices to the coolant fluid is critically dependent on the choice of the ultimate cooling medium and method of cooling.

1.6.3.1 Liquid cooling and change of phase

Liquid cooling methods such as atomised spray, jet impingement and coldplates are better suited for cooling power electronics due to the heat fluxes generated and the high heat capacity of liquids compared to the ambient air. Spray and impingement cooling are able to cool electronic devices generating heat fluxes of over $100W/cm^2$ [31]. Atomised spray cooling with change of phase can produce very high heat transfer coefficients due to the thermal energy absorbed by the latent heat of vaporisation of the working fluid. Implementing such a spray cooling system requires precision components, a sophisticated control and monitoring system and a finely filtered working fluid. This is only practical in a stable and stationary environment due to the effect of g-forces and vibration on the spray droplets. The spray droplet size and saturation conditions at the cooled surface must be finely controlled due to the reduction in heat transfer resulting from either wetting of the surface or dry out. Difficulties associated with change of phase; dry out and cavitation of the heat transfer surface, could potentially rule out atomised spray cooling for use in an avionic system at the present time.

1.6.3.2 Potential of jet impingement

Jet impingement cooling with submerged jets can produce very high heat transfer coefficients at a reasonable pressure drop for a single phase liquid cooling system. The arrays of jets enhance the heat transfer to the coolant fluid by reducing the thickness of the thermal boundary layer resulting in a high temperature gradient near to the heat transfer surface. Due to the high

heat transfer coefficients generated by the impinging jets a heat spreader plate is not always required, greatly reducing the physical and thermal mass of the system. Unlike a microchannel system, the jet impingement cooler geometry does not need to be machined from metal or a material with high thermal conductivity but can be made from light weight plastics or other materials as the thermal properties are not crucial to the performance of the cooler. A traditional coldplate cooler could be simply replaced by a jet impingement cooler in most installations. Whereas a spray cooling system with change of phase would require a number of substantial modifications and added complexity to the coolant circuit.

There is great potential to increase the efficiency of jet impingement cooling systems in the context of power electronic cooling if the jet arrays are specifically designed to match the heat fluxes underneath the electronic devices. Mathematical modelling and simulations using computational fluid dynamics (CFD) have been attempted but are presently unable to provide conclusive predictions of the thermal heat transfer performance and the associated pressure drop produced by working geometries which are required to optimise the jet arrays [32].

Due to the impressive performance characteristics of jet impingement and the ability for it to be used as part of a direct cooling system it was decided to look further into this technology due to the potential reliability benefits if integrated properly into a power module. Jet impingement cooling is covered more fully in Chapter 3.

1.7 Structure of the thesis

The background material presented in the first chapter has identified that there is a need to improve and optimise the cooling of power electronic devices in order to improve the operational reliability of power modules. Potential improvements to reliability can be achieved by integrating the cooler as part of the power module thus reducing the number of bonded interfaces which are prone to failure. Jet impingement cooling has been identified as a cooling method which has great potential and will be investigated further in the context of power electronic cooling.

Chapter Two

This chapter looks into the limitations of heat transfer and the impact on the design of the heat transfer path through the power module. The thermal and mechanical properties of the individual material layers which make up the power module are analysed further and an overview of reliability and points of failure is given. The necessity or in some cases the redundancy of a heat spreader depending on the heat transfer coefficient produced by the cooler is analysed.

Chapter Three

In this chapter initial experimental tests involving jet impingement cooling are described. A power module was cooled by three different coolers in differing configurations. The cooling performance of a traditional serpentine coldplate is compared to the cooling performance of a jet impingement cooler, directly cooling the baseplate of the power module and a second jet impingement cooler, directly cooling the underside of the DBC substrate tiles. The results of the experimental tests indicate that direct jet impingement cooling of the DBC substrate tile cooled the power electronic devices most effectively.

Chapter Four

An experimental test rig was designed and constructed to allow a range of jet impingement array geometries to be tested and their cooling performance determined. In this set of tests the jet-to-target distance was held constant. The experimental results indicated that there is an optimum jet array geometry which can cool a given heat source most efficiently.

Chapter Five

Following on from the experiments performed in chapter four, a new experimental test rig was constructed to test the performance of a single 6×6 jet array directly cooling the substrate tile beneath a single diode. The test rig is designed to be similar to how such a system would be implemented in practice. Two series of tests were performed: The first involved varying the jet-to-target distance. The second involved varying the jet-to-jet spacing. The experimental results were analysed and the optimum jet array geometry was determined.

1.8 Chapter summary

In this chapter an overview of the power module and its uses are presented. Power modules are increasingly used in a variety of applications. Power modules generate heat and need to be adequately cooled in order to operate reliably and prevent thermal failure. When individual factors such as size, weight, power density and efficiency of the power modules becomes very important there are different approaches to the design and materials which are used to construct the module. The general construction of a power module with Silicon based devices soldered onto DBC ceramic substrates tends to be consistent, with most variations involving the choice of specific materials in the layered stack, the method of cooling and the interface between the power module and the cooler. A variety of cooling methods are described, jet impingement cooling is identified as showing great potential if integrated into the power module. An outline of the structure of the thesis is listed with a brief summary of the contents of each chapter.

Chapter 2

2 The heat transfer path

2.1 Introduction

In this chapter the issues relating to the long term operational reliability of power modules are explored with a focus on the material layers constituting the module. The properties of the material layers and interfaces making up the thermal path from heat source to heat sink are defined. The limitations of heat transfer within the module and the impact on the design of the heat transfer path are discussed. Reliability issues and weak points in the power module stack which are prone to failure are identified. The necessity or in some cases the redundancy of a heat spreader depending on the heat transfer coefficient produced by the cooler is analysed.

2.2 Reliability is largely a thermal problem

Long term failures of power modules which are operating within their designed range are caused by thermal problems. The likelihood of cracking of solder joints at edges, delamination of bonded surfaces, heel cracks or lift-off of wirebonds increases with number of power cycles [33]. These types of failure are exacerbated by thermal cycling. As the failure grows, for example a crack at the edge of a solder joint, the conduction of heat through the layered stack deteriorates due to the lower surface area available for heat transfer. This results in an increase in the thermal resistance between the device and the cooler. The higher component operating temperature results in thermal cycles of larger amplitude; this increases mechanical stresses and increases the crack growth, ultimately resulting in thermal failure of the module as the device overheats.

2.2.1 Thermal expansion and layers

The fabrication of electronic devices that will not fail by material and joint fatigue under high cycling rates and operating temperatures is a significant challenge. As temperatures and cycling rates increase, the mismatch of CTE and expansion rates for each layer of material in the module becomes critical as the de-bonding of materials becomes more likely [34]. In order

to improve the long term reliability of power modules, material and solder changes or more advanced layering schemes may be required.

2.3 The elements of the thermal path and integration

In a conventional power module heat is generated within the *Si* die at the top of the assembly and passes through a variety of solid materials, across interfaces and finally to the coolant fluid. The three main elements of the thermal path from heat source to sink can therefore be summarised as follows:

- Conduction of heat through materials.
- Heat flow across interfaces between different materials.
- Heat transfer to the coolant fluid by convection.

Improving each of the elements of the thermal path as part of an integrated system can greatly improve the reliability, performance and efficiency of power modules.

2.4 Thermal resistance of the power module

The thermal resistance, R_{th} , of a power module is the ratio of the temperature difference across the module from the electronic die to the coolant fluid per *Watt* of energy transferred as defined in Equation 1. Thermal resistance is typically expressed as: K/W or $^{\circ}C/W$.

$$R_{th,j-a} = \Delta T_{j-a} / Q$$

Equation 1 – Definition of thermal resistance from junction to ambient.

A low thermal resistance is desirable in order to minimise the temperature rise of the electronic devices per *Watt* of heat generated. The thermal resistance of a system is the sum of each individual layer's thermal resistance, which depends on the thermal conductivity and thickness of the material [35]. Figure 23 shows the thermal conductivity and Figure 24 shows the thermal resistance of the materials arranged in the order that they would be found in a typical power module cooled with a coldplate generating a heat transfer coefficient of $10,000W/m^2K$ [36] (see Figure 3). The thermal resistance of each layer is summed to give the total thermal resistance for the module, typically described as $R_{th,j-a}$ (junction-to-ambient), where the ambient is the surrounding air or the coolant fluid.

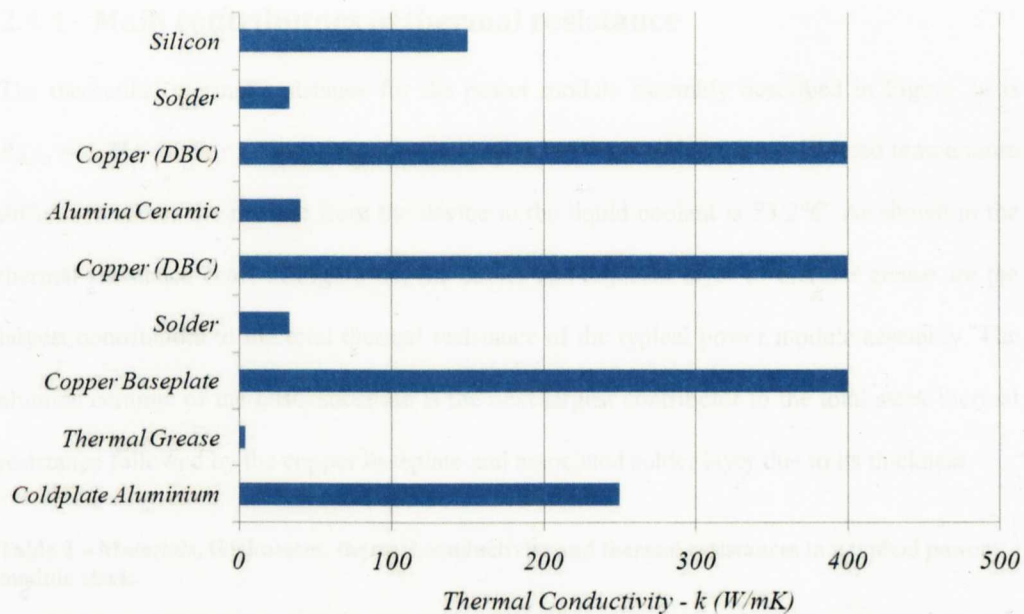


Figure 23 – Thermal conductivity of each individual layer in the stack. Arctic Silver thermal grease thermal conductivity $k = 4W/mK$ [37].

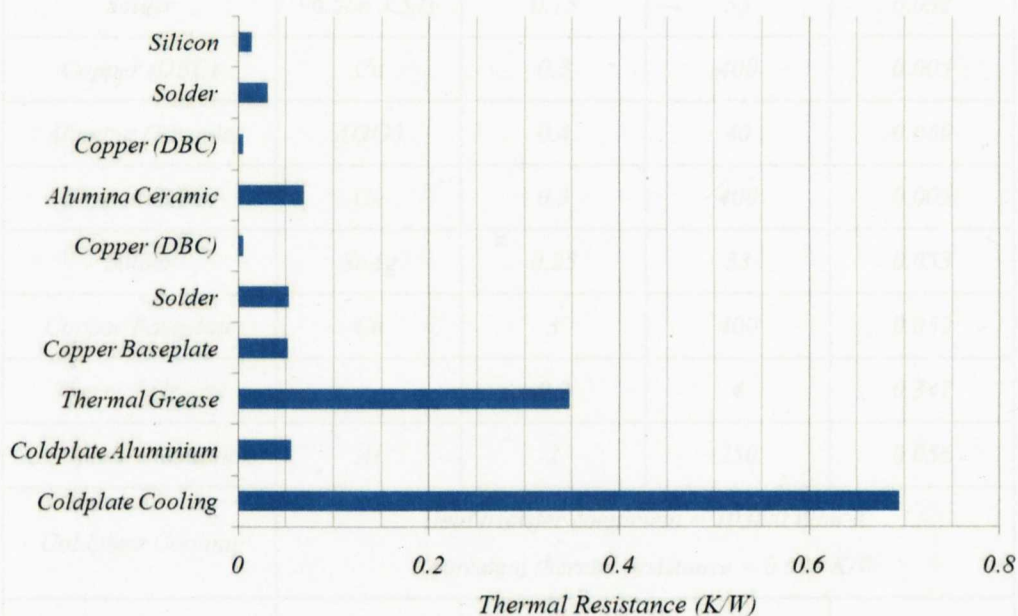


Figure 24 – Thermal resistance (R_{th}) of the individual layers making up the power module stack.

The values for the thermal resistance and temperature drop across each layer in the stack presented in Figure 24 and Table 2 were calculated ignoring end effects and lateral heat spreading through the stack. 100Watts of heat was transferred through the stack and the device measured 12mm x 12mm.

2.4.1 Main contributors of thermal resistance

The theoretical thermal resistance for the power module assembly described in Figure 24 is $R_{th,j-a} = 1.33K/W$. For a Silicon device dissipating $100Watts$ of heat, the calculated temperature difference across the module from the device to the liquid coolant is $75.2^{\circ}C$. As shown in the thermal resistance chart in Figure 24, the cooler and adjacent layer of thermal grease are the largest contributors to the total thermal resistance of the typical power module assembly. The alumina ceramic of the DBC substrate is the next largest contributor to the total stack thermal resistance followed by the copper baseplate and associated solder layer due to its thickness.

Table 2 – Materials, thicknesses, thermal conductivities and thermal resistances in a typical power module stack.

<i>Layer name</i>	<i>Chemical Symbol</i>	<i>Thickness (mm)</i>	<i>Thermal conductivity k (W/mK)</i>	<i>Thermal Resistance R_{th} (K/W)</i>
<i>Silicon</i>	<i>Si</i>	<i>0.3</i>	<i>150</i>	<i>0.014</i>
<i>Solder</i>	<i>96.5Sn 3.5Ag</i>	<i>0.15</i>	<i>33</i>	<i>0.032</i>
<i>Copper (DBC)</i>	<i>Cu</i>	<i>0.3</i>	<i>400</i>	<i>0.005</i>
<i>Alumina Ceramic</i>	<i>Al₂O₃</i>	<i>0.4</i>	<i>40</i>	<i>0.069</i>
<i>Copper (DBC)</i>	<i>Cu</i>	<i>0.3</i>	<i>400</i>	<i>0.005</i>
<i>Solder</i>	<i>SnAg</i>	<i>0.25</i>	<i>33</i>	<i>0.053</i>
<i>Copper Baseplate</i>	<i>Cu</i>	<i>3</i>	<i>400</i>	<i>0.052</i>
<i>Thermal Grease</i>		<i>0.2</i>	<i>4</i>	<i>0.347</i>
<i>Coldplate Aluminium</i>	<i>Al</i>	<i>2</i>	<i>250</i>	<i>0.056</i>
<i>Coldplate Cooling</i>	<i>Heat transfer coefficient = 10,000 W/m²K</i> <i>Equivalent thermal resistance = 0.694 K/W</i>			
<i>Water</i>	<i>H₂O</i>		<i>0.58</i>	

2.5 Choice of materials

The materials making up individual layers of the thermal stack from source to sink are carefully chosen based on an appropriate balance between a number of different material properties such as: thermal conductivity, electrical conductivity, CTE matching, elasticity,

manufacturability and cost. The tradeoffs between the choice of different materials are often defined by the target application or specification of the power module. Depending on the criteria of the final application a number of layers in the assembly are necessary and cannot be removed or improved much, whereas other layers are either unnecessary, or can be improved significantly.

2.5.1 Matching the thermal expansion coefficient

The CTE of *Si* and *SiC* is 3.5ppm/K and 3.7ppm/K respectively, this is a relatively low value and becomes the target value for the other materials in the stack (Table 3). Copper (17ppm/K) and aluminium (25ppm/K) stand out for their good electrical and thermal conductivity and low cost but are amongst the worst materials in the stack in terms of matching the CTE to adjacent layers. Baseplate heatspreaders also tend to be made from aluminium and copper due to the combination of low cost and high thermal conductivity. More exotic baseplate materials such as *AlSiC* have been developed in order to address the problem of improving heat transfer while minimising the effect of CTE mismatch. *AlSiC* has a high thermal conductivity of 180W/mK at 25°C and a low density of 3g/cm^3 compared to copper with a density of 9g/cm^3 . The CTE of *AlSiC* is 8ppm/K which is compatible with *AlN* substrates and can withstand many thousands of thermal cycles without delamination, which is a common failure in copper baseplate equivalents in similar operating conditions [11]. In Table 3 the Young's modulus is listed as well as the CTE of the various materials in the stack. The Young's modulus, also known as the tensile modulus, is a measure of the stiffness of an elastic material and is a quantity used to characterize materials. It is defined as the ratio of the uniaxial stress over the uniaxial strain in the range of stress in which Hooke's Law holds. Young's modulus is the ratio of stress, which has units of pressure, to strain, which is dimensionless; therefore, Young's modulus has units of pressure. Stiff or hard materials have a high value of Young's modulus, approaching 1000GPa (for example: Graphene) whereas soft, bendy or elastic materials have a lower value, for example, solder has a Young's modulus of 41GPa .

Table 3 – Young’s Modulus, CTE values and temperature drop between layers in the stack.

<i>Layer name</i>	<i>Young's Modulus</i>	<i>CTE</i>	<i>CTE difference to next layer</i>	<i>Mean temperature difference to next layer</i>
	<i>GPa</i>	<i>ppm/K</i>	<i>ppm/K</i>	<i>°C</i>
<i>Silicon</i>	<i>150</i>	<i>3.5</i>	<i>-16.5</i>	<i>2.3</i>
<i>Solder</i>	<i>41</i>	<i>20</i>	<i>3</i>	<i>1.8</i>
<i>Copper (DBC)</i>	<i>110</i>	<i>17</i>	<i>10.5</i>	<i>3.7</i>
<i>Alumina Ceramic</i>	<i>370</i>	<i>6.5</i>	<i>-10.5</i>	<i>3.7</i>
<i>Copper (DBC)</i>	<i>110</i>	<i>17</i>	<i>-3</i>	<i>2.9</i>
<i>Solder</i>	<i>41</i>	<i>20</i>	<i>3</i>	<i>5.2</i>
<i>Copper Baseplate</i>	<i>110</i>	<i>17</i>	<i>-8[#]</i>	<i>20.0</i>
<i>Thermal Grease</i>	<i>-</i>	<i>-</i>	<i>-</i>	<i>20.1</i>
<i>Coldplate Aluminium</i>	<i>68</i>	<i>25</i>	<i>-</i>	<i>-</i>

CTE difference given between Copper Baseplate and Coldplate Aluminium as the layer of thermal grease is not a bonded interface.

2.5.1.1 CTE and stresses

The objective of selecting materials based on their CTE value is really to avoid excessive stress, which tends to involve strain matching more than simple CTE matching. When a large temperature gradient is present across the module the designer might choose to have appropriate differences in CTE in adjacent materials. In addition, elasticity is desirable to allow strain differences to be absorbed without inducing cracks in the materials. Solders and other bonding materials particularly should have significant elasticity. The outcome of the interaction of all of the important material properties requires sophisticated modelling [34].

2.5.1.2 Stress induced failure

A typical failure pattern for a power module is due to thermal fatigue resulting in a crack along the solder layer between the DBC substrate tile and the copper baseplate of the power module [38]. A layer of solder with a minimum thickness of $200\mu\text{m}$ is recommended as a compromise between the benefit to reliability of the thicker solder to absorb the strain difference and the additional thermal resistance between the die and coolant. Simulations of the thermal stresses induced in the power module stack have been performed [39]. The simulations indicate stress concentrations along the edges and at corners of bonded material layers. The stress concentrations found along the edges and at corners mirrors observations of delamination of DBC substrates in failed power modules (Figure 25).

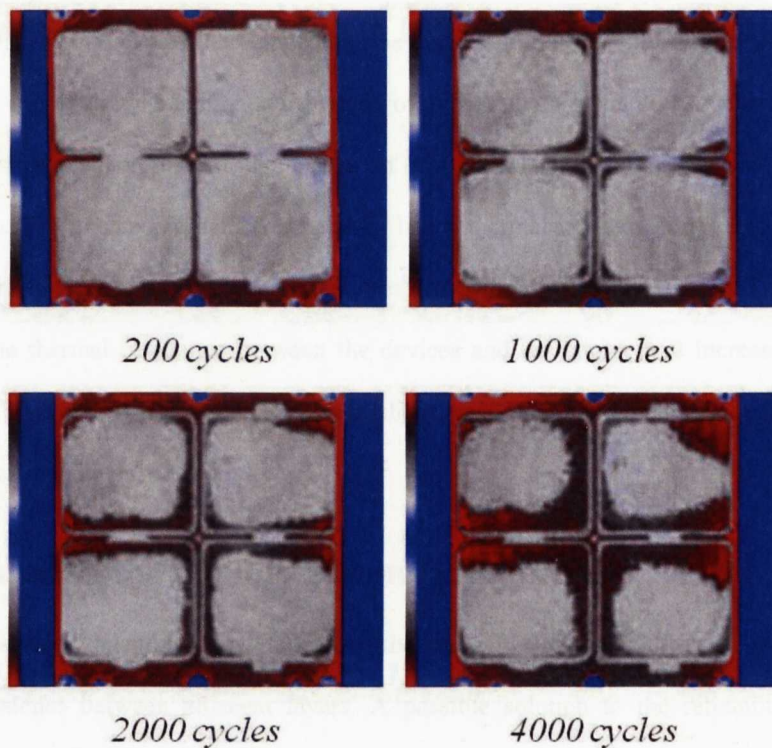


Figure 25 – Scanning Acoustic Microscope (SAM) images of a power module consisting of 4 substrate tiles undergoing thermal cycling. The grey area represents the solder layer between the substrate tiles and the baseplate. Cracks along the solder layer reduce the effectiveness of the bonded interface ultimately resulting in thermal failure of the module as the devices overheat.

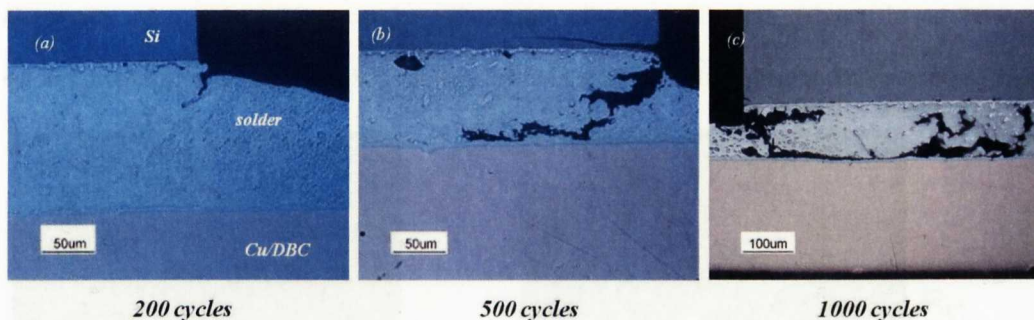


Figure 26 – Crack propagation in the solder joint between the *Si* device and the DBC substrate after thermal cycling. The cracks tend to propagate from edges or corners due to stress concentrations at these locations.

In Figure 25 four DBC tiles soldered onto a baseplate heatspreader have been subjected to thermal cycling. The grey area represents the solder layer between the DBC substrates and the baseplate. After 1000 cycles there appears to be degradation of the solder layer at the corners of the tiles, with more degradation at the centre of the baseplate. After 4000 cycles the edges of the DBC substrates closest to the centre of the baseplate have experienced substantial degradation. The cracked solder layer behaves like a thermal insulator, impeding the flow of heat from the devices to the cooler and therefore increasing the thermal resistance of the power module. The thermal resistance between the devices and the cooler will increase to a level where the devices will be operating above their maximum rated temperature resulting in thermal failure of the power module.

2.6 Reducing the number of bonded interfaces

Bonded interfaces delaminate and fail when thermally cycled due to stresses induced from CTE mismatches between adjacent layers. A possible solution to the reliability problems caused by bonded interfaces is to use a pressure contact to reduce the thermomechanical forces between adjacent layers in the assembly. A suitable thermal interface material must be chosen to enhance the heat transfer between the power module and the heat sink.

2.6.1 Thermal interface materials (TIMs)

TIMs can reduce the contact resistances by filling microscopic voids and grooves caused by surface asperities of the heat-generating and heat-dissipating devices, as well as bridging the macroscopic gaps generated by warpage as shown in Figure 27. In the wider context of

electronics applications, TIMs can be rather arbitrarily categorized as polymer-based TIMs, solders, composite materials, metallic foils, sintered metallic TIMs and carbon nano-tubes.

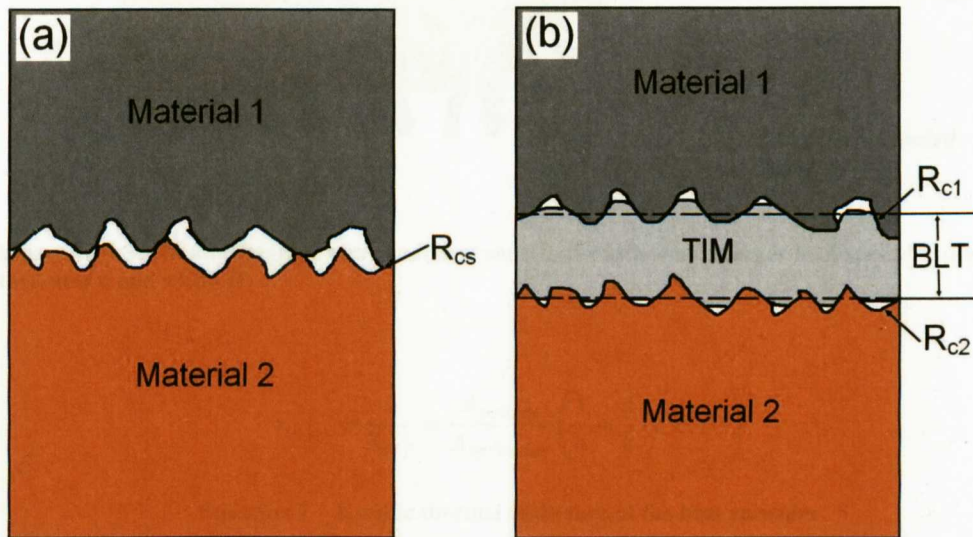


Figure 27 - Schematic representations of the surfaces of two materials (a): Actual contact area is much less than the apparent area of solid-solid contact due to surface asperities; (b) Enhanced contact using a thermal interface material (TIM) with a bond line thickness of BLT.

2.7 The need for a heat spreading baseplate

The DBC substrate tiles in a power module are typically soldered onto a metal heat spreading baseplate which aids the cooling of the power electronic devices. The solid plate expands the heat flow area and can be viewed as a mechanism for amplifying the heat transfer to the coolant fluid as shown in Figure 28. The performance of the heat spreader is a function of the size of the heat source, the thermal properties of the spreader itself and the heat transfer coefficient generated by the cooler as described in Equation 2. Intuitively, in Equation 2, if the thickness of the heat spreader is increased, the thermal resistance will increase also, whereas if the thermal conductivity of the heat spreader is increased the thermal resistance will be lower. With no heat spreader, the die temperature would be determined solely by the heat transfer coefficient, h . A higher h would result in a lower die temperature. F is a geometrical factor which depends on the shape of the die, it is always greater than zero and it does not depend on the size of the die or the heatspreader.

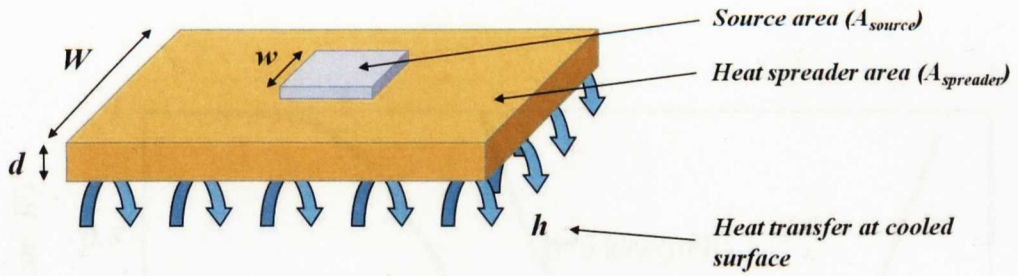


Figure 28 – Schematic diagram of a small heat source of width w on a larger heat spreader plate of thickness d and width W .

$$r_{th,sp} = \frac{1}{h_{eff}} = \frac{A_{source}}{A_{spreader}} \left(\frac{1}{h} + \frac{d}{k} (1 + F) \right)$$

Equation 2 – Specific thermal resistance of the heat spreader

Where: $r_{th,sp}$ is the specific thermal resistance (Km^2/W), k is the conductivity of the heatspreader material (W/mK), F is the spreading resistance factor ($F > 0$).

$$R_{th} = r_{th}/Area$$

Equation 3 – Definition of thermal resistance and specific thermal resistance

2.7.1 Heat spreader performance

The heat spreader performance is a function of heat source size, spreader material and heat transfer coefficient. For example: a $5mm$ square heat source is bonded onto a $10mm$ square copper heat spreader. In Figure 29 the effect of spreader thickness on total thermal resistance and efficiency of the heat spreader is shown for three different heat transfer coefficients (note that the units are for specific thermal resistance, r_{th}). A thin spreader is not effective, as seen towards the left side of the figure, thermal resistance increases as the thickness of the spreader decreases. In Figure 30 the temperature profile is plotted for a $0.01mm$ thick spreader cooled with a heat transfer coefficient of $10kW/m^2K$. As the thickness of the spreader is increased, so the performance improves until a minimum r_{th} is reached. Here a flatter temperature profile is produced with a lower device peak temperature as shown in Figure 31. Increasing the thickness of the spreader further has a retrograde effect of increasing the thermal resistance.

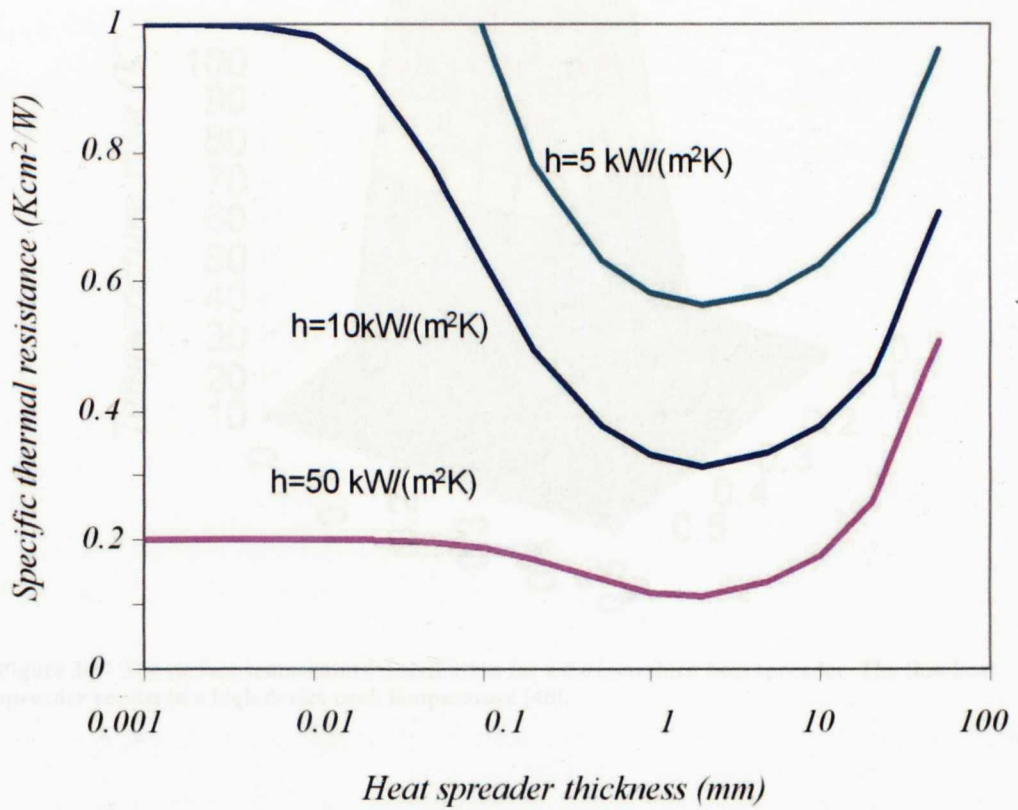


Figure 29 = The effect of increasing the heat transfer coefficient and heat spreader thickness for a 5mm source on a 10mm copper heat spreader [40].

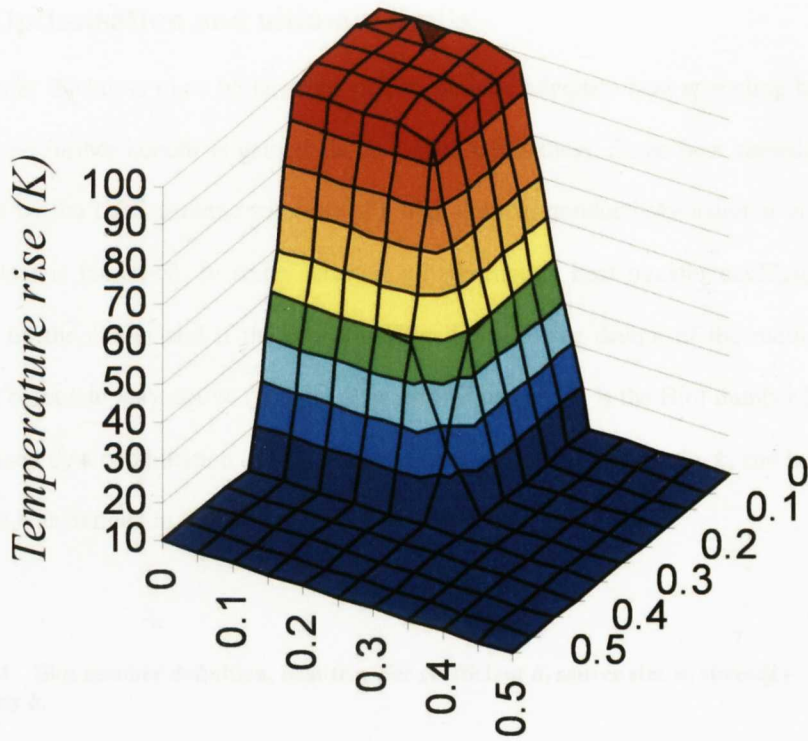


Figure 30 – The surface temperature distribution for a 0.01mm thick heat spreader. The thin heat spreader results in a high device peak temperature [40].

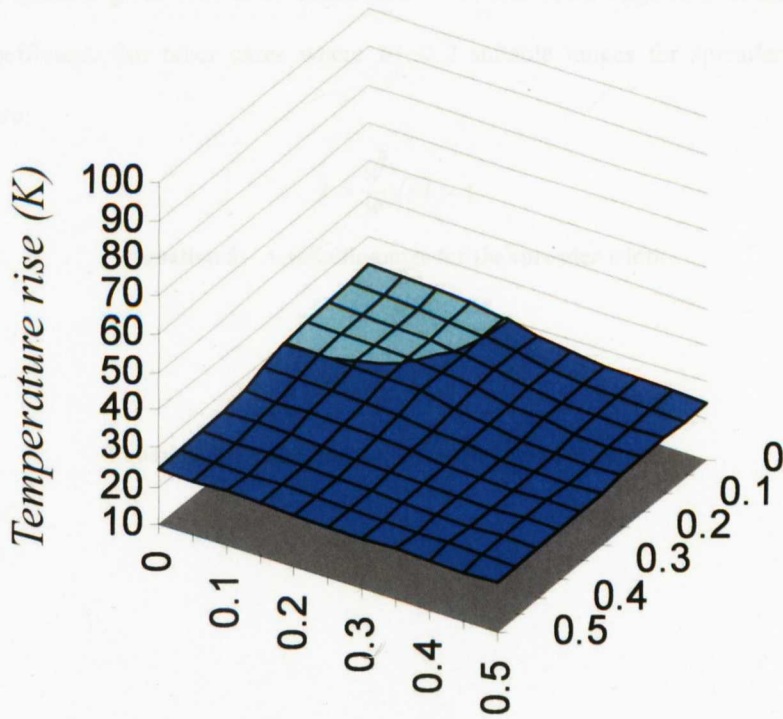


Figure 31 – The temperature distribution for a 2mm thick heat spreader is much flatter overall with a lower peak temperature [40].

2.7.2 Optimisation and ultimate limits

The spreader thickness must be large enough to provide adequate heat spreading but as with the width no further benefit is gained above a certain thickness. Some heat spreading can be performed by the DBC ceramic substrate if a high thermal conductivity material is used or if the thickness is increased. In some cases, if a high enough heat transfer coefficient can be produced by the cooler and if there is some flexibility in the design of the module, a heat spreading baseplate may not be required. The critical parameter is the Biot number (Bi) which is determined by a combination of heat source size w , spreader conductivity k , and heat transfer coefficient h as defined in Equation 4.

$$Bi = \frac{hw}{k}$$

Equation 4 – Biot number definition, heat transfer coefficient h , source size w , spreader conductivity k .

2.7.3 Heat spreader design choices

For a semi-infinite spreader, the specific thermal resistance tends to a constant value of: $r_{ih} = 0.56w/k$. A spreader gives little or no benefit if $Bi > 2$, that is, for large sources or a high heat transfer coefficient. For other cases where $Bi < 2$ suitable ranges for spreader width and thickness are:

$$2 > \frac{W}{w} \sqrt{Bi} > 1$$

Equation 5 – A suitable range for the spreader width

$$0.15 > \frac{d}{w} \sqrt{Bi} > 0.07$$

Equation 6 – A suitable range for the spreader thickness

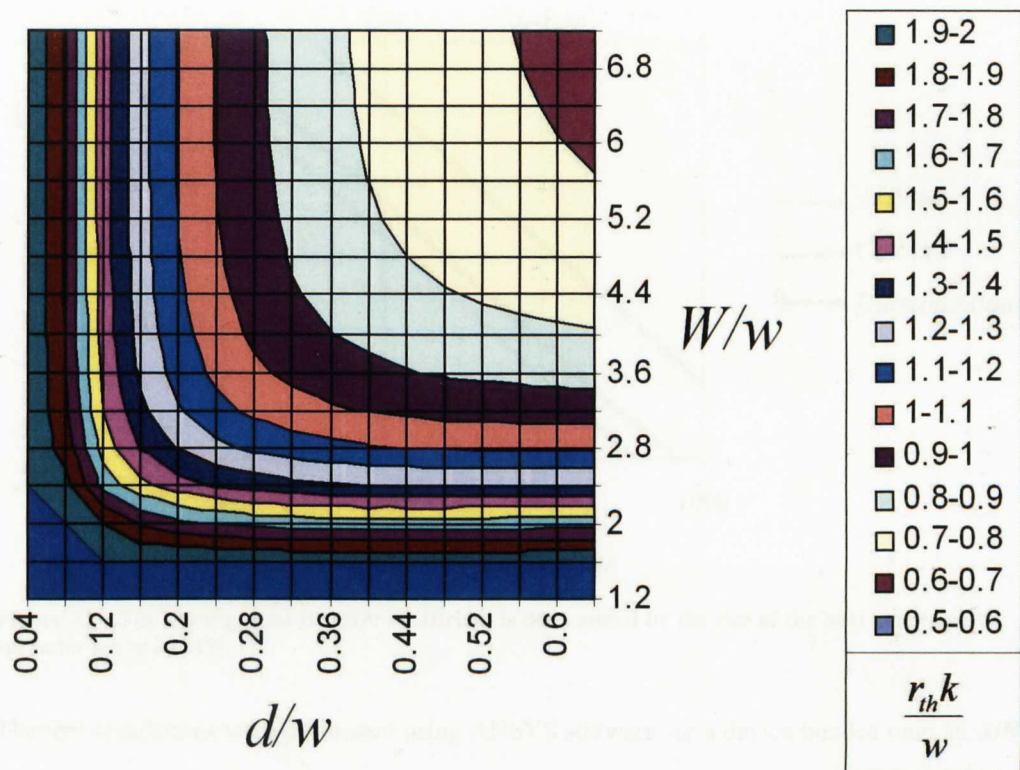


Figure 32 – Normalised specific thermal resistance plotted against normalised spreader width and thickness for a Biot number $Bi = 0.5$ [40].

2.7.4 The impact of varying the heat transfer coefficient on the need for a baseplate heatspreader

In Figure 33 the limiting heat transfer coefficient is plotted for three baseplate materials over a range of heat source sizes. Typical dies benefit from heat spreading for effective heat transfer coefficients below $\sim 50 \text{ kW/m}^2\text{K}$, whereas typical modules benefit from heat spreading for effective heat transfer coefficients below $\sim 5 \text{ kW/m}^2\text{K}$.

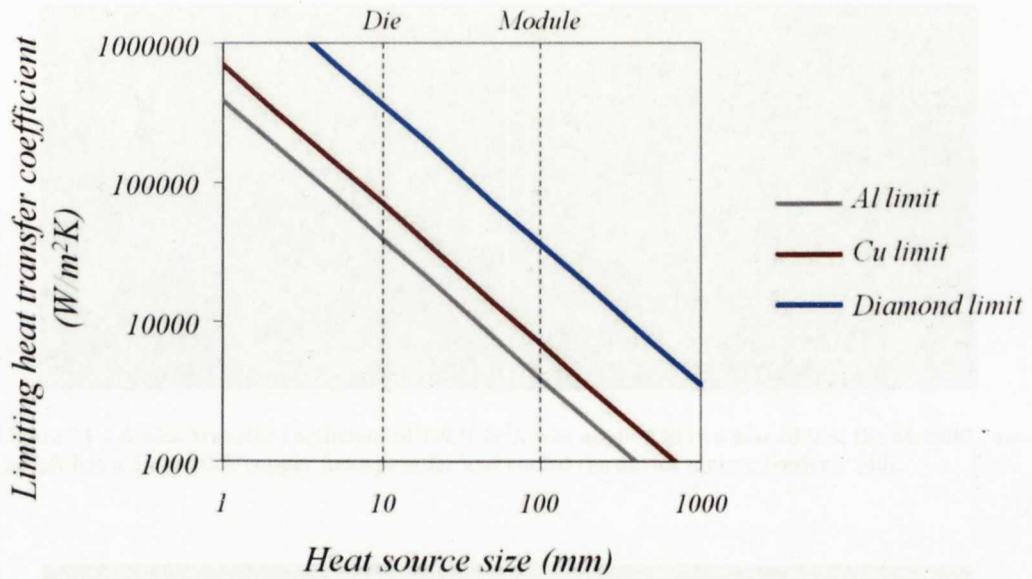


Figure 33 – The limiting heat transfer coefficient is determined by the size of the heat source and spreader material [40].

Thermal simulations were performed using ANSYS software for a device bonded onto an *AlN* substrate with and without a 3mm thick copper heat spreader as part of the assembly. In Figure 34 a heat transfer coefficient of $10\text{kW/m}^2\text{K}$ was applied to both cases and in Figure 35 a heat transfer coefficient of $50\text{kW/m}^2\text{K}$ was applied. The peak device temperature of each of the four simulations is summarised in Table 4. For a heat transfer coefficient of $10\text{kW/m}^2\text{K}$ a heatspreader is required in the assembly as the device temperature increases by over 16°C if the heatspreader is removed. Whereas, when the heat transfer coefficient is increased to $50\text{kW/m}^2\text{K}$ the peak device temperature of the assembly without a heatspreader is lower than the assembly with a heatspreader. The results of the simulations indicate that the need for a heatspreader is related to the heat transfer coefficient generated by the cooler. If a high enough heat transfer coefficient can be attained, then a heat spreading baseplate is no longer required in the power module assembly as it merely adds to the thermal resistance of the package and increases the device temperature. The simulations indicate that directly cooling the underside of the DBC substrate with a suitable high heat transfer cooling method can result in lower device peak temperatures and potentially improve the operational reliability of the power module.

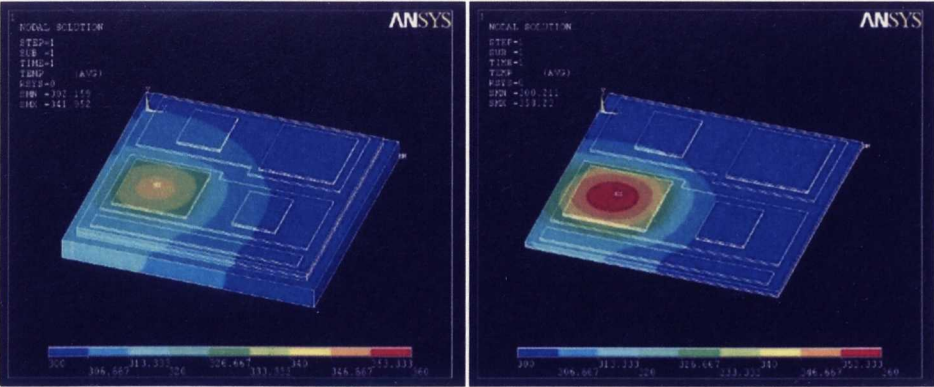


Figure 34 – A heat transfer coefficient of $10\text{ kW/m}^2\text{K}$ was applied to two assemblies, the assembly on the left has a 3 mm thick copper heatspreader and cooled the device more effectively [40].

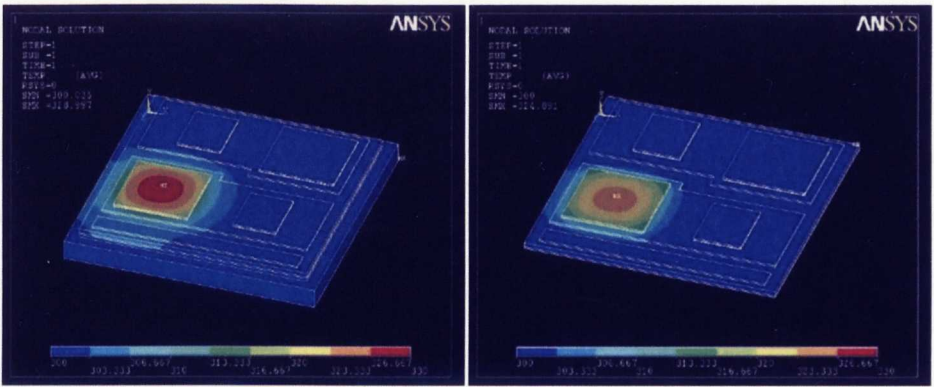


Figure 35 – The heat transfer coefficient was increased $50\text{ kW/m}^2\text{K}$ and the simulations were repeated. At this higher heat transfer coefficient the device in the assembly without the heatspreader was cooled more effectively [40].

Table 4 – Peak temperature rise above the coolant temperature for the four simulations displayed in Figure 34 and Figure 35.

<i>Heat transfer coefficient ($\text{W/m}^2\text{K}$)</i>	<i>Peak temperature rise with baseplate heatspreader ($^{\circ}\text{C}$)</i>	<i>Peak temperature rise without baseplate heatspreader ($^{\circ}\text{C}$)</i>
10,000	41.952	58.230
50,000	28.997	24.091

2.8 Chapter summary

Power module failure is exacerbated by thermal cycling which induces stresses between material layers with different coefficients of thermal expansion. Reliable operation of power modules can be prolonged if the materials within the stack are carefully selected based on properties such as their thermal conductivity, CTE and elasticity. Changes in the way the module is designed and integrated with the cooling system can reduce the number of thermal interfaces between different materials within the stack. In a typical power module assembly, the layer of thermal grease between the power module baseplate and the cooler, and the solder layer between the DBC substrate and the baseplate, account for a large proportion of the total module thermal resistance. If a cooling method producing a high enough heat transfer coefficient is used to cool the power module, a metal heatspreader plate may not be required in the assembly. The number of bonded interfaces which are a cause of failure can therefore be reduced. An integrated design can reduce the overall thermal resistance of the power module allowing the devices to operate more reliably at lower temperatures or in harsher environments.

Chapter 3

3 Liquid Cooling

3.1 Introduction

In this chapter liquid cooling of power modules is investigated in combination with reducing the number of layers in the power module stack. Jet impingement has been identified as a cooling method which can produce very high heat transfer coefficients. It is postulated that a power module can be cooled more efficiently if the number of layers in the thermal stack between the heat source and coolant fluid are reduced and the underside of the substrate tile is cooled directly by jet impingement. Two jet impingement coolers were designed and constructed to directly cool a power module with and without a baseplate as part of the assembly. The power module was also cooled by a traditional coldplate as a comparison. Experimental tests were performed in order to confirm that directly cooling the substrate tile with jet impingement is more efficient than cooling the power module using a traditional coldplate.

3.2 Context of the Problem

In a typical power electronic module the heat generated by the devices is removed by means of a conduction path through the substrate tile followed by the copper baseplate to the final fluid swept surface at which convection occurs. The baseplate is mounted onto a cooler in the form of a coldplate using a thermal conducting paste. In this case there are nine thermal interfaces between the die junction (where heat is generated) and the coolant fluid, as illustrated in Figure 36. In order to adequately cool the electronic devices it is desirable for there to be as little thermal resistance between the hot die and the surface where heat transfer by convection to the cooling fluid occurs. The reduction in thermal resistance between the source and the coolant fluid can be achieved in a number of ways: by using high conductivity materials, by thinning each layer, or by reducing the number of layers in the package.

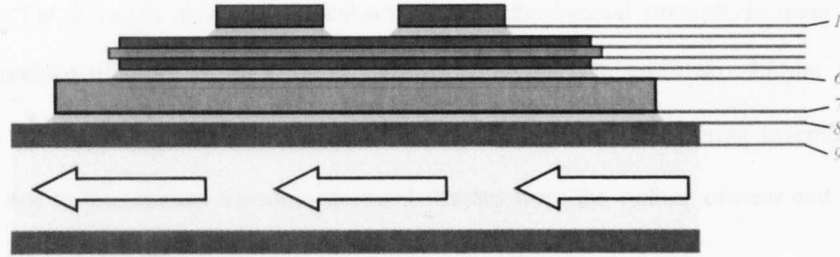


Figure 36 – Cross section of a typical power module structure. The arrows indicate the direction of coolant flow and the lines to the right indicate each of the nine interfaces of the layered structure.

The nine thermal interfaces identified in Figure 36 are:

1. Die / Solder
2. Solder / Copper
3. Copper / Ceramic
4. Ceramic / Copper
5. Copper / Solder
6. Solder / Baseplate
7. Baseplate / Thermal Paste
8. Thermal Paste / Water Plate
9. Water Plate / Water Coolant

3.2.1 Reducing the thermal resistance of the stack

The thermal resistance of the stack between heat source and sink can be reduced by increasing the thermal conductivity and reducing the thickness of each layer of material. In principle each of the material layers and bonded interfaces can be improved. For example, materials such as aluminium nitride (AlN) and alumina (Al_2O_3) have been used to reduce the thermal resistance of the ceramic isolation substrates. Alumina has a thermal conductivity of $30W/mK$ whereas AlN has a thermal conductivity of $210W/mK$, which is high for a ceramic material. Thin alumina substrates of thickness $\sim 300\mu m$ have decreased the substrate tiles' thermal resistance to values similar to those of the solder layers in the base plates. The use of very high thermal conductivity materials such as diamond based substrates is typically not cost effective for most commercial power modules. A certain thickness of dielectric material is necessary so that the substrate can perform its role in electrically isolating the power electronic devices. For example the dielectric breakdown strength of alumina is $16.7kV/mm$, however the limiting factor is not

normally the dielectric ability of the substrate but its mechanical strength. In mass produced power modules it is rare for the ceramic substrate to be much thinner than $\sim 250\mu\text{m}$. Very thin ceramic substrates can crack during the manufacturing process and during assembly of the module due to the residual thermomechanical stresses from the etching process and when the devices are soldered on.

3.2.2 Reducing the number of thermal layers

In a typical power electronic assembly there are nine thermal interfaces between the semiconductor die and the coolant fluid. Referring to Table 2, the solder layer between the substrate tile and the baseplate and the thermal interface between the baseplate and the cooler account for 30% of the total thermal resistance of the module. It is possible to cool the baseplate of the power module by having the coolant liquid in direct contact with it. By cooling the baseplate of the power module directly with liquid (shown schematically in Figure 37) two thermal interfaces can be removed, namely the layer of thermal paste and the wall of the coldplate. If a cooling method generating a sufficiently high heat transfer coefficient is employed a heat spreading baseplate may not be necessary. The number of thermal interfaces can be further reduced by not including the baseplate in the assembly and cooling the substrate tile directly (as shown in Figure 38). Two further layers have been removed, namely the copper baseplate and a $200\mu\text{m}$ layer of solder, reducing the number of layers between silicon die and coolant fluid to five.

3.3 Initial Jet Impingement study

Jet impingement has been known to produce high heat transfer coefficients for cooling power electronic devices [41]. Jet impingement arrays can cool flat surfaces and therefore this cooling method lends itself to direct cooling of power modules. It was decided to conduct experimental tests to evaluate the potential of jet impingement cooling compared to a more traditional cooling method. As this was an initial proof of concept test the impingement array designs were not optimised in any way. The arrays were sized to fit the footprint area of the power module and to provide a way of comparing similar cooling architecture used to cool the power module in configurations with and without the copper baseplate as part of the assembly.

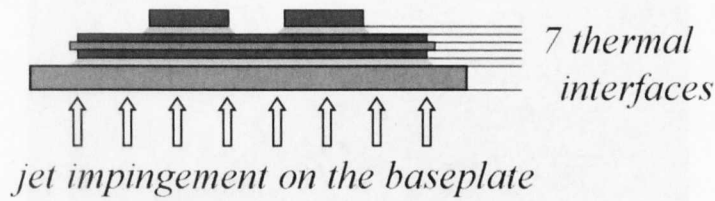


Figure 37 - Direct cooling of the baseplate with water jet impingement resulting in 7 thermal interfaces between the electronic dies and the coolant fluid.

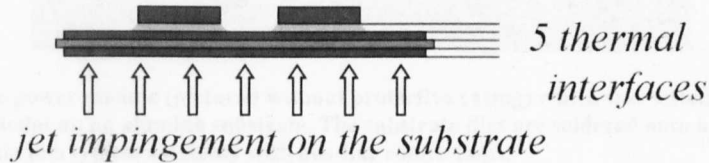


Figure 38 - Direct cooling of the substrate tile and the removal of the baseplate from the package reduces the number of thermal interfaces to 5.

3.3.1 Description of the power module used for the tests

A commercially available half-bridge module was used for the tests (Figure 39). The design, choice of materials and layout of the electronic components had not been optimised for use with direct baseplate cooling or jet impingement cooling. The power module was made up of two direct-bonded-copper (DBC) substrate tiles each measuring $56\text{mm} \times 37\text{mm}$. The tiles consisted of a $380\mu\text{m}$ thick alumina substrate with a $300\mu\text{m}$ layer of copper bonded on both sides. The substrate tiles were soldered onto a 3mm thick copper baseplate with a layer of solder with a thickness of approximately $200\mu\text{m}$. Soldered onto each substrate tile were three diodes measuring $9.5\text{mm} \times 7.5\text{mm}$ and three IGBTs measuring $12\text{mm} \times 12\text{mm}$. There were six IGBTs and six diodes in total. For the purpose of the tests the six IGBTs were used as a heat source dissipating over 1kW of power in total.

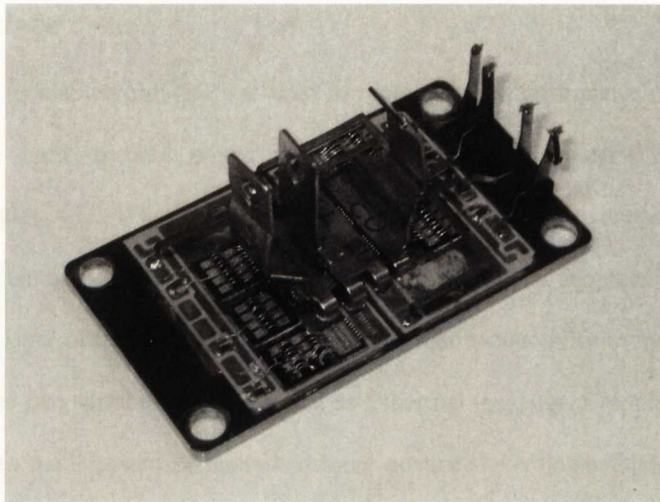


Figure 39 – The power module (pictured without protective casing) which was tested consisting of 6 IGBTs and 6 diodes on an alumina substrate. The substrate tiles are soldered onto a 3mm thick copper baseplate in a typical assembly with bus-bar connections.

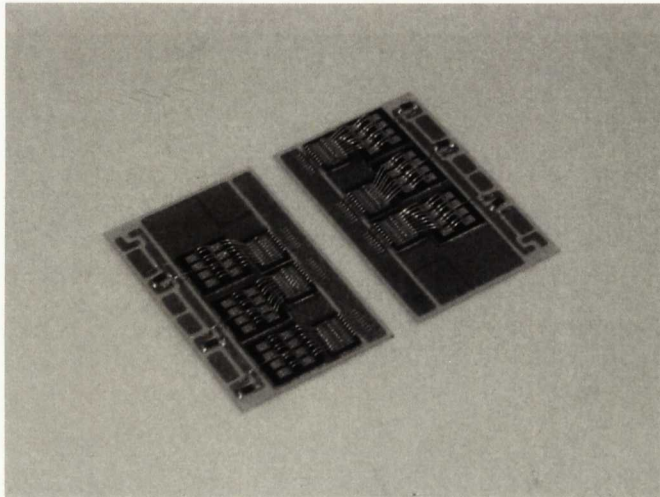


Figure 40 – The substrate tiles alone.

3.4 The coolers

The power module was cooled by three different coolers: A commercially available coldplate was chosen and two jet impingement coolers were designed and built to cool the IGBT half bridge power module in various assemblies. Each cooling method was tested experimentally to determine the performance of each cooler and quantify any advantages gained by direct cooling.

3.4.1 Coldplate

A commercially available coldplate was used to represent the performance of a typical water cooler currently used to cool power electronic modules in industrial and commercial applications (Figure 41). Water simply flows through a serpentine copper pipe which is embedded in an aluminium block. The power module baseplate is mounted directly onto the coldplate with a layer of thermal paste to improve thermal conductivity by preventing pockets of air between the two surfaces which may act as a thermal insulator. Coldplates are relatively straightforward to manufacture compared to more advanced cooling methods. The effective heat transfer coefficient is not very high compared to more advanced cooling methods and is typically around $8,000 \text{ W/m}^2\text{K}$, measured at the interface between the coldplate and the baseplate of the power module.

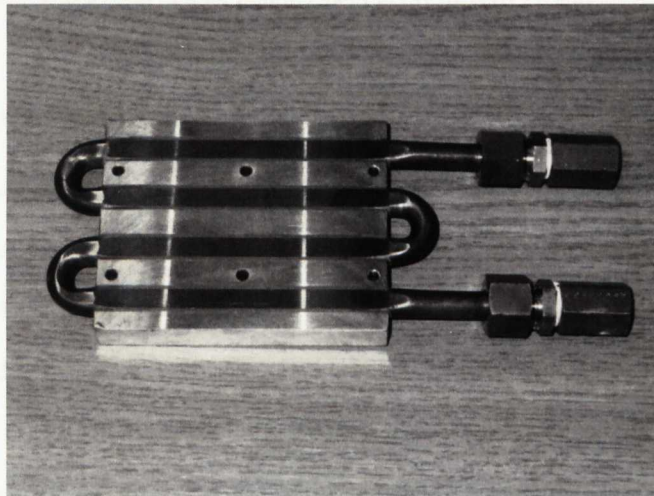


Figure 41 – A picture of the commercially available coldplate consisting of a copper pipe embedded in an aluminium block which was used in the tests.

3.5 Water jet impingement

3.5.1 Description

In a jet impingement cooler, water is sprayed through an array of narrow jets with diameter typically less than 1mm onto the flat impingement surface (shown schematically in Figure 42). An impingement cell incorporates arrays of jets from which the spent fluid exhausts in a single direction. The fluid flows in series through the cells, with the exhaust fluid from one jet array panel cascading into the downstream jet array panels. Excessive crossflow can cause the

downstream jets to be swept away from the adjacent target surface. As a result, the downstream jets become less effective and therefore the overall convective heat transfer coefficient is degraded [42]. Two jet impingement coolers were designed and built with differing arrangements of jets and cells to cool the baseplate of the power module (Figure 43) and the substrate tiles directly (Figure 49).

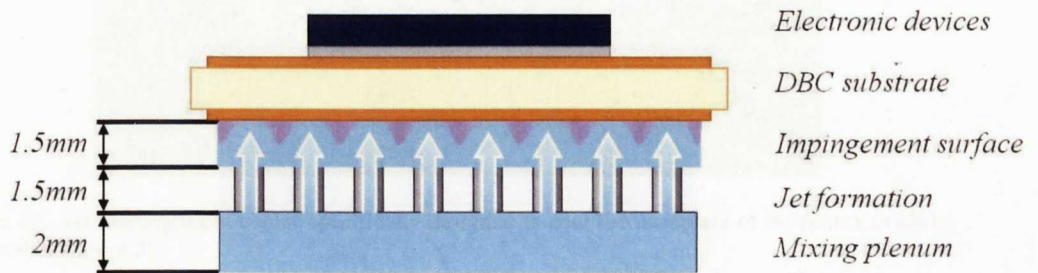


Figure 42 – Simple cross-section of a jet impingement array directly cooling a DBC substrate tile (not to scale).

3.5.2 Design of the direct baseplate cooler

The power module baseplate measured $105\text{mm} \times 60\text{mm}$. The surface area of the baseplate was divided into 12 cells, 11 of which contained a 6×8 array of 1mm diameter holes with centres spaced at 2mm (48 jets per cell, see Figure 43 for detail). The final cell was used as the exit for the fluid and did not contain any impingement jets although some heat transfer will still be provided by the flow of fluid across the surface of the baseplate. The spray plate thickness is 1.5mm and the spray distance is 1.5mm . The plenum chamber above the jets is slightly larger at a height of 2mm to promote mixing of the fluid. Following impingement on the baseplate, the spent coolant water is collected, and via the discharge slot, fed to the next plenum. The impingement process continues in the subsequent jet array panels with the appropriate use of discharge slots to divert (sometimes at right angles to the upstream slot direction) the coolant route (as shown in Figure 46). The cooler, pictured in Figure 43, was manufactured from stainless steel using a laser sintering process which could accommodate the three-dimensional nature of the geometry of the impingement cells. The baseplate of the power module had grooves machined into it as shown in Figure 44. A 1mm diameter bead of silicone sealant was injected into the grooves to aid the sealing of the impingement cells.

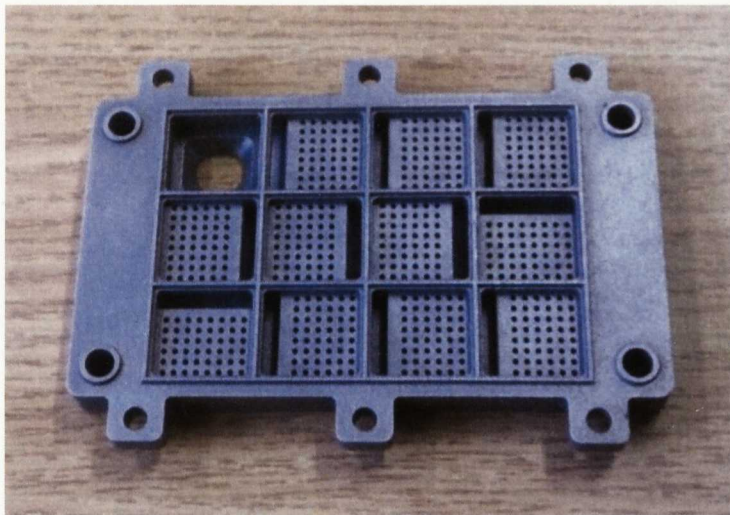


Figure 43 - Jet impingement cooler specifically designed to cool the baseplate of the power module pictured in Figure 39.



Figure 44 – The flat baseplate of the power module had grooves machined into it to aid the sealing of the impingement cells.

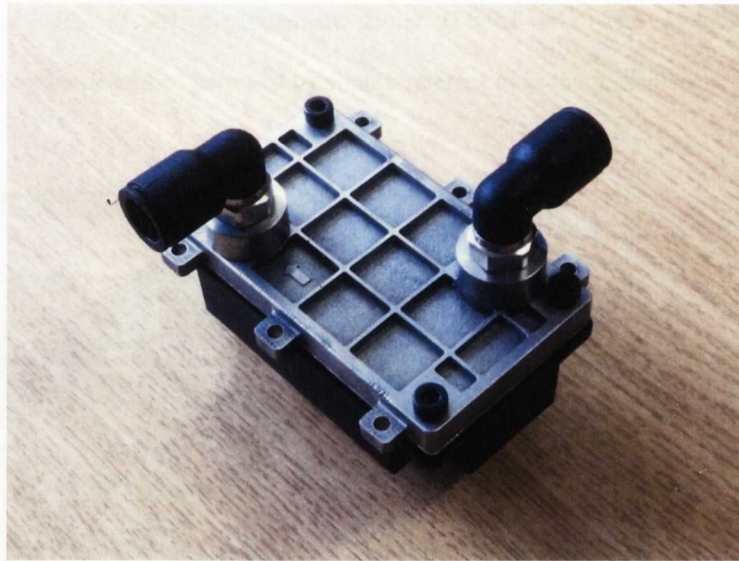


Figure 45 – The assembled direct baseplate impingement cooler showing inlet and outlet water connections.

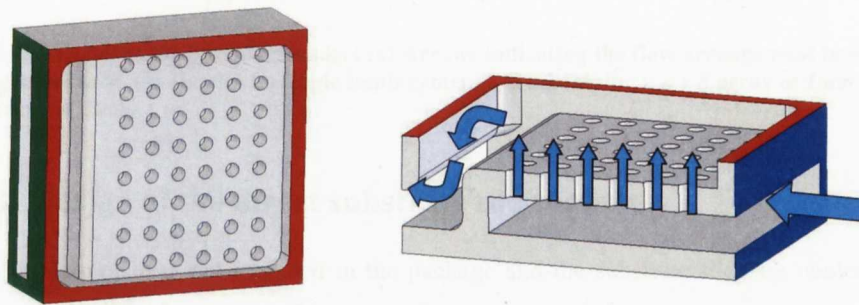


Figure 46 – Detail and cross section of a single jet impingement cell for the direct baseplate cooler containing a 6×8 array of 1mm diameter jets spaced at 2mm . The arrows indicate direction of water flow. The coolant enters the plenum through the slot in the blue plane, the red plane indicates the impingement surface, the coolant exits to the left through the slot in the green plane into the plenum of the adjacent cell.

A 6×8 arrangement of impingement holes was selected in order to reduce the effects of downstream crossflow of spent fluid while properly utilising the impingement area of the IGBT heat spreader plate. The use of small jet arrays e.g. 3×3 would increase the number of panels over the footprint of the IGBT spreader plate. This would increase the area occupied by the solid barrier walls and the discharge slots, thus reducing the effective area for the impingement heat transfer. A larger number of smaller panels would also increase the parasitic pressure drop through the slots that collect spent flow. This impingement cooler design is compatible with most commercial power electronics modules which are built on a flat heat spreader plate. The power module baseplate was machined flat to remove the pre-bowed shape. Grooves were machined into the baseplate and a fine thread of silicone sealant was used to seal

the individual cells of the impingement cooler (Figure 44). The direct baseplate jet impingement cooler described here will be simply referred to as the ‘baseplate cooler’.

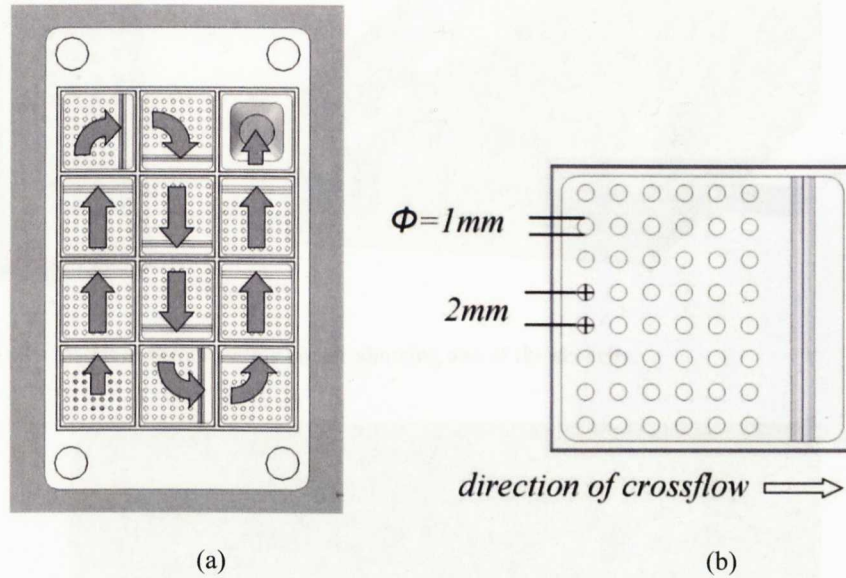


Figure 47 - Detail of the baseplate cooler: (a) Arrows indicating the flow arrangement between impingement cells. (b) Detail of a single impingement cell containing a 6×8 array of 1mm diameter jets spaced at 2mm .

3.5.3 Design of the direct substrate tile cooler

When the baseplate is not included in the package and the substrate tiles are cooled directly there will be less heat spreading as the distance between the IGBT die (where heat is generated) to the coolant fluid (where heat is dissipated) is reduced from 4mm to 1mm . Therefore it was decided to modify the design so that the impingement cells were aligned underneath the IGBTs and diodes on the substrate tile. In contrast to the baseplate cooler, the substrate cooler design has 6 cells with jets in a 4×14 arrangement (4 jets parallel to the flow and 14 tangential giving 56 jets per cell). Assuming an equal distribution of flow rate between each of the jets in the impingement array for the same volume flow rate of water, the average jet velocity in the baseplate cooler is a factor of 1.166 faster than the average jet velocity of the substrate cooler. The direct substrate tile jet impingement cooler described here will be simply referred to as the ‘substrate cooler’.

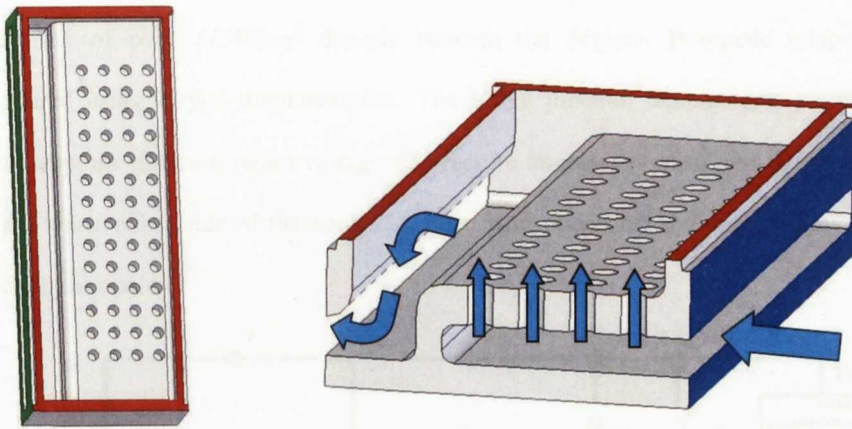


Figure 48 – Detail of the substrate cooler showing one of the six cells.

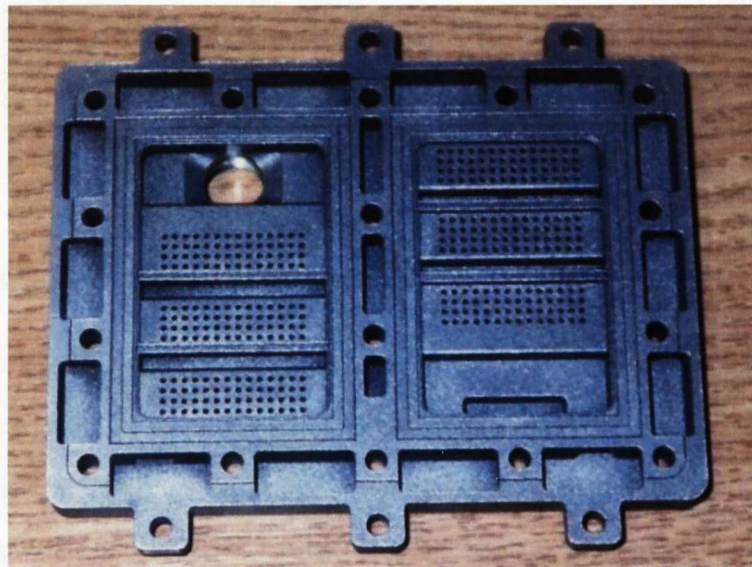


Figure 49 – Direct substrate jet impingement cooler with 6 impingement cells, manufactured from stainless steel using a laser sintering process.

3.6 Experimental Testing

3.6.1 Apparatus

A water test rig was used to characterise the performance of the three coolers. A pump rated with a constant flow rate of 5 litres/minute was used to circulate water from a tank, through the cooler and back, forming a closed loop circuit. A bypass valve was used to manually vary the flow rate through the cooler. The cooling circuit contains a heat exchanger which allows it to maintain the coolant water at a constant temperature. During tests the temperature of the water at the inlet of the cooler was maintained at 40°C. A low voltage, high current power supply

was used to drive the IGBTs. $1,038W$ of heat was dissipated by the IGBTs, corresponding to a heat flux of over $115W/cm^2$ directly beneath the devices. Baseplate temperatures were measured using k-type thermocouples. The IGBT junction temperatures were obtained by measuring the device forward voltage V_f . Pressure transducers measured the absolute pressure of the water either side of the cooler. A flow meter measured the volume flow rate of water through the cooler.

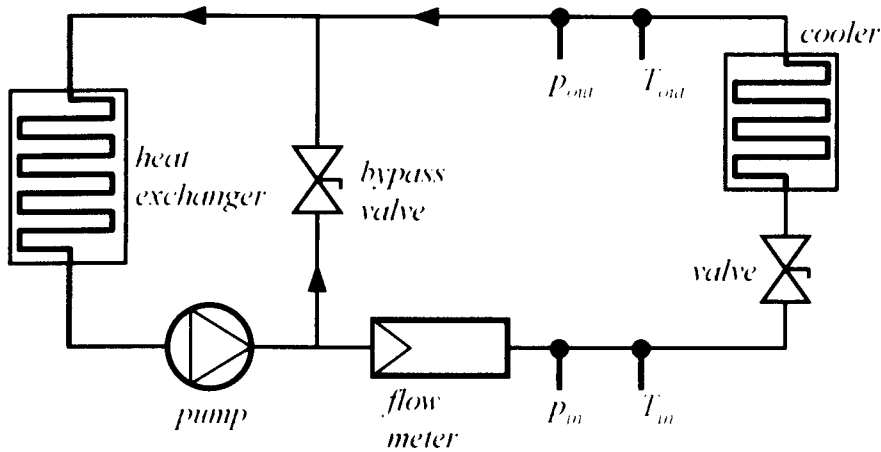


Figure 50 – Schematic diagram of the coolant circuit.

During each test the following data were collected via a data acquisition system: inlet and outlet temperature of the water through the cooler; volume flow rate of the water through the cooler; pressure drop across the cooler; electrical power input to the IGBTs or cartridge heaters; temperature of the IGBT die; temperature at the heat transfer surface.

3.7 Testing Procedure

3.7.1 Pumping power

Pressure drop, ΔP , is an important parameter when comparing different coolers since it determines the power that is required to pump (or to draw) a certain amount of fluid through a cooler. The pumping power required to circulate the coolant is related to the pressure drop across the cooler and the volumetric flow rate of the coolant. This can be summarised by Equation 7.

$$PumpingPower(Watts) = \frac{\Delta P \dot{V}}{\mu}$$

Equation 7

Where ΔP is the pressure drop across the cooler in Pa , \dot{V} is the volumetric flow rate of the liquid coolant in m^3/s and μ is the pump efficiency.

3.7.2 Heat transfer coefficient

Using calorimetry it is possible to calculate the power transferred to the coolant at the heat transfer surface (Equation 8).

$$\dot{Q} = \dot{m}c\Delta T$$

Equation 8

Where \dot{m} is the mass flow rate of the water coolant in kg/s , c is the specific heat capacity of the water and ΔT is the temperature rise of the water in *Kelvin*. The amount of pumping power required to achieve a certain amount of heat transfer is a good measure of presenting how efficiently a cooler operates. Due to heat spreading differences between the substrate, baseplate and coldplate cooled systems it is difficult to accurately infer a surface heat transfer coefficient using only the IGBTs or diodes alone as a heat source. To overcome this difficulty an additional series of tests were performed with electrical cartridge heaters embedded in copper blocks in order to generate a relatively uniform heat flux at the cooled surface. Thermocouples were placed in the copper blocks to measure the temperature *1mm* below the water cooled heat transfer surface. The effective heat transfer coefficient generated by each cooler was calculated using Equation 9.

$$h = Q / A\Delta T$$

Equation 9

h – Heat transfer coefficient

Q - Heat transfer in Watts

A - The heat transfer surface area.

ΔT - The temperature difference between the surface of the baseplate and the mean coolant temperature.

In each of the three tests, four cartridge heaters dissipated a total of *1,038 Watts* of heat (corresponding to the amount of heat dissipated by the IGBTs in the tests involving the power modules). The heat transferred to the coolant water was calculated by calorimetry using

Equation 8. The heat transfer surface area for each cooler is known and therefore the heat flux can be calculated. The average temperature of the heat transfer surface and the average temperature of the coolant are known, therefore an effective surface heat transfer coefficient can be calculated over a range of flow rates for each cooler.

3.7.3 Thermal Impedance Characteristic

In a second series of tests, the performance of the coolers was evaluated by passing current through the six IGBT devices in the power module thus creating a heat source. *1,038Watts* of heat was dissipated by the six IGBTs. The heating current was alternately switched on and off to allow measurement of the thermal step response. During the cooling periods, the temperature of the IGBT was determined by passing a small current of *50mA* through the IGBT and measuring the forward voltage V_f across it. There is a linear relationship between V_f and temperature allowing the instantaneous device temperature to be determined. The thermal impedance of the system is determined by the package thermal resistance and the rate at which heat is transferred to the cooler. This governs the effect of thermal transients, high heat loads and power cycles on the system. By analysing the cooling curves it is possible to determine the thermal impedance characteristic of the package. This can be used to predict how the package and cooler react to cyclic inputs of heat.

3.8 Experimental Results

3.8.1 Pressure drop and flow rate

The thermal performance of each of the three coolers was tested up to a flow rate of *4 litres/minute*. The pressure drop across a cooler at a given flow rate indicates how much energy is required to pump the coolant around the fluid circuit (Table 5). At a flow rate of *4 litres/minute* the coldplate cooler produced the lowest pressure drop of *0.26 bar* (Figure 51). At a flow rate of *4 litres/minute* the baseplate cooler produced a pressure drop of *1.49 bar*, which is almost six times higher than the pressure drop produced by the coldplate. The high pressure drop produced by the baseplate cooler is due to the large number of impingement cells in series. The baseplate cooler has 11 impingement cells in series compared to the 6 wider cells of the substrate cooler.

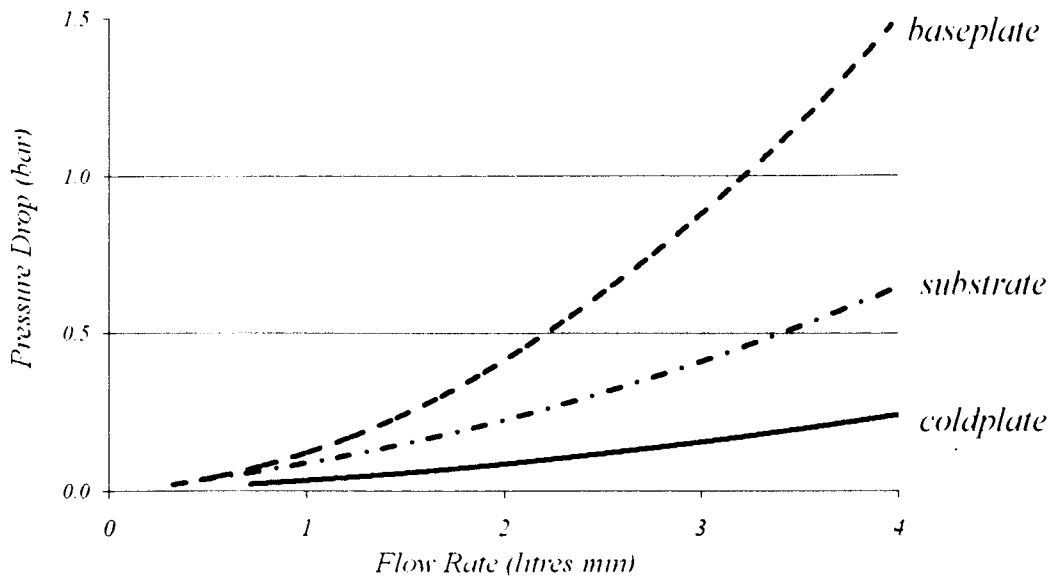


Figure 51 – Pressure drop versus flow rate for the three coolers tested.

Table 5 – Pressure drop and pumping power for the three coolers at a water flow rate of 4 litres/minute.

<i>Cooler</i>	<i>Pressure drop (bar)</i>	<i>Pumping power (Watts)</i>
<i>Coldplate</i>	<i>0.26</i>	<i>1.75</i>
<i>Baseplate</i>	<i>1.49</i>	<i>9.93</i>
<i>Substrate</i>	<i>0.65</i>	<i>4.33</i>

3.8.2 Heat Transfer Coefficient

The heat transfer coefficient generated by each of the three coolers over a range of flow rates was determined using Equation 9 and is plotted in Figure 52. The coldplate cooler offers the lowest cooling performance of the three coolers tested, producing a heat transfer coefficient of $8,480 \text{ W/m}^2\text{K}$ at a water flow rate of 4 litres/minute, requiring 1.75 W of pumping power (Table 6). The substrate and baseplate jet impingement coolers generated a heat transfer coefficient of $14,950 \text{ W/m}^2\text{K}$ and $16,450 \text{ W/m}^2\text{K}$ respectively for 1.75W of pumping power. The cooling performance of the two jet impingement coolers is therefore much higher compared to the coldplate. The jet impingement baseplate cooler generated an effective heat transfer coefficient of $22,440 \text{ W/m}^2\text{K}$ at a flow rate of 4 litres/minute requiring 9.9W of pumping power.

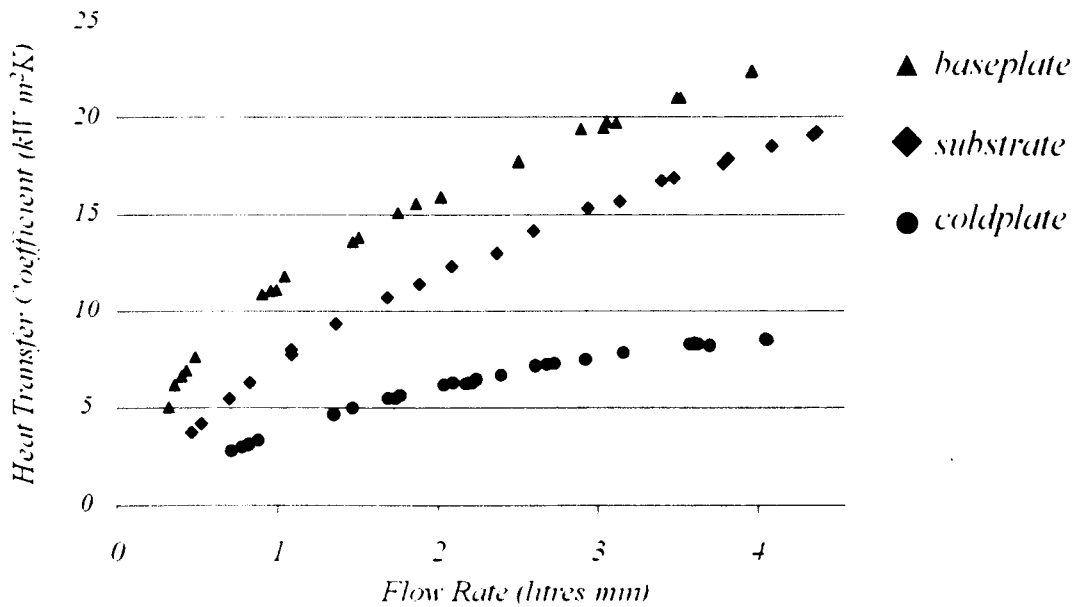


Figure 52 – Heat transfer coefficient versus flow rate for the three coolers.

Table 6 – Heat transfer coefficient and pumping power required at a flow rate of 4 litres/minute

<i>Cooler</i>	<i>Heat transfer coefficient (W/m²K)</i>	<i>Pumping power (Watts)</i>
<i>Coldplate</i>	8480	1.75
<i>Baseplate</i>	22440	9.93
<i>Substrate</i>	18289	4.33

Over the range of flow rates tested the baseplate cooler produced a higher heat transfer coefficient than the substrate cooler. However, the baseplate cooler also produces a high pressure drop across it requiring more energy to drive the coolant through it compared to the substrate cooler and the coldplate. In Figure 53 pumping power is plotted on a logarithmic scale and it can be seen that there is a diminishing rate of return regarding the increase in heat transfer coefficient with pumping power. This is related to the pressure drop characteristic of the coolers in which the pressure drop across the cooler is proportional to the square of the flow rate; In order to gain a small increase in heat transfer coefficient a large increase in power is required to pump the coolant through the cooler at a higher flow rate.

When operating at a low pumping power (up to 0.5 Watts) the baseplate cooler generates a higher heat transfer coefficient compared to the substrate cooler. But at higher flow rates the heat transfer performance of the substrate cooler almost matches the baseplate cooler. The data presented in Figure 53 indicates that the heat transfer performance of both coolers could be equal at a higher coolant flow rate.

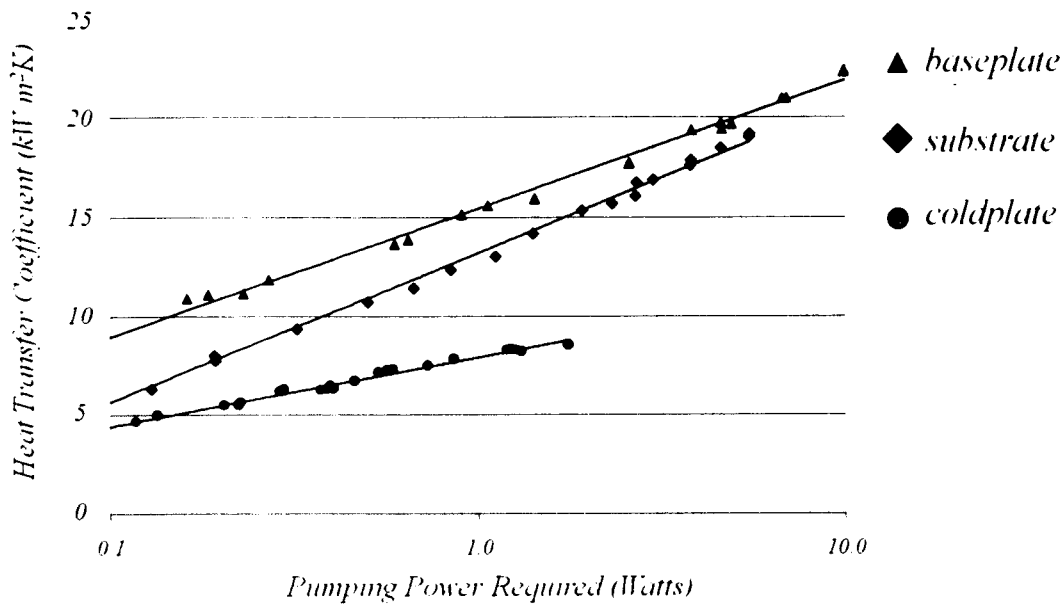


Figure 53 - Heat transfer coefficient against pumping power for the three coolers over a range of flow rates up to 4 litres/minute.

3.8.3 Thermal Impedance

For the thermal impedance tests the power module was cooled in various configurations. In Figure 54 the cooling curves for the three coolers are presented at a water flow rate of 4 litres/minute, where the IGBTs are dissipating $1,038\text{ W}$ of power and then switched off at $t=0$. For the coldplate cooler the steady state temperature difference between the IGBT die and the coolant water is 47.8°C . For the direct baseplate cooler this is reduced to 33.7°C and reduced further to 30.8°C for the direct substrate cooler. This is an interesting result because at a coolant flow rate of 4 litres/minute the baseplate cooler produces a higher heat transfer coefficient than the substrate cooler, yet the IGBTs operate at a lower temperature when the substrate tile is cooled directly by jet impingement. This result supports the hypothesis that a heat spreader is not necessary if a sufficiently high heat transfer coefficient is used to cool the power module.

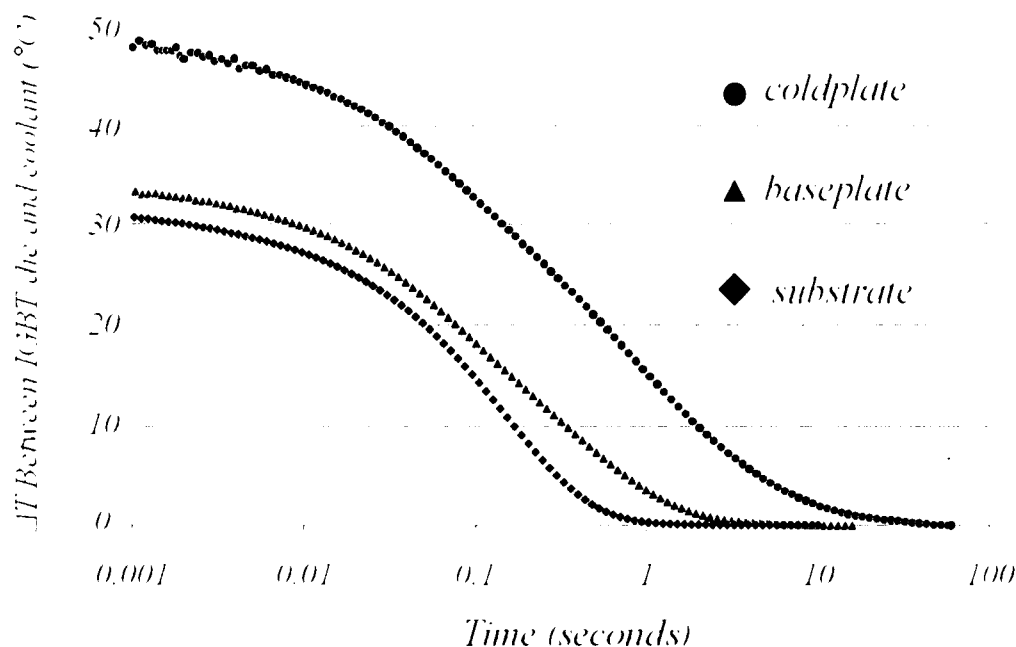


Figure 54 - Temperature difference between IGBT and the average coolant temperature as a function of time. Cooling curves for the three coolers operating at a flow rate of 4 litres/minute.

The cooling curves for the three coolers are of a similar shape and they do not cross or overlap each other. The data presented in Figure 54 indicates that under the same operating conditions the temperature of the IGBT devices will always be highest when cooled by the coldplate compared to when the baseplate is cooled directly, and the temperature of the devices will always be lowest when the substrate tile is cooled directly by jet impingement.

Table 7 – IGBT temperature rise above coolant temperature for the three coolers over a range of flow rates.

	<i>Water flow rate</i>			
<i>Cooler</i>	<i>1 litre/min</i>	<i>2 litres/min</i>	<i>3 litres/min</i>	<i>4 litres/min</i>
<i>coldplate</i>	58.46	51.89	49.26	47.83
<i>baseplate</i>	46.03	38.39	35.42	33.69
<i>substrate</i>	48.36	37.5	33.48	30.76

3.8.4 Power Cycling

The cooling curves are of interest in the context of power cycling because Figure 54 indicates that if there is an adequate cooling method present providing a high heat transfer coefficient then there is no additional benefit gained by including a heat spreader plate between the

substrate tile and the cooler. It is shown that the heat spreader plate reduces performance of the system by increasing the package thermal resistance. A lower package thermal resistance allows the electronic devices to operate at a lower peak temperature.

From the data presented in Figure 54, if the components are power cycled at a frequency higher than say 1kHz , the amplitude of the variation of temperature with time (dT/dt) for all three coolers would be similar, although the devices cooled by the coldplate will be operating at a significantly higher temperature compared to the baseplate and substrate cooled devices. This is because the structure of the module from the devices to the bottom of the DBC substrate is identical for all three cases. But when the devices are switched at a frequency of say 20Hz the IGBTs cooled by the coldplate would experience temperature cycles of larger amplitude compared to the direct and substrate cooled IGBTs. For slower cycles of the order of tens of seconds, when the devices are switched off the IGBTs which are cooled by the coldplate cool by 48°C and the direct and substrate cooled IGBTs cool by 34°C and 31°C respectively which is significantly less.

3.8.5 Reducing the number of thermal interfaces

The die temperature cooling curves offer an interesting insight into the potential advantages of removing thermal layers and interfaces from the IGBT packaging and electronic assembly. In a conventional power module the DBC substrate tiles are soldered onto a metal baseplate heat spreader. The heat spreader plate is typically the single heaviest component in a power electronic package. A baseplate is designed to reduce hot spots generated underneath the electronic components and to provide a stable mechanical base for the power module so that it can be clamped onto a cooler. As the device is thermally cycled the difference in the coefficient of thermal expansion between the baseplate and the substrate tile results in mechanical stresses and strains which will lead to fatigue failure of the bonding solder layer. When cooling the ceramic substrate tile directly, due to the nature of the sealing of the coolant circuit, the DBC tile is mounted in a more forgiving package where it is not rigidly clamped. This allows it to move relative to the cooler (with temperature cycles) without producing the high mechanical stresses introduced when the tiles are soldered onto a heat spreader plate.

3.9 Summary of initial jet impingement tests

In this chapter the performance of three coolers was characterised experimentally. The tests demonstrated the improvement found by removing thermal layers in the package and cooling the baseplate and substrate tile of a power module directly with liquid jet impingement. A commercially available coldplate was chosen to represent the performance of a typical water cooled system used in industry. Two liquid jet impingement coolers were designed and built to cool a power module comprising two substrate tiles each populated with three IGBTs and three diodes in a half bridge arrangement. The first jet impingement cooler was designed to cool the baseplate of the power module while the second jet impingement cooler was designed to cool the underside of the DBC substrate tile directly. When the substrate tile was cooled directly the electronic devices operated with a lower peak temperature and exhibited a smaller amplitude of thermal cycling compared to the baseplate cooled and coldplate cooled methods.

Measurements of transient thermal impedance (cooling curves in Figure 54) revealed that the impingement coolers offered lower thermal resistance at all times during the cooling transient with the direct substrate cooler giving the best performance. Thus the added thermal mass of the baseplate gives no advantage in absorbing thermal transients and in fact merely adds to the thermal resistance. As a consequence, the impingement coolers will produce lower amplitude thermal cycling for any load (power) cycling regime, giving potential improvements in module reliability. Further improvements in reliability can be expected from the removal of interfaces between the baseplate and cooler and the substrate tile and baseplate (in the case of the direct substrate cooler).

Chapter 4

4 Direct Substrate Cooling with Jet Impingement

4.1 Introduction

In the previous chapter a power module was cooled with arrays of water jets impinging directly onto the underside of the DBC substrate tile onto which the electronic devices were soldered. Direct substrate cooling with jet impingement was found to be more effective at cooling the power module compared to a traditional serpentine coldplate and direct baseplate cooling with jet impingement. This chapter aims to build on the experimental results from the previous chapter and focuses on direct substrate cooling with jet impingement. The parameters affecting the performance of jet arrays are covered in detail. Rather than cooling the entire surface area of the substrate tile it is postulated that more efficient cooling of the electronic devices can be achieved by targeting the hot spot beneath each device with a carefully designed array of impinging jets. An apparatus allowing various jet array geometries to be tested was constructed and 12 different jet array designs were tested. The performance of each jet array was characterised in order to determine which array geometry produced the most efficient cooling.

4.2 Direct substrate cooling

In direct substrate cooling of power electronics the coolant fluid is in direct contact with the underside of the DBC substrate tile. There are a number of advantages found by cooling the underside of the substrate tile directly: The removal of the baseplate in the package results in a shorter thermal path and therefore a lower thermal resistance between the power electronic components and the coolant fluid. The overall power module package can therefore be smaller in size and have a reduced weight. Having fewer thermal layers in the package reduces the number of interfaces between materials with different coefficients of thermal expansion (CTE). The reduced mechanical stresses induced by differences in CTE improves the reliability of the package especially by the removal of the solder layer between the substrate tile and the baseplate heatspreader.

4.3 Reducing redundancy in the cooling system

4.3.1 Small heat sources and heat spreading

In the context of cooling, power electronic devices soldered onto substrate tiles can be described as small heat sources. The temperature profile at the cooled surface of the substrate tile or baseplate is not uniform over the area; there are hot spots. Traditionally power module cooling systems have been designed to produce relatively uniform heat transfer coefficients over the entire area of the cooled surface onto which the module is mounted. The two jet impingement coolers tested in the previous chapter cooled almost the entire surface area of the underside of the power module. However the heat profile produced by the power module is not uniform over the surface area. The electronics which were being cooled (3 IGBTs and 3 diodes per substrate tile) only accounted for an area of 646mm^2 which is 31% of the total surface area of the substrate tile.

When the entire surface area of the substrate tile is cooled directly by jet impingement a significant proportion of the jets are redundant and have a minimal contribution to the cooling of the devices. There is unnecessary pumping power being used to drive the coolant fluid through the impinging jets in these redundant areas, whereas hot spots located directly underneath the electronic devices do not receive any additional cooling. It is possible to improve the efficiency of the cooling system for a non-uniform heat source. Gains in efficiency can be found by reducing the redundancy in the cooling system and by improving the efficiency of the jet impingement arrays themselves. A more efficient solution might be to target the hotspots with a higher rate of cooling. This will require a more integrated design as the cooling will need to target the areas where the highest heat fluxes are found.

4.3.2 Improving the efficiency of the impingement arrays

The tests performed in the previous chapter indicated that liquid jet impingement coolers can produce high heat transfer coefficients efficiently for a given amount of pumping power. The initial study produced promising results for jet impingement cooling and for the concept of the direct cooling of the underside of a substrate tile without having a metal heatspreader plate in the package. The jet impingement arrays in the initial tests were not optimized in any way and

there is thus scope to improve the performance of the impingement geometry for direct substrate cooling. It was decided to explore this idea further with the aim being to improve the efficiency of jet impingement arrays specifically designed for direct substrate cooled power modules.

4.4 Custom substrate tile

The design layout of the half bridge modules tested in the first set of liquid cooling experiments had not been optimised for use with jet impingement cooling. The layout of the devices can be modified in order to improve the thermal performance of the power module. In order to progress with this idea further it was proposed to design a new substrate tile rather than use ones which were available commercially.

4.4.1 Thickness and robustness of the ceramic substrate tile

The substrate tiles tested in the previous chapter consisted of a $300\mu\text{m}$ layer of alumina double side bonded with copper and were not intended for use with direct cooling as they were designed to be soldered onto a metal baseplate. The initial impingement tests were performed on a test rig with a pressurised coolant circuit reaching a pressure of up to 3bar above atmospheric pressure. When the coolant system was pressurised some of the thin alumina tiles cracked due to the pressure difference across them and were permanently deformed. A picture of the direct substrate cooled module is shown in Figure 55. Once a tile has deformed and lifted off from the cooler the impingement arrays do not perform properly as the fluid leaks across into adjacent cooling cells without passing through the impingement geometry properly. The plastic mounting which held the tiles in place was thus redesigned (as shown in Figure 56) incorporating cross pieces which pressed the substrate tile down onto the impingement arrays to prevent it from flexing upwards due to the water pressure. The custom designed substrate tile should be thicker than the thin $300\mu\text{m}$ alumina tiles in order to be more robust and have more mechanical strength. Due to the increased thickness a ceramic material with higher thermal conductivity than alumina should be used in order to keep the thermal resistance between heat source and heat sink as low as possible.

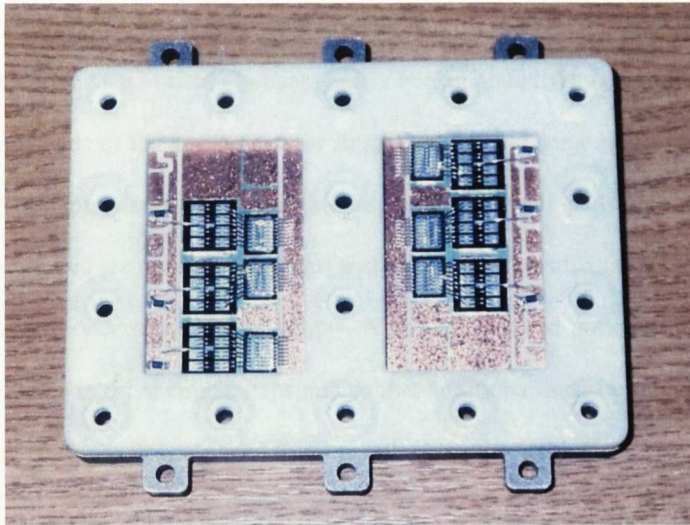


Figure 55 – The IGBTs and diodes are clearly visible in the direct substrate cooled module.

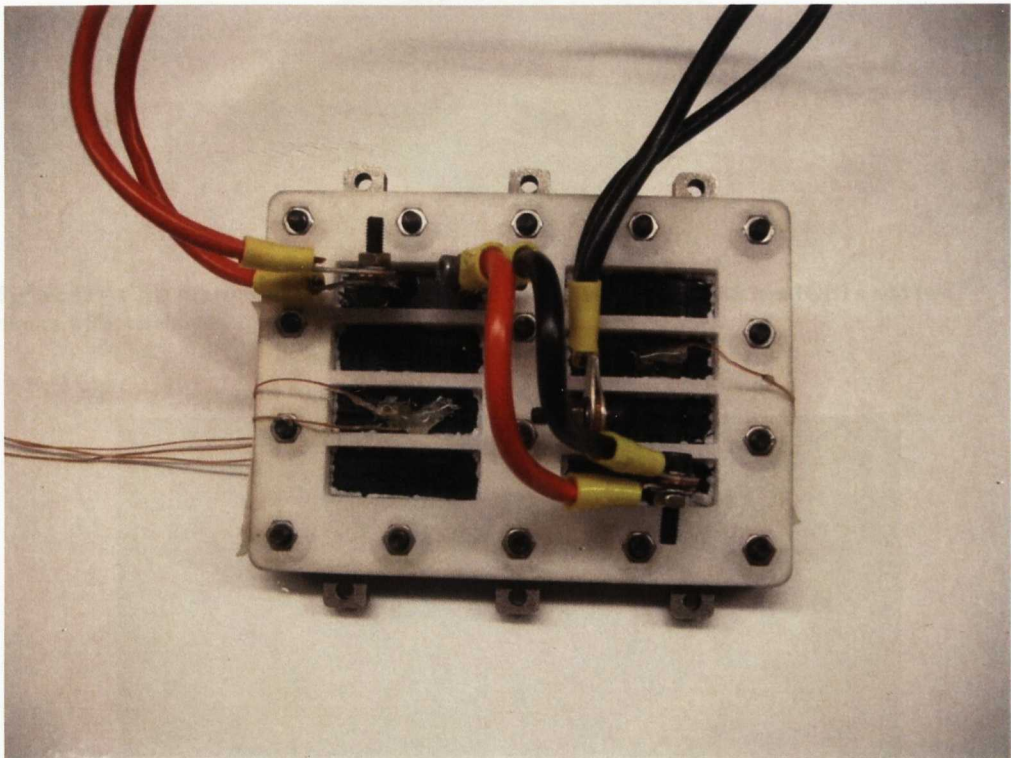


Figure 56 – The plastic cover was redesigned with additional support pieces to prevent the substrate tile from flexing due to the water pressure.

4.4.2 Design of the substrate tile

The final design layout was intended for two IGBTs and two diodes arranged as a half-bridge on a single tile in order to decrease the size of the inductance loop for high-frequency operation and to aid cooling (CAD drawing shown in Figure 57). Two IGBTs measuring $13\text{mm} \times 13\text{mm}$ and two diodes measuring $9.5\text{mm} \times 7.5\text{mm}$ can be soldered onto the tile. The tile has

overall dimensions of $40\text{mm} \times 40\text{mm}$ and is double side bonded with copper of thickness $300\mu\text{m}$ using an active metal brazing process and is Nickel plated. The ceramic material chosen was Aluminium Nitride of thickness 1mm for strength and to act somewhat as a heatspreader as there will be no heatspreader plate used in this assembly. The main pads onto which the IGBTs and diodes are soldered are spaced 2mm apart and have corners with a radius of 1mm to reduce the chance of arcing occurring at sharp points. Along the top and bottom edges smaller pads were added for the gate drive connections and so that additional measurements could be taken from these pads. The *AlN* substrate tiles were manufactured by Denka.

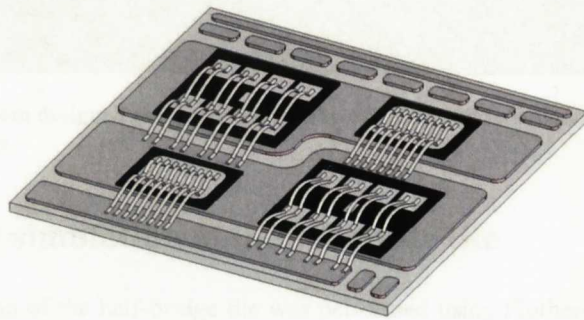


Figure 57 – CAD drawing of the custom designed *AlN* tile populated with two IGBTs and two diodes with wirebonds.

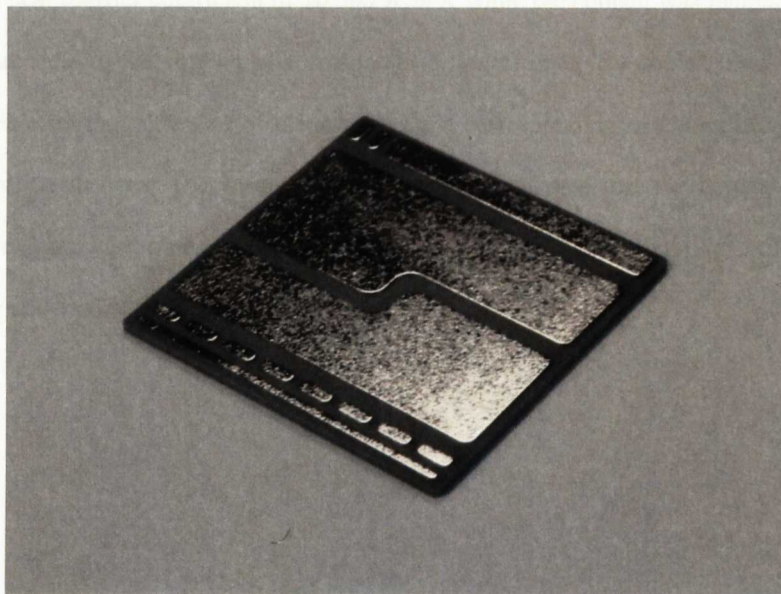


Figure 58 – The custom designed *AlN* substrate tile as received from the manufacturer (Denka). The direct bonded copper is plated with nickel resulting in a silver appearance.

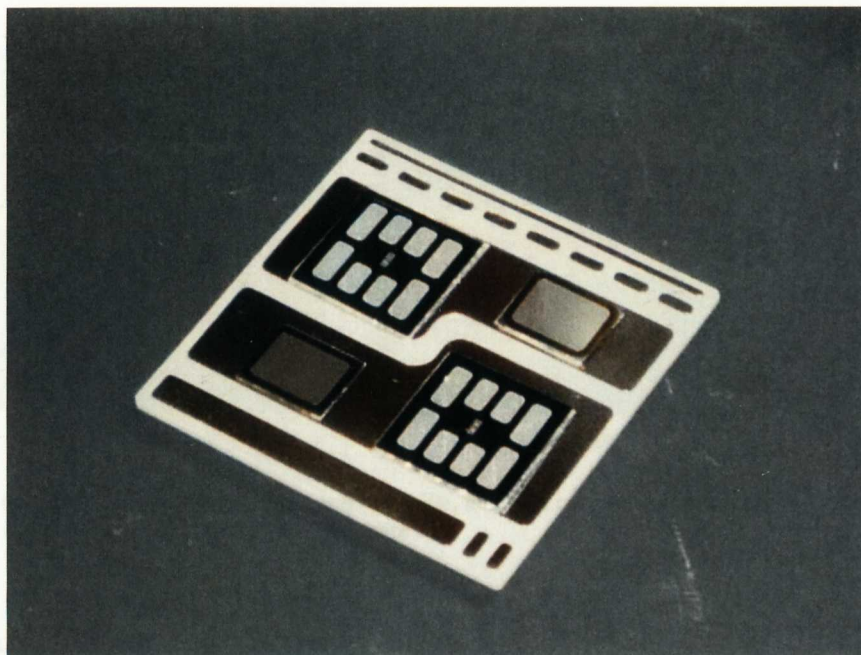


Figure 59 – The custom designed substrate tile with two IGBTs and two diodes soldered on, forming a half-bridge.

4.5 Thermal simulation of the substrate tile

A thermal simulation of the half-bridge tile was performed using Flotherm software using the material properties listed in Table 8. In the model $400W$ of heat was dissipated by the two *Si* diodes ($200W$ each) while the underside of the substrate tile was cooled by an evenly distributed heat transfer coefficient of $10,000\text{ W/m}^2K$ while the coolant was maintained at $0^\circ C$. This is equivalent to the cooling performance of a typical coldplate cooler. Two hotspots are clearly visible on the underside of the substrate tile corresponding to the location of the two heat dissipating devices. The results of the simulation indicate that the hottest 50% of the temperature range on the underside of the substrate tile accounts for only 22% of the surface area on the underside of the tile.

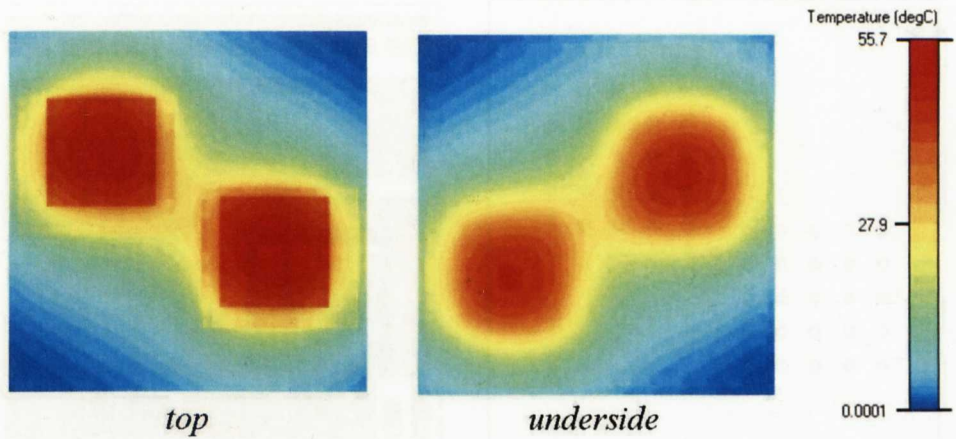


Figure 60 - Thermal simulation of the substrate tile, hotspots corresponding to the two devices are clearly visible on the underside of the substrate tile.

Table 8 – Material properties for the thermal simulation.

<i>Description</i>	<i>Material</i>	<i>Thermal Conductivity (W/mK)</i>	<i>Thickness (mm)</i>
<i>Silicon Device</i>	<i>Si</i>	<i>105</i>	<i>0.33</i>
<i>Solder</i>	<i>Sn-3.5Ag</i>	<i>33</i>	<i>0.1</i>
<i>DBC Copper</i>	<i>Cu</i>	<i>400</i>	<i>0.3</i>
<i>Aluminium Nitride</i>	<i>AlN</i>	<i>230</i>	<i>1</i>
<i>DBC Copper</i>	<i>Cu</i>	<i>400</i>	<i>0.3</i>

4.5.1 Reducing redundancy

Rather than cooling the entire surface area of the underside of the substrate tile with an evenly distributed heat transfer coefficient it may be more efficient to provide increased cooling at the hotspots located underneath the IGBTs. It is possible to design jet impingement arrays which will cool the hotspots directly with the remaining surface area of the substrate tile being cooled by the spent fluid as it leaves the cooler (Figure 61). In order to design more efficient cooler geometries for the direct cooling of power electronics it is important to understand more about jet impingement. The aim being to design efficient jet impingement array geometries to cool individual power electronic components with a surface area of approximately 1cm^2 soldered onto a DBC ceramic substrate tile.

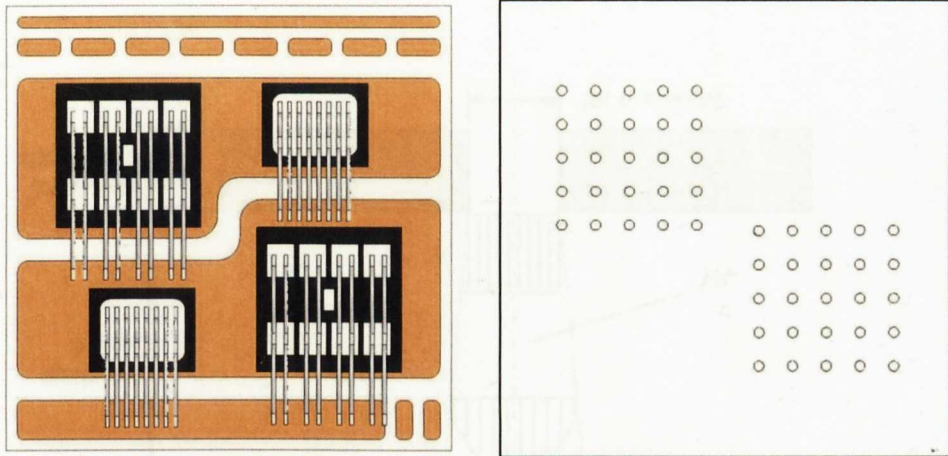


Figure 61 – CAD drawings showing an example of a sprayplate (right) featuring two 5 x 5 jet impingement arrays intended to cool the IGBTs on the populated substrate tile (left).

4.6 Jet impingement cooling

In jet impingement cooling the fluid passes through an array of holes in the sprayplate and impinges perpendicularly onto the cooled surface (Figure 62). As the fluid passes through the holes in the sprayplate its velocity increases and it effectively becomes a jet. A high heat transfer coefficient can be attained at the cooled surface due to the small thermal boundary near to where the jet impinges.

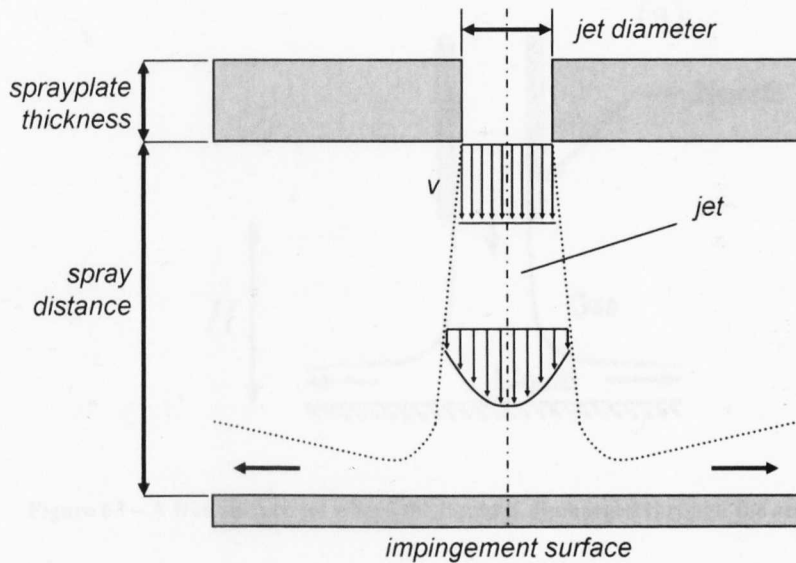


Figure 62 – A schematic diagram of an impinging jet indicating important variable parameters, boundary layers and velocities.

4.6.1 Types of jet impingement

Impinging jets can be classified as either free-surface, submerged or confined-submerged. In free-surface jets the liquid is discharged from the jet nozzle through the ambient gas before impinging upon the target surface [43] (Figure 63). Submerged jets exude through the same fluid in the same state, that is liquid into liquid or gas into gas and can be described as being confined or unconfined. In the unconfined case, the nozzle plate is far enough away from the target surface to have little or no influence on the flow structure of the jets (Figure 64). However, in the confined case (Figure 65), the nozzle plate is close enough to the target surface to influence the flow structure and create a recirculation zone [44]. Pann and Webb [45] observed a transition at $H/d = 2$ from the jets being confined and submerged to free surface as H/d was increased to 5.

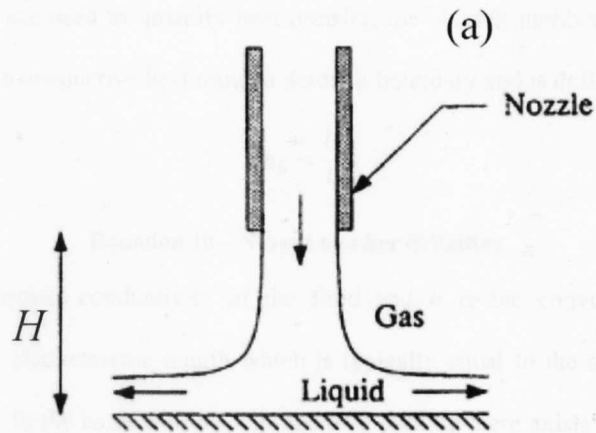


Figure 63 – A free surface jet where the liquid is discharged through the ambient gas [44].

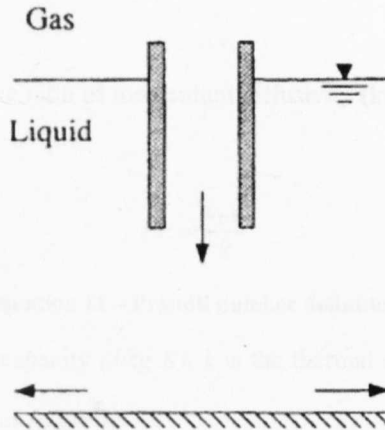


Figure 64 – A submerged jet where the liquid discharges through liquid [44].

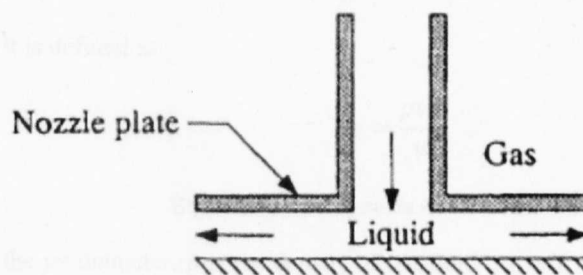


Figure 65 – A confined submerged jet, no gas is present [44].

4.6.2 Heat transfer coefficient profile

Various parameters are used to quantify heat transfer, the Nusselt number (Nu) describes the ratio of convective to conductive heat transfer across a boundary and is defined as:

$$Nu_L = \frac{hL}{k_f}$$

Equation 10 – Nusselt number definition

Where k_f is the thermal conductivity of the fluid and h is the convective heat transfer coefficient. L is the characteristic length which is typically equal to the distance over which heat transfer occurs. In the context of jet impingement cooling there exists a certain amount of ambiguity in determining the characteristic length due to the spent fluid after impingement having a cooling effect also. L is often defined as the length of the array of jets, for example a 3 x 3 array of jets, spaced at 2mm would have a characteristic length, $L = 6mm$.

The Prandtl number (Pr) is the ratio of momentum diffusivity (kinematic viscosity) to thermal diffusivity and is defined as:

$$Pr = \frac{c_p \mu}{k}$$

Equation 11 – Prandtl number definition

Where c_p is the specific heat capacity ($J/kg K$), k is the thermal conductivity (W/mK) and μ is the dynamic viscosity, ($Pa s$) or (Ns/m^2).

The Reynolds number gives a measure of the ratio of inertial forces to viscous forces and consequently quantifies the relative importance of these two types of forces for given flow conditions. It is defined as:

$$Re = \frac{\rho v d}{\mu}$$

Equation 12 – Reynolds number definition

Where d is the jet diameter, ρ is the density of the fluid (kg/m^3), v is the kinematic viscosity ($v = \mu/\rho$) (m^2/s).

The heat transfer coefficient on the impingement surface from a single jet has generally been found to demonstrate a bellshaped distribution, with the local maximum occurring at the

stagnation point [46] (Figure 66). Secondary peaks in local Nusselt number have also been located in the region between 1.5 and 2.5 jet diameters from the stagnation point [47]. These peaks have been accredited to a transition to turbulence in the wall-jet region. The magnitude and distribution of the heat transfer coefficient has been found to be dependent on a number of parameters including, but not limited to: the Prandtl number (Pr), Reynolds number (Re), jet diameter (d), jet-to-target spacing (H/d) and the physical geometry of the jets and target surface [46].

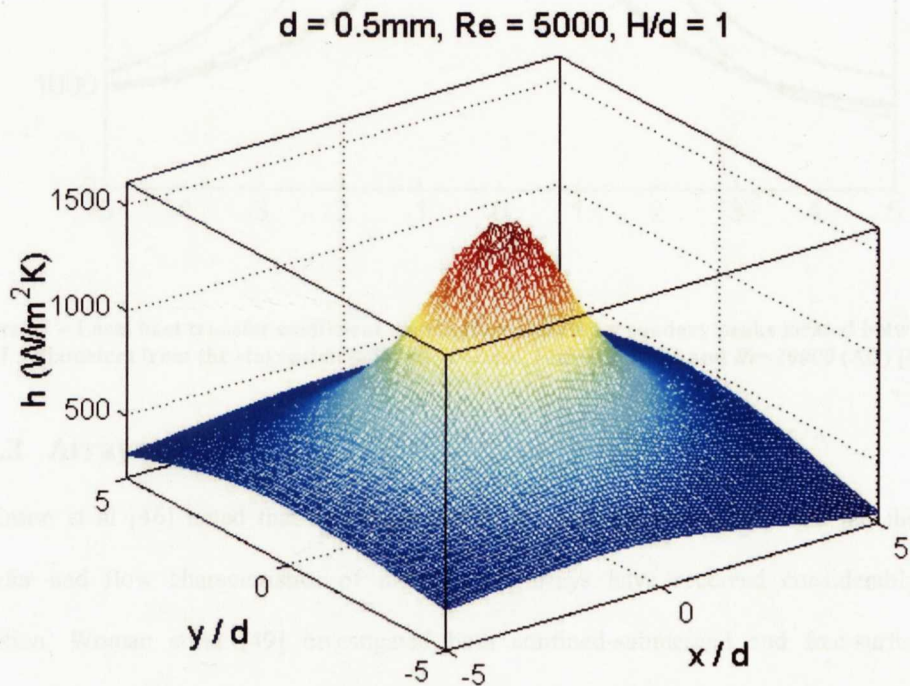


Figure 66 – Three dimensional local heat transfer coefficient distribution for $d=0.5\text{mm}$, $Re=5000$ and $H/d=1$ (Air) [48].

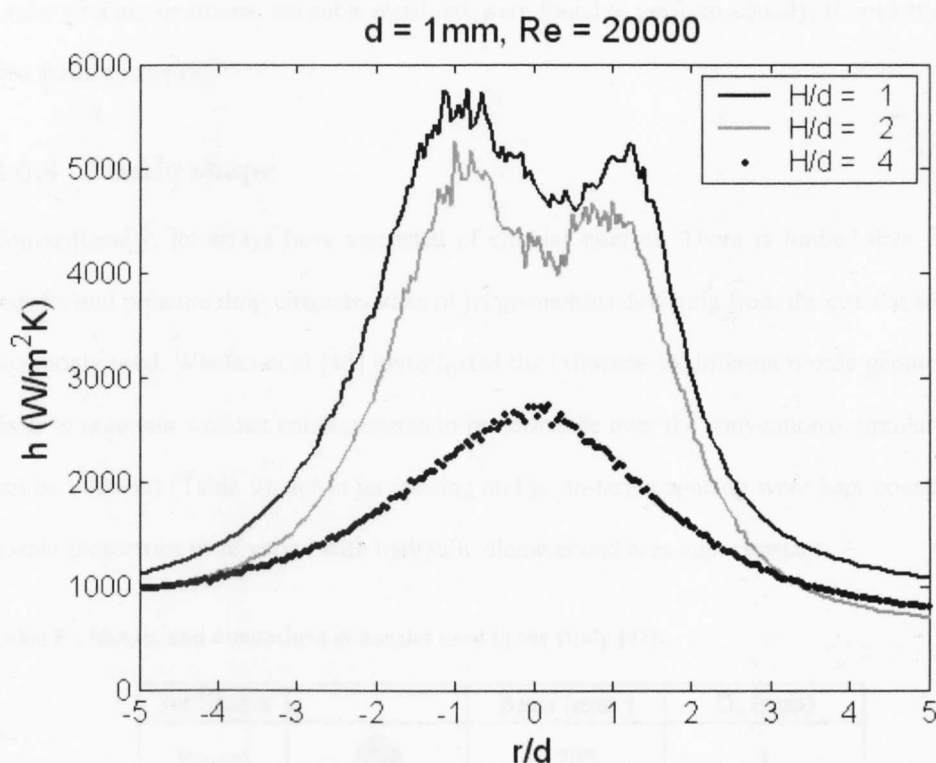


Figure 67 – Local heat transfer coefficient distribution showing secondary peaks located between 1 and 1.5 diameters from the stagnation point for $d=1\text{mm}$, $H/d=1, 2$ and 4 and $Re=20000$ (Air) [48].

4.6.3 Arrays of jets








Robinson et al [46] noted that in comparison to jet impingement of a single jet, the heat transfer and flow characteristics of multiple jet arrays have received considerably less attention. Womac et al [49] investigated both confined-submerged and free-surface jet impingement heat transfer, using water and FC-77 as the coolants. Arrays of 2×2 and 3×3 circular jets were tested for jet diameters of 0.513mm and 1.02mm over various jet-to-jet spacing. When the volumetric flow rate was held constant, it was observed that heat transfer increased with decreasing values of d and N , which was attributed to increased jet velocity. When values of flow rate, d and N were held constant, heat transfer was discovered to increase with decreasing values of jet-to-jet spacing, with interference between neighbouring cells and/or a possible reduction in the wall-jet region associated with each jet attributed to this enhancement. Experiments conducted for the confined-submerged liquid jet arrays found that the heat transfer coefficient was somewhat insensitive to jet-to-target spacing within the range of $2 \leq H/d \leq 4$ due to the target surface being within the potential core of the issuing jets.

Under similar conditions, the submerged jets were found to perform equally, if not better, than free surface jets [49].

4.6.4 Nozzle shape

Conventionally, jet arrays have consisted of circular nozzles. There is limited data for heat transfer and pressure drop characteristics of jet geometries deviating from the circular jets most commonly used. Whelan et al [43] investigated the influence of different nozzle geometries in order to ascertain whether enhancements in performance over the conventional circular nozzle can be obtained (Table 9). Jet-to-jet spacing and jet-to-target spacing were kept constant, the nozzle geometries were varied with hydraulic diameter and area kept constant.

Table 9 – Shapes and dimensions of nozzles used in the study [43].

Jet Shape		Area (mm ²)	D _h (mm)
Round		0.785	1
Chevron		1.07	1
		0.785	0.73
Triangle		1.3	1
		0.785	0.77
Square		1	1
		0.785	0.89
Cross		1.8	1
		0.785	0.66
Medal		2.63	1
		0.785	0.54
Star		2.79	1
		0.785	0.73

The results of the study indicated that for jets with the same hydraulic diameter, the commonly used circular jets produced the highest heat transfer coefficient for a given amount of pumping power (Figure 68), followed by the square, triangular and chevron shaped jets.

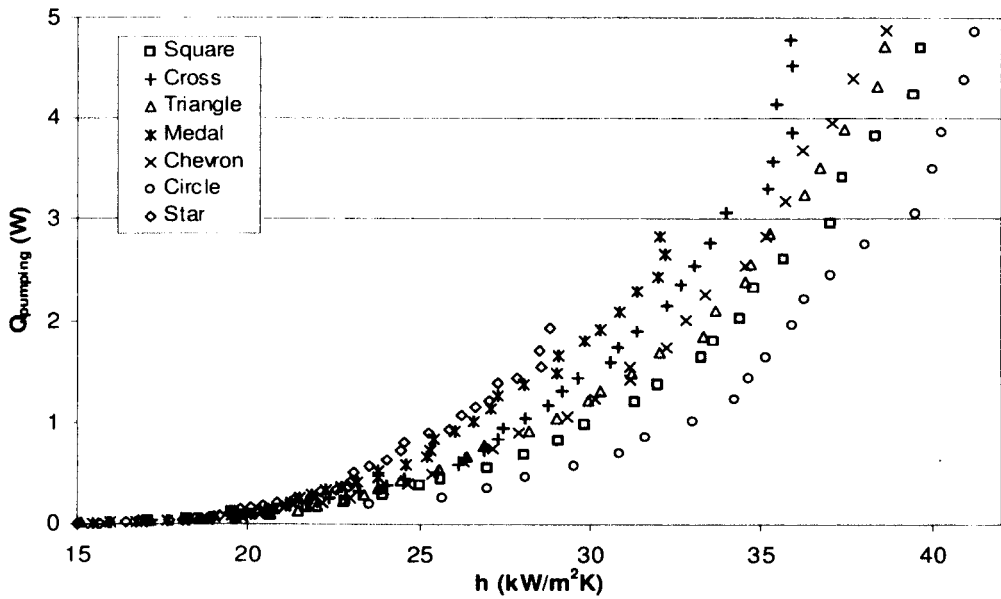


Figure 68 – Pumping power versus average heat transfer coefficient for different nozzle geometries of constant hydraulic diameter [43].

4.6.5 Erosion of the heat transfer surface

For jet impingement at high velocities ($> 10\text{m/s}$) erosion of the heat transfer surface material must be considered. Rao and Buckley [50] and Janakiram [51] have investigated erosion rates for liquid impingement on copper using a rotating disk device. A filtered water jet of diameter $d=1.5\text{mm}$ with an average velocity of 125m/s impinging on copper placed in ambient air gave an erosion rate of 0.092 mm/hour . It is noted that the velocity of 125m/s used in this study is particularly high compared to the velocity of jets in the impingement coolers tested in the previous chapter, which were tested up to a maximum jet velocity of 0.2m/s . From the result mentioned above we can see that erosion is a concern and the long term effect of the erosion of the heat transfer surface due to the impinging jets should be investigated.

4.6.6 Parameters affecting heat transfer performance

The key parameters affecting the performance of jet impingement arrays include:

- Jet velocity - V
- Jet-to-target distance - H
- Jet diameter - d
- Jet spacing - r
- Sprayplate thickness - l
- Number of jets in the array - N
- Total size of the array - $r(\sqrt{N} - 1)$

The parameters are often paired to simplify the analysis and understanding of experimental data, namely:

- Ratio of jet-to-target distance to jet diameter - H/d

This is a measure of the spray distance and how confined the jet is in relation to the spent fluid.

- Ratio of jet spacing to jet diameter - r/d

A measure of the density of the jets per unit area.

- Ratio of jet diameter to sprayplate thickness - d/l

This describes whether the jets produced are similar to those which exude from an orifice plate or from a cylindrical pipe.

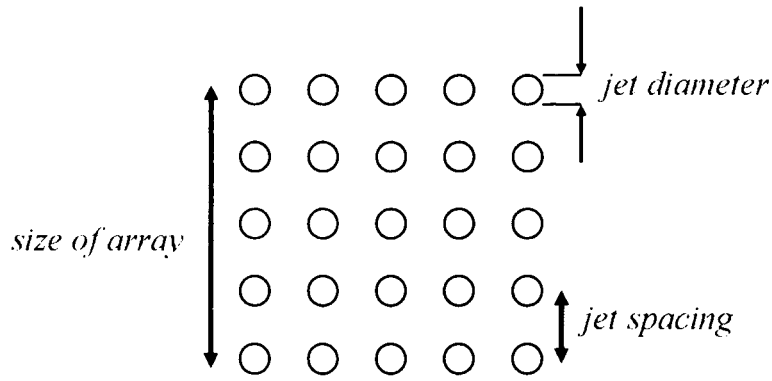


Figure 69 - A square 5 x 5 impingement array with key parameters defined.

A number of trade-offs exist when designing a jet impingement array. If there are many jets located near to one another, spent fluid from the central jets prevents the outer jets from impinging fully at the heat transfer surface and cooling performance is reduced. The opposite is true if there are a small number of jets spaced far apart, as the full cooling potential of each impinging jet is not being utilized. If the holes in the impingement array are too narrow the jet of fluid may degrade before it reaches the cooled surface and full impingement may not be achieved. Whereas, if the jet diameter is too large, the thickness of the thermal boundary layer at the cooled surface will increase due to the increased amount of crossflow from the spent fluid which reduces the amount of cooling achieved.

4.7 Heat transfer correlations

A number of correlations exist for the heat transfer which can be obtained from certain jet array geometries. The correlations tend to only be valid over very specific ranges of array geometries for example: specific ranges of jet diameters and jet-to-jet spacing, number of jets in the array or Reynolds numbers of the coolant fluid flow. There is not a single correlation which can fully describe all jet arrays ranging from single jets to large arrays consisting of hundreds of jets over a wide range of flow rates. At present there is limited data available for the pressure drop and associated pumping power required to generate a certain value of heat transfer coefficient for confined liquid jet arrays.

Lienhard's paper on liquid jet impingement cooling [52] is commonly referenced when researching the parameters affecting jet impingement cooling. He finds that for jets issuing

from long tubes, the flow will be turbulent for $Re_d \geq 2000$. A typical result for stagnation zone heat transfer is given in Equation 13 which is valid for fully turbulent jets of non-metallic liquids ($Pr > 1$) and $25000 \leq Re_d \leq 85000$. Such results show that the heat transfer coefficient is larger for smaller diameter jets and increases with jet velocity, owing to thinning of the boundary layer [52].

$$Nu_d = hd/k = 0.278Re_d^{0.633}Pr^{1/3}$$

Equation 13

For laminar jets ($2000 \geq Re_d$) the jet can be smaller than the nozzle diameter if the nozzle produces a strong contraction (as does a sharp-edged orifice). The velocity profile from a laminar jet is also very sensitive to the nozzle shape. For jets issuing from tubes at $2000 \leq Re_d$, the profile is parabolic, while for jets issuing from sharp-edged orifices at any Re_d , the profile is uniform after the jet contracts. Non-uniform velocity profiles can more than double the stagnation zone heat transfer, provided that the nozzle is placed within a few nozzle diameters of the target, so that the profile is unable to dissipate toward the mean jet velocity. For example, a parabolic-profile laminar jet has:

$$Nu_d = 1.648Re_d^{1/2}Pr^{0.368}$$

Valid for $1 \leq Pr \leq 10$

Equation 14

While a uniform profile laminar jet has:

$$Nu_d = 0.745Re_d^{1/2}Pr^{1/3}$$

Equation 15

4.7.1 Submerged jets and pressure drop

Fabbri and Dhir [53] were one of the first to consider both heat transfer to the jet arrays and pressure drop across the jet plate. The study investigated microjet arrays within a Reynolds number range of $73 \leq Re_d \leq 3813$, and jet diameter range of $65\mu m \leq d \leq 250\mu m$ using water and FC40 as the coolants. Increases in Re_d and Pr , as well as decreases in r/d were observed to lead to enhancements in the average surface heat transfer coefficient.

Robinson and Schnitzler [46] conducted experiments investigating water jet impingement cooling for both free-surface and confined-submerged jet arrays. Jet diameters of $1mm$ were

used, with a jet-to-jet spacing range of $3 \leq r/d \leq 7$. Averaged heat transfer and pressure drop data was recorded for a dimensionless jet-to-target spacing range of $2 \leq H/d \leq 30$ and Reynolds number range of $650 \leq Re_d \leq 6500$. For the submerged jets, it was found that heat transfer was insensitive to jet-to-target spacing changes in the range of $2 \leq H/d \leq 3$. A monotonic decrease in heat transfer was observed with increasing jet-to-target spacing in the range of $5 \leq H/d \leq 20$. It was reported that, for a constant Reynolds number, increasing the jet-to-jet spacing incurred a detrimental effect on heat transfer. It was also found that a stronger dependence on jet-to-jet spacing was encountered for smaller jet-to-target spacing. Free-surface jets were observed to behave as submerged jets within the range of $2 \leq H/d_n \leq 10$. Beyond this value, entirely free jet flow occurs with the heat transfer coefficient showing marginal improvement with increasing jet-to-target spacing. Robinson and Schnitzler correlated their heat transfer data for free-surface jets as:

$$\frac{Nu_L}{Pr^{0.4}} = 7.8 Re_{dn}^{0.49} \exp\left(-0.025 \frac{S}{d_n}\right)$$

Equation 16 – Robinson-Schnitzler correlation for free-surface jets

A Nusselt number correlation for the confined-submerged data was also presented as:

$$\frac{Nu_L}{Pr^{0.4}} = 23.39 Re_{dn}^{0.46} \exp\left(\frac{S}{d_n}\right)^m \left(\frac{H}{d_n}\right)^n \quad 2 \leq H/d_n \leq 3, \quad 3 \leq S/d_n \leq 7 \quad \begin{cases} m = -0.442 \\ n = -0.00716 \end{cases}$$

Equation 17 – Robinson-Schnitzler correlation for confined-submerged jets

Where S = nozzle to target separation, d_n = jet diameter.

In comparison to the free-jet flows, the submerged jets at small jet-to-target spacing were found to provide the required heat transfer coefficient at the smallest pumping power requirement. Other notable correlations for the heat transfer generated by impingement arrays were developed by Martin and Womac et al.

The Martin correlation [54] for multiple circular submerged jets:

$$\left(\frac{Nu}{Pr^{0.42}}\right)_{AN} = K(S_{NP}/d, \alpha_j) G(S_{NP}/d, \alpha_j) F(Re_j)_{AN}$$

$$K(S_{NP}/d, \alpha_j) = \left[1 + \left(\frac{S_{NP}/d}{0.6/\sqrt{\alpha_j}}\right)^6\right]^{-0.05}$$

$$G(S_{NP}/d, \alpha_j) = \frac{2\sqrt{\alpha_j}(1 - 2.2\sqrt{\alpha_j})}{1 + 0.2(S_{NP}/d - 6)\sqrt{\alpha_j}}$$

$$F(Re_j)_{AN} = 0.5Re_j^{2/3}$$

$$2000 \leq Re_j \leq 100000; 0.004 \leq \alpha_j \leq 0.04; 2 \leq S_{NP}/d \leq 12$$

Equation 18 – The Martin correlation for multiple circular submerged jets

Where $\alpha_j = (\pi d^2)/(4A_{corr.})$, d = nozzle diameter, S_{NP} = nozzle-to-target separation, $Nu = h_{avg}d/k$, $Re_j = \rho v d/\mu$, $Pr = \mu C_p/k$, AN stands for array of nozzles, and $A_{corr.}$ is the area corresponding to a single jet.

Womac et al. Correlation [49] for multiple circular submerged jets:

$$\frac{Nu_l}{Pr^{0.4}} = C_1 Re_d^m \left(\frac{l}{d}\right) A_r + C_2 Re_L^n \left(\frac{l}{L}\right) (1 - A_r)$$

$$L = \frac{[(\sqrt{2}L_e/2) - 1.9d] + [(L_e/2) - 1.9d]}{2}$$

$$A_r = N\pi (1.9d)^2/l^2$$

$$5000 \leq Re_d \leq 20000; 0.5 \leq d \leq 1.0 \text{ mm}; 2 \leq S_{NP}/d \leq 4; N = 4 \text{ or } 9 \text{ jets}; l = 12.7 \text{ mm}; m = 0.5; n = 0.8; C_1 = 0.509; C_2 = 0.0363$$

Equation 19 – The Womac correlation for multiple circular submerged jets

Where, d = nozzle diameter, S_{NP} = nozzle-to-target separation, l = length of the side of the square heat source, L = average length of the wall jet region, L_e = length of nozzle unit cell for an array, $Nu_l = h_{avg}l/k$, $Re_d = \rho v d/\mu$, $Re_L = \rho v L/\mu$ and $Pr = \mu C_p/k$.

Table 10 – Properties of water at 25°C

$\rho \text{ (kg/m}^3\text{)}$	998
$C_p \text{ (J/kgK)}$	4182
$\mu \text{ (Ns/m}^2\text{)}$	0.001003
$K \text{ (W/mK)}$	0.60
Pr	7.0

4.7.2 Heat transfer correlations and power module cooling

A power module consists of a number of heat dissipating devices each of which can be cooled by its own impingement array. Each of the heat transfer correlations described have been derived from experimental tests where after impingement the spent fluid exhausts equally in all directions. However when implementing a jet impingement cooling system for a typical power module consisting of multiple devices, the spent fluid from each impingement array is likely to exhaust in a single direction. The crossflow from the spent fluid will disrupt and interfere with the heat transfer performance and related pressure drop of the impingement array. Therefore the existing heat transfer correlations for the ideal case of a single jet array exhausting equally in all directions may not be directly applicable for the design of multiple jet arrays for the cooling of power modules.

4.7.2.1 Applying the Correlations

In the previous chapter, two different jet impingement coolers were tested. It was decided to compare the experimental results with heat transfer figures calculated using the correlations. The direct baseplate impingement cooler, consisted of 11 impingement cells each containing a 6×8 array of jets and produced an average heat transfer coefficient of $22440 \text{ W/m}^2\text{K}$ at a water flow rate of 4 litres/minute . The cooled area was 0.003723 m^2 and a pressure drop of 149 kPa was measured across the cooler. The cooler contained a total of 528 jets and assuming an evenly distributed heat transfer coefficient over the cooled area, each jet cooled an area of 7.05 mm^2 .

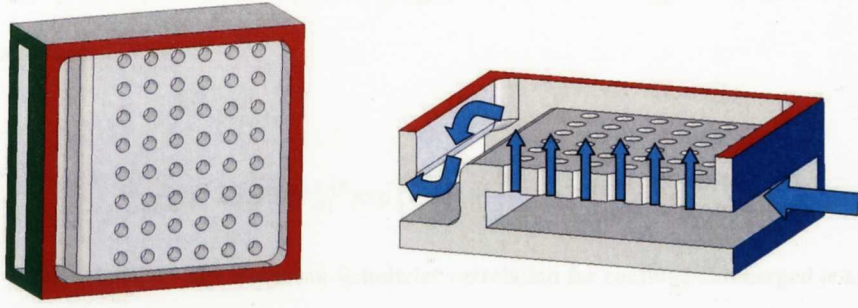


Figure 70 – Detail of a single cell from the direct baseplate impingement cooler.

The pressure drop across the cooler is a function of the flow rate and can be described as:

$$\Delta P_{cooler} = 8390\dot{V}^2 + 4050\dot{V}$$

Equation 20 – The pressure drop across the cooler in terms of the flow rate

Where ΔP_{cooler} is the pressure drop across the cooler in *Pa* and \dot{V} is the volumetric flow rate in *litres/minute*.

The heat transfer correlations tend to refer to the average fluid velocity through a single jet. In this case, the pressure drop relating to a single jet in the cooler, ΔP_{jet} , in terms of the average jet velocity, v_{jet} , can be described as:

$$\Delta P_{jet} = 9837 v_{jet}^2 + 190.85 v_{jet}$$

Equation 21 – The pressure drop across a single jet in terms of the average jet velocity

Where ΔP_{jet} is the pressure drop across a single jet in *Pa* and v_{jet} is the average jet velocity in *m/s*.

From Figure 53, the heat transfer coefficient generated by the cooler is related to the pumping power over the range, $1 \leq \dot{V} \leq 4$ (where \dot{V} is expressed in *litres/minute*) as:

$$h = 2810.9 \ln(Q) + 15440$$

Equation 22 –The heat transfer coefficient generated by the cooler in terms of pumping power

Where the units of heat transfer coefficient, h , are *W/m²K*, and Q is the total pumping power in *Watts*.

The average heat transfer coefficient generated by a single jet can be described in terms of the jet velocity as:

$$h = 2810.9 \ln(2153.9v^3 + 41.6v^2) + 15440$$

Equation 23 –The heat transfer coefficient generated by the cooler in terms of jet velocity

Where v is the average jet velocity in *m/s*.

The array geometry of the baseplate impingement cooler was applied to three heat transfer correlations:

$$\frac{Nu_L}{Pr^{0.4}} = 23.39 Re_{dn}^{0.46} \exp\left(\frac{S}{d_n}\right)^m \left(\frac{H}{d_n}\right)^n \quad \begin{cases} m = -0.442 \\ n = -0.00716 \end{cases}$$

Equation 24 - The Robinson-Schnitzler correlation for confined-submerged jets

$$\left(\frac{Nu}{Pr^{0.42}}\right)_{AN} = K(S_{NP}/d, \alpha_J) G(S_{NP}/d, \alpha_J) F(Re_J)_{AN}$$

Equation 25 - The Martin correlation for multiple circular submerged jets

$$\frac{Nu_l}{Pr^{0.4}} = C_1 Re_d^m \left(\frac{l}{d}\right) A_r + C_2 Re_L^n \left(\frac{l}{L}\right) (1 - A_r)$$

Equation 26 - Womac et al. Correlation for multiple circular submerged jets

Table 11 – Parameters for use with the heat transfer correlations.

<i>Jet-to-jet spacing (m)</i>	<i>S</i>	0.002
<i>Characteristic length (m)</i>	<i>L</i>	0.002
<i>Jet diameter (m)</i>	<i>dn</i>	0.001
<i>Jet to target distance (m)</i>	<i>S_{NP}</i>	0.0015
<i>Area corresponding to a single jet</i>	<i>A_{corr}</i>	7.05×10^{-6}
<i>Length of the square heat source</i>	<i>l</i>	0.006
<i>Number of jets in array</i>	<i>N</i>	9
<i>Length of single cell (m)</i>	<i>L_e</i>	0.002

The values for the parameters from Table 11 were substituted into the correlations. The effective heat transfer coefficient was calculated for a range of jet velocities up to 0.2m/s (corresponding to a flow rate of 5litres/minute through the baseplate cooler) and compared with the experimental data from the baseplate impingement cooler (Table 12). It is interesting to see how the correlations compare to the measured heat transfer coefficient for the baseplate cooler over the range of jet velocities tested, that is: $v \leq 0.2\text{m/s}$. There appears to be a large variation in the value of the heat transfer coefficient predicted by the three correlations when compared to the experimental data. The Womac correlation appears to be the closest whereas

the Robinson-Schnitzler and Martin correlations appear to underestimate the heat transfer by a factor of 2 and 4 respectively.

Table 12 – Comparison of heat transfer coefficients calculated at a jet velocity of 0.2m/s.

<i>Correlation</i>	<i>Heat Transfer Coefficient (W/m²K)</i>
<i>Baseplate Cooler (experimental data)</i>	23701
<i>Womac</i>	20135
<i>Martin</i>	5765
<i>Robinson-Schnitzler</i>	10557

In Figure 71 the heat transfer coefficient predicted by each of the three correlations is plotted along with the experimental data and in Figure 72 the value of the heat transfer coefficient is normalised at $v = 0.2m/s$ so that the shape of the curves can be compared to see which correlation most closely matches the profile from the experimental data. The Womac and Robinson-Schnitzler correlations have a similar shape over the range of jet velocities displayed in the normalised graph. The Martin correlation produces a more linear dependence on heat transfer compared to the measured data and the other two correlations. In Figure 72 the measured data follows closely to the Womac and Robinson-Schnitzler correlations from a jet velocity of approximately 0.04m/s onwards.

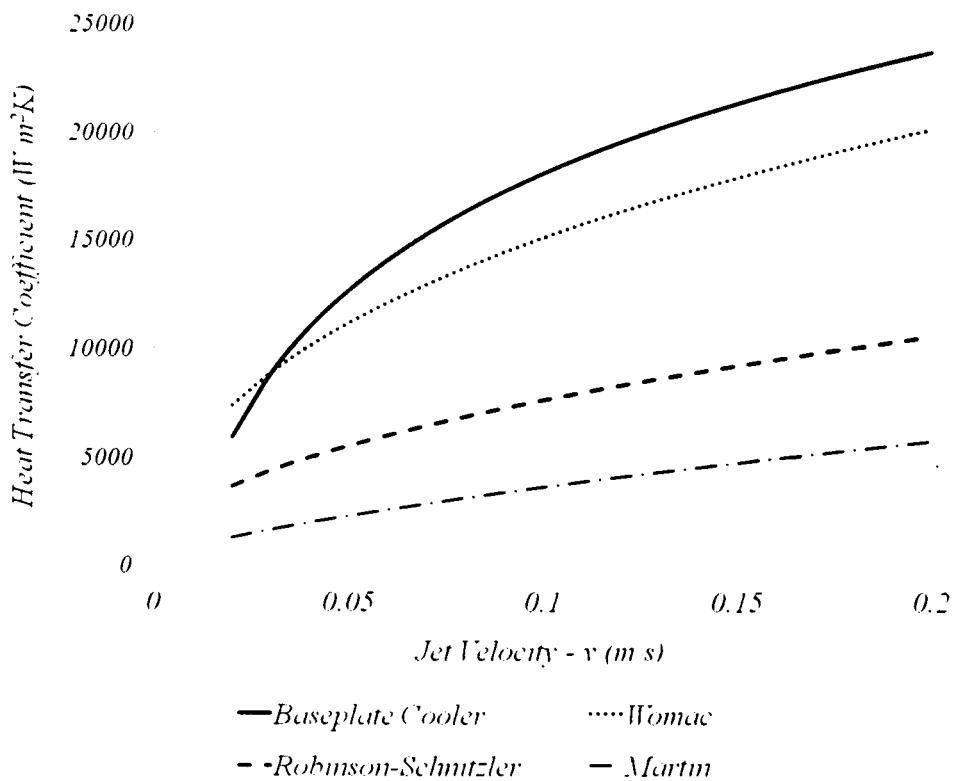


Figure 71 – Heat transfer coefficients predicted by the correlations compared to the experimental data

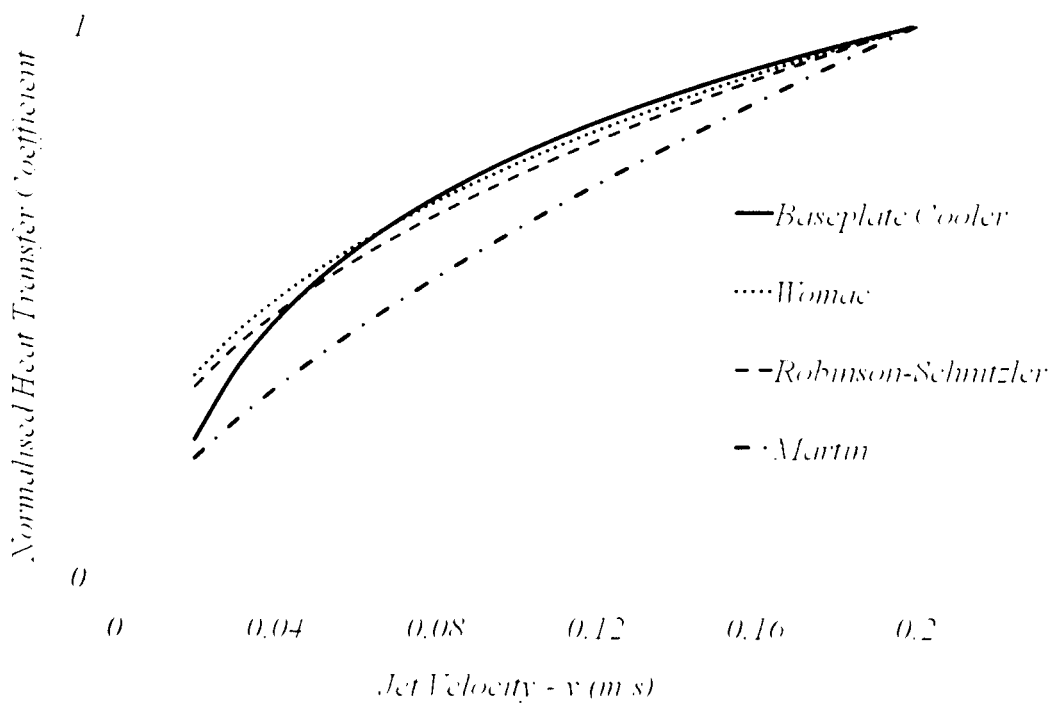


Figure 72 – Normalised heat transfer coefficient versus jet velocity for the three correlations and the experimental data for the baseplate impingement cooler.

The data within Table 12 and Figure 72 indicate that existing heat transfer correlations may not always be applicable or accurate enough to be solely used to design or optimise impingement arrays for the cooling of multiple power electronic devices. The heat transfer performance predicted by the Womac correlation provides the closest match to the experimental data of the three chosen correlations. However, the correlations do not indicate the amount of pressure drop and therefore pumping power required to drive the coolant through the jet arrays; without which the jet arrays cannot be optimised for efficiency. Experimental testing will be required in order to determine the most effective jet array geometry for the cooling of the hotspot directly beneath the device.

4.7.3 An optimal jet array configuration

Fabbri and Dhir noted that the pressure drop across the nozzle required to form the jet is not necessarily connected to the heat transfer mechanism at the impingement surface [53]. This establishes the attractive possibility of an optimal nozzle configuration in which, for a required heat transfer coefficient, volumetric flow rate and pumping power can be minimized. A study was performed in order to further improve the efficiency of the jet impingement coolers by testing a variety of array geometries designed to cool devices soldered onto the custom made *AlN* substrate tile described earlier.

4.8 Experimental testing

The aim of the study is to test a number of impingement array geometries by directly cooling two diodes measuring $12.7\text{mm} \times 12.7\text{mm}$ soldered onto the $40\text{mm} \times 40\text{mm}$ *AlN* substrate tile described earlier in the chapter. Each diode will be cooled by a jet array aligned to cool the hotspot directly beneath it. Due to the number of parameters which can be varied when constructing the geometry of a jet impingement array it is necessary to carefully design the various arrays using the findings from the research.

4.8.1 The sprayplates and jet arrays

The arrays were designed to operate as submerged jets as they were found to perform equally, if not better, than free jets [49]. The highest heat transfer rates were found to come from the smallest diameter jets [53]. The smallest diameter of jets for this set of experiments was set at

0.5mm as this was believed to be the lowest acceptable diameter of jet hole which could be used on an automotive water-glycol cooling circuit without risk of being clogged. Once the smallest jet diameter has been set at 0.5mm, this allows the jet-to-target distance, H , to be determined. For submerged liquid jet arrays a jet-to-target spacing within the range of $2 \leq H/d \leq 4$ was found to be most effective due to the target surface being within the potential core of the issuing jets. For $H/d = 3$, and for jets of diameter 0.5mm, the spray distance, H , that is the distance between the sprayplate and the underside of the substrate tile, was kept constant at 1.5mm. The sprayplates were manufactured from Al_2O_3 of thickness 1mm and the holes for the jet arrays were laser cut.

4.8.2 Jet diameter

The diameter of the holes in the impingement arrays affects the jet velocity of the fluid. If there are an identical number of holes in the array, the array with the narrower holes will generate a higher average jet velocity at a given flow rate compared to the same array with larger diameter jets (Figure 73). The range of jet diameters which were tested were: $0.5mm < d < 1.5mm$ producing a ratio of jet spacing to jet diameter: $2 < r/d < 8$.

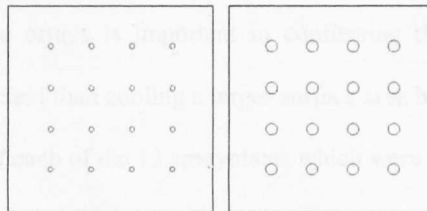


Figure 73 - Comparison of sprayplate 5 (left) and sprayplate 11 (right). Both have a jet spacing of 4mm in a 4 x 4 array. Sprayplate 5 has jets of diameter 0.5mm with a total jet surface area of $3.1mm^2$ while sprayplate 11 has jets of diameter 1.125mm with a total jet area of $15.9mm^2$

4.8.3 Ratio of jet spacing to jet diameter

The ratio of jet spacing, r , to jet diameter, d , (r/d) is an important factor in the performance of an impingement array. Five sprayplates with jet diameter 0.5mm were manufactured to produce a 12mm square array with the spacing of the jets varying from 1mm up to 4mm with r/d (ratio of jet spacing to jet diameter) varying from 2 to 8 (Figure 74).



Figure 74 - Sprayplates 1 – 5 with jet diameter 0.5mm in a 12mm array with increasing jet-to-jet spacing.

4.9 Size of the array

For this set of experiments the size of the jet array is defined in Figure 69 as the distance in millimetres between the centres of two corner jets located along one side of the square array and can be calculated using $r(\sqrt{N} - 1)$, where r is the jet-to-jet spacing and N is the total number of jets in the array. For example, using this definition for the size of an array, a 4×4 array with 1mm jets spaced at 4mm is the same size as a 7×7 array with 0.5mm jets spaced at 2mm , that is 12mm . Sprayplates 3, 6 and 7 each have arrays of 0.5mm jets spaced at 2mm ($r/d = 4$). Sprayplate 7 has a 6×6 array of jets producing an array size of 10mm , sprayplate 3 has a 7×7 array producing an array size of 12mm square corresponding approximately to the size of the diodes and sprayplate 6 has an 8×8 array of jets giving an array size of 14mm . The relative performance of these three arrays is important in confirming the hypothesis that hot spot targeting may be more efficient than cooling a larger surface area beneath the devices. Table 13 lists the array geometries of each of the 12 sprayplates which were tested.

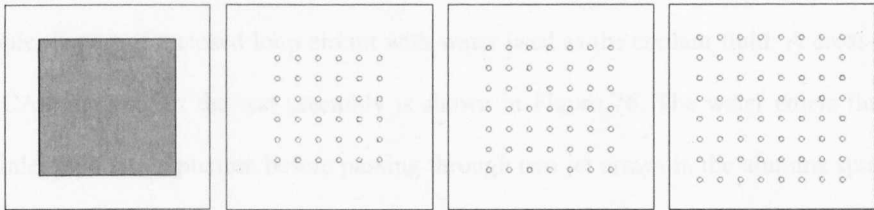


Figure 75 - From left to right: Size of diode die for comparison. Sprayplate 7 with a 6×6 array measuring 10mm . Sprayplate 3 with a 7×7 array measuring 12mm . Sprayplate 6 (far right) with an 8×8 array measuring 14mm .

Table 13 - Jet impingement sprayplate geometries.

<i>Sprayplate number</i>	<i>Jet diameter (mm)</i>	<i>Jet spacing (mm)</i>	<i>r/d (ratio of jet spacing to diameter)</i>	<i>Array</i>	<i>Array size (mm)</i>
1	0.5	1	2	13 x 13	12
2	0.5	1.5	3	9 x 9	12
3	0.5	2	4	7 x 7	12
4	0.5	3	6	5 x 5	12
5	0.5	4	8	4 x 4	12
6	0.5	2	4	8 x 8	14
7	0.5	2	4	6 x 6	10
8	0.75	1.5	2	9 x 9	12
9	1	2	2	7 x 7	12
10	0.9	3	3.33	5 x 5	12
11	1.125	4	3.56	4 x 4	12
12	1.5	6	4	3 x 3	12

4.10 Experimental test rig

A test rig was built in order to perform the heat transfer experiments. The same substrate tile and electronic devices were used for the entire set of experiments. The substrate tile was mounted in a plastic holder at the top of the cooler assembly. The test rig was manufactured in such a way as to allow the alumina sprayplates to be exchanged after each set of experiments. The cooler is part of a closed loop circuit with water used as the coolant fluid. A cross-section of the CAD drawing of the test assembly is shown in Figure 76. The water enters through a single inlet pipe into a plenum before passing through two jet arrays in the alumina sprayplate. The water then impinges onto the underside of the substrate tile, directly underneath the diodes. The water subsequently exhausts in two opposite directions and then feeds into a single return pipe back to the pump.

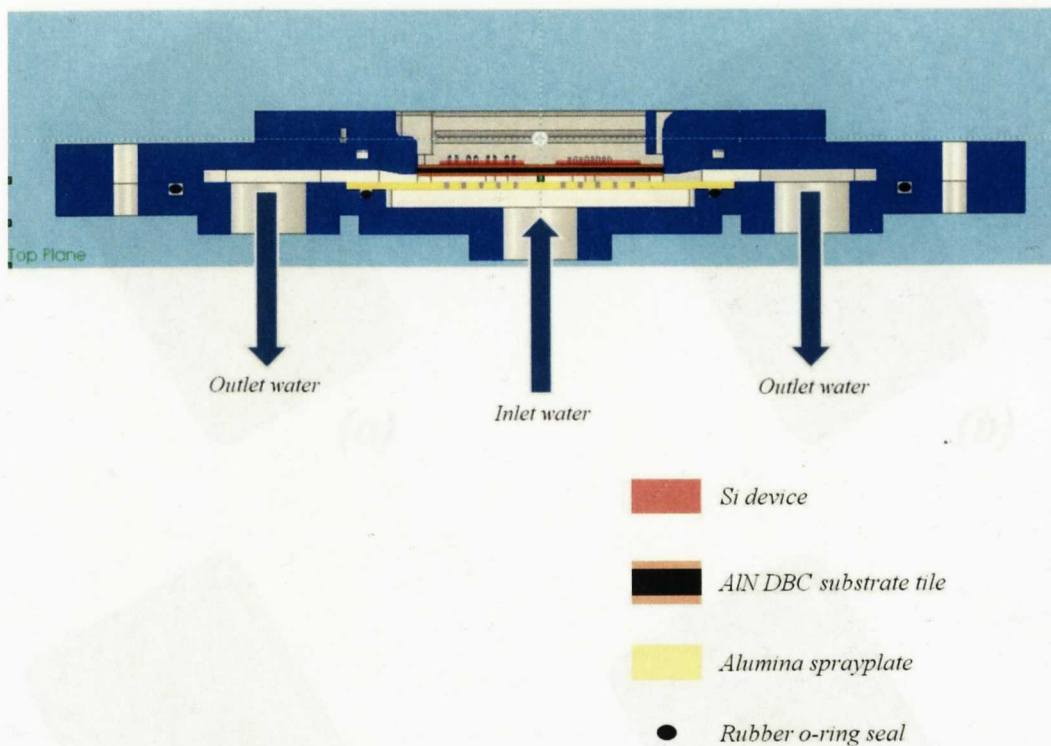


Figure 76 – A cross-section of the CAD drawing of the impingement cooler.

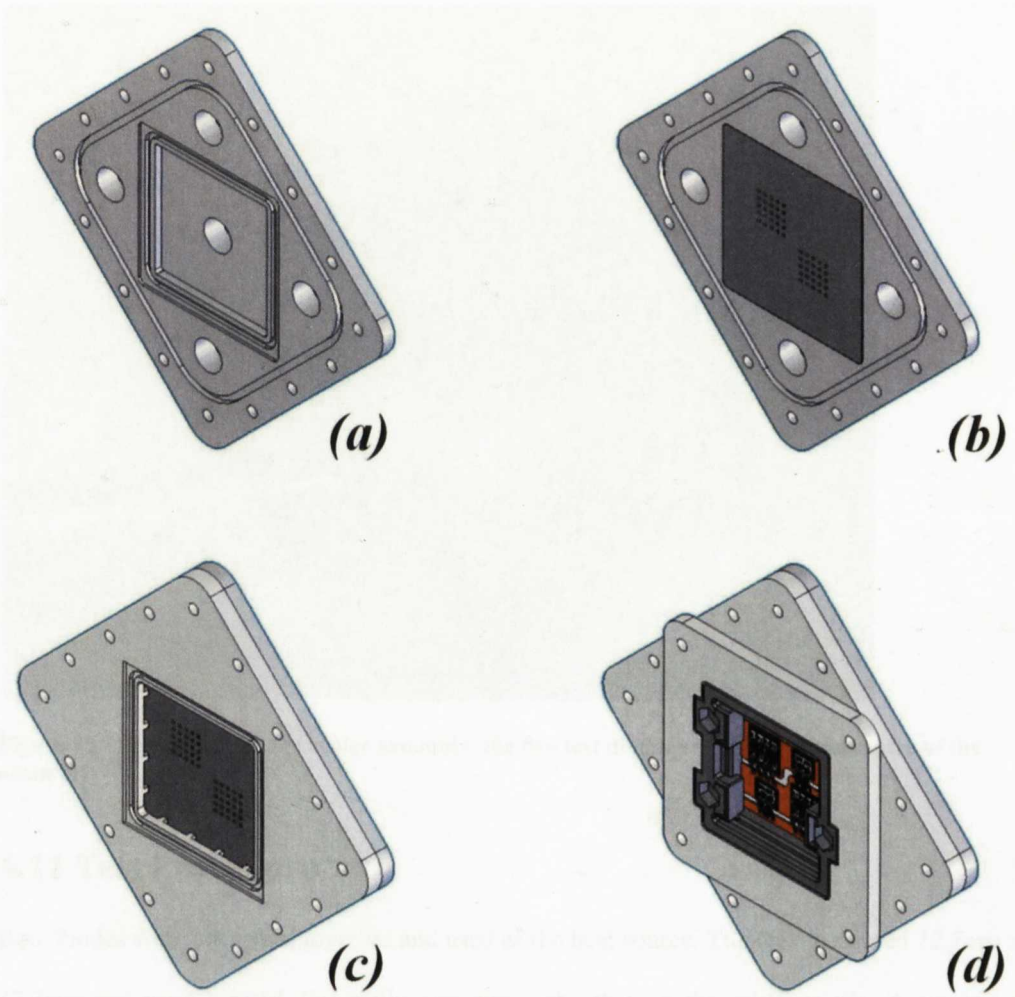


Figure 77 – CAD drawings detailing the assembly of the test apparatus:

- (a) Bottom part, containing inlet and outlet fixtures and recesses for two o-rings.**
- (b) An alumina sprayplate has been inserted. Each sprayplate has a different geometry of jets.**
- (c) The top part compresses the two o-rings to seal the assembly.**
- (d) The substrate tile is mounted into a plastic holder which is held in place with a clamp at the top of the assembly.**

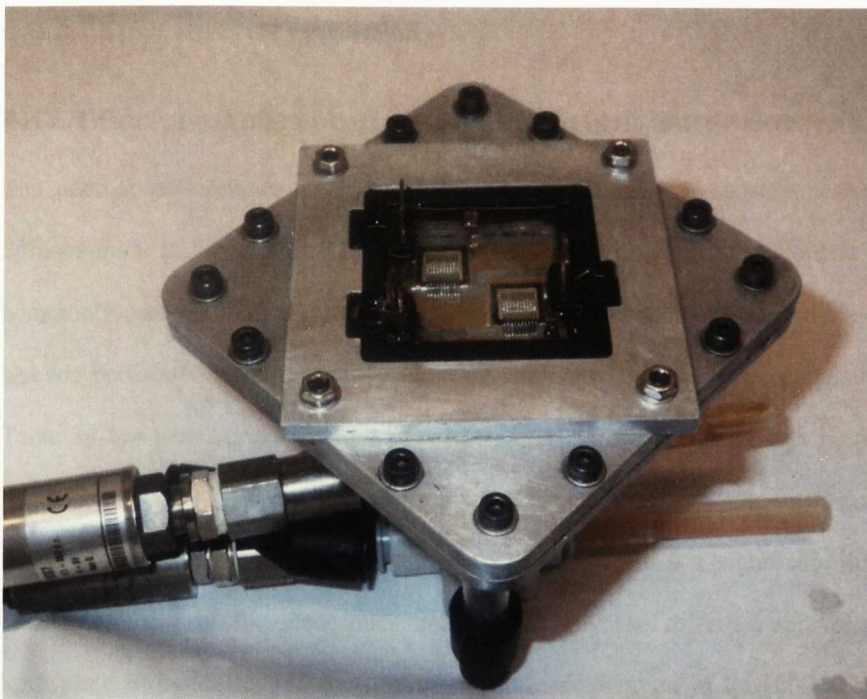


Figure 78 - Photograph of the cooler assembly, the two test diodes are visible at the centre of the assembly.

4.11 Test Procedure

Both diodes were energized together and used as the heat source. The dies measured $12.7\text{mm} \times 12.7\text{mm}$ and were located diagonally opposite each other on the substrate tile. A single jet impingement sprayplate containing two jet arrays was thus used to provide the cooling. Each of the sprayplates was subjected to the same set of tests. A high current power source was used to pass current through both of the diodes in series resulting in 300Watts of power in total being dissipated by the two diodes. The dissipated power was measured using a current probe and a voltmeter across the power connections closest to the diodes. The diodes were operating near their rated current of 100Amps . The temperature of the water was maintained at 45°C by the heat exchanger. The water flow rate through the cooler was varied from 1 to 4 litres/minute using a bypass valve. Pressure transducers were used to determine the pressure drop across the cooler assembly. A flow meter was used to measure the water flow rate through the cooler and two thermocouples measured the temperature of the water at the inlet and outlet of the cooler respectively. The temperature of the diodes was measured using the forward voltage across a single diode taken at a high sample rate of 10kHz giving the thermal step response.

4.12 Experimental Results

4.12.1 Performance comparison at constant water flow rate

The cooling performance of each of the 12 sprayplates at a constant water flow rate of *2litres/minute* is listed in Table 14. Cooling performance at a given coolant flow rate is a commonly used method of comparing the cooling performance of different coolers. The same test was performed without a sprayplate in the cooler and the data is presented also. The data in Table 14 has been sorted in order of temperature rise of the diodes, that is, the temperature difference between the diode die and the water coolant at a flow rate of *2litres/minute* when *300W* of heat is being dissipated by the two diodes. There is a significant difference in the temperature rise of the electronics being cooled by the different sprayplate geometries. Sprayplate 5 is able to maintain the diodes at a temperature of *33.19°C* above the coolant temperature, this is over *20°C* cooler than sprayplate 9. Sprayplates 1 to 7 which have *0.5mm* diameter jets cooled the diodes more effectively than sprayplates 8 to 12 which have larger diameter jets. Each of the twelve sprayplates tested offered significantly better cooling performance compared to not having a sprayplate in the cooler.

Table 14 – Cooling performance of impingement sprayplates at a water flow rate of 2 litres/minute.

<i>Sprayplate number</i>	<i>Temperature rise (°C)</i>	<i>Pressure drop (bar)</i>	<i>Pumping power (Watts)</i>
5	33.19	1.576	5.252
4	34.04	0.665	2.217
7	34.84	0.352	1.172
3	35.81	0.294	0.979
2	38.67	0.139	0.463
6	39.28	0.140	0.466
11	45.24	0.093	0.309
1	45.38	0.083	0.278
10	45.41	0.081	0.271
12	48.28	0.108	0.360
8	51.75	0.056	0.188
9	53.98	0.054	0.180
no sprayplate	68.32	0.042	0.141

4.12.2 Pumping Power Comparison

When the sprayplates are compared at a constant water flow rate as in Table 14, sprayplates 5, 4 and 7 offer the best cooling performance in terms of temperature rise of the electronics however there is a large variation in the amount of pressure drop produced across the cooler. At a water flow rate of 2litres/minute sprayplate 5 produces over four times more pressure drop across it compared to sprayplate 7 for a cooling enhancement of only 5%. Pumping power is the product of the pressure drop across the cooler in *Pascals* and the flow rate in m^3/s . In order to operate the cooler geometry of sprayplate 5, over four times as much pumping energy is required to circulate the coolant fluid compared to sprayplate 7 in return for a small gain in cooling performance as shown in Figure 79. The data in Figure 79 shows a general trend of diminishing rate of return regarding the amount of cooling generated for the amount of pumping power required.

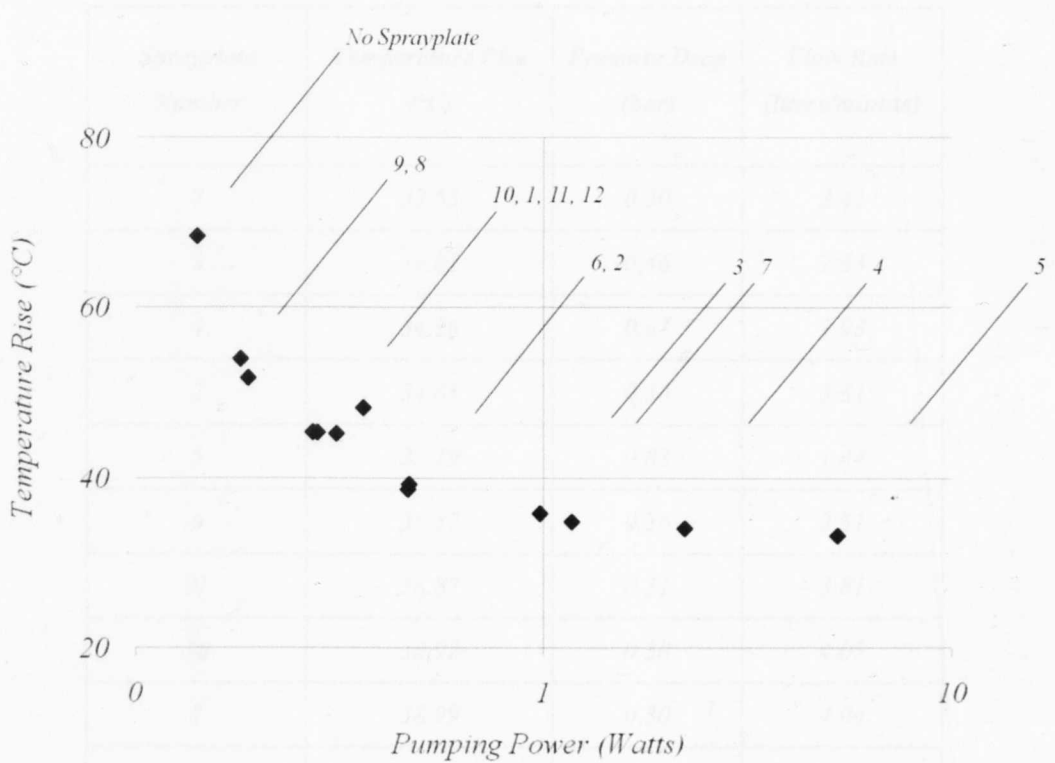


Figure 79 – Temperature rise versus pumping power at a flow rate of 2litres/minute for the 12 sprayplates tested. (Diodes dissipating 300Watts of heat. Pumping power is plotted on a logarithmic scale).

The amount of pumping power required in order to pass the water through the cooler to achieve a certain level of cooling is a way of comparing the true performance of the various sprayplate geometries. In Table 15 the performance of each sprayplate is given at a pumping power of 2Watts, the most efficient jet arrays produce the lowest temperature rise of the electronic devices. Sprayplates 8 to 12 which have jets of diameter greater than 0.5mm produced the poorest cooling of the sprayplates tested. Sprayplates 2 to 7 with 0.5mm diameter jets produced the best cooling performance. Sprayplates 2 to 7 produced similar cooling performance at a pumping power requirement of 2Watts, ranging from a temperature rise of 33.55°C for sprayplate 7 to 35.57°C for sprayplate 6. Sprayplates 7 and 3 both have jets spaced at 2mm with sprayplate 7 having a 6 x 6 array compared to the larger 7 x 7 array of sprayplate 3 indicating that of the pieces tested that a jet-to-jet spacing of 2mm produces the most efficient cooling.

Table 15 - Performance of impingement sprayplates at constant pumping power of 2Watts

<i>Sprayplate Number</i>	<i>Temperature Rise (°C)</i>	<i>Pressure Drop (bar)</i>	<i>Flow Rate (litres/minute)</i>
7	33.55	0.50	2.41
3	34.05	0.46	2.63
4	34.26	0.62	1.93
2	34.88	0.36	3.31
5	35.19	0.83	1.44
6	35.57	0.36	3.31
11	38.87	0.31	3.81
10	38.92	0.30	4.05
1	38.99	0.30	4.04
12	41.58	0.32	3.72
8	42.68	0.25	4.74
9	43.80	0.25	4.81
no sprayplate	53.62	0.22	5.38

4.12.3 Jet diameter (d)

Four pairs of arrays (sprayplates 2 & 8, 3 & 9, 4 & 10, 5 & 11) contained the same number of jets, spaced at the same distance with different jet diameters, the properties of the paired arrays are listed in Table 16. The cooling results from these pairs of arrays offer insight into the effect of jet diameter on cooling performance. When the sprayplates were operating at a pumping power of 2Watts the jet arrays with the smaller 0.5mm diameter jets cooled the devices more effectively as show in Figure 80.

Table 16 – Jet array properties for Sprayplates 2-5 and 8-11.

<i>Sprayplate number</i>	<i>Jet diameter (mm)</i>	<i>r/d (ratio of jet spacing to jet diameter)</i>	<i>Jet spacing (mm)</i>	<i>Array</i>	<i>Array size (mm)</i>
2	0.5	3	1.5	9 x 9	12
8	0.75	2			
3	0.5	4	2	7 x 7	12
9	1	2			
4	0.5	6	3	5 x 5	12
10	0.9	3.33			
5	0.5	8	4	4 x 4	12
11	1.125	3.56			

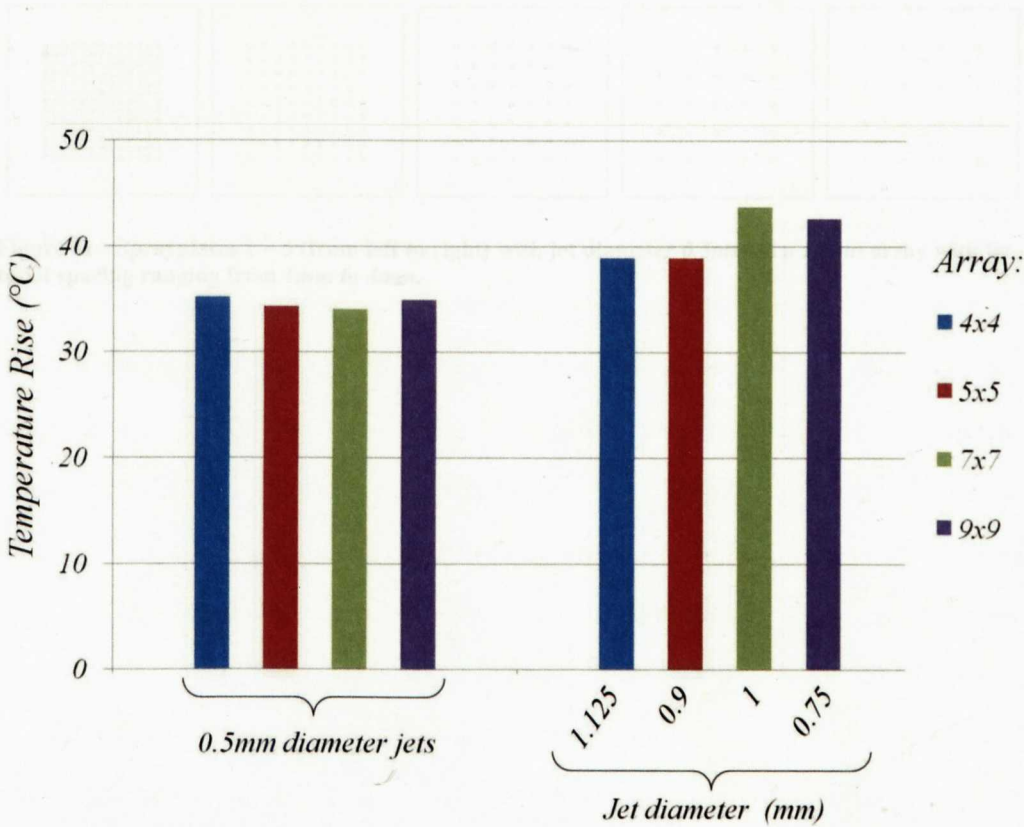


Figure 80 – Bar graph displaying temperature rise for pairs of jet arrays with different jet diameters at a pumping power of 2Watts.

4.12.4 Ratio of jet spacing to jet diameter (r/d)

Sprayplates 1 to 5 have jets of diameter 0.5mm with the jet spacing varying from 1mm up to 4mm in an array which is 12mm square. In Figure 82 the thermal performance of the five sprayplates is plotted against r/d (the ratio of jet spacing to jet diameter) at a constant pumping power of 2Watts. When r/d is low cooling performance deteriorates significantly. Sprayplate 1 with a 13x13 array of jets spaced at 1mm cools the diodes to 38.99°C above the coolant temperature, which is the poorest cooling performance of the arrays with 0.5mm diameter jets. Cooling performance also deteriorates when spacing of the jets is too high. Sprayplate 3 with a jet-to-jet spacing of 2mm in a 7 x 7 array (r/d = 4) produced the best cooling performance of the five arrays, cooling the diodes to 34.05°C above the coolant temperature. From the data presented in Figure 82 it appears that there is an optimum ratio of jet spacing to jet diameter of approximately r/d = 4.

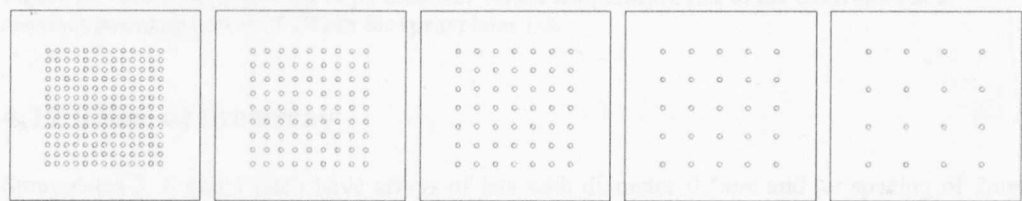


Figure 81 - Sprayplates 1 – 5 (from left to right) with jet diameter 0.5mm in a 12mm array with jet-to-jet spacing ranging from 1mm to 4mm.

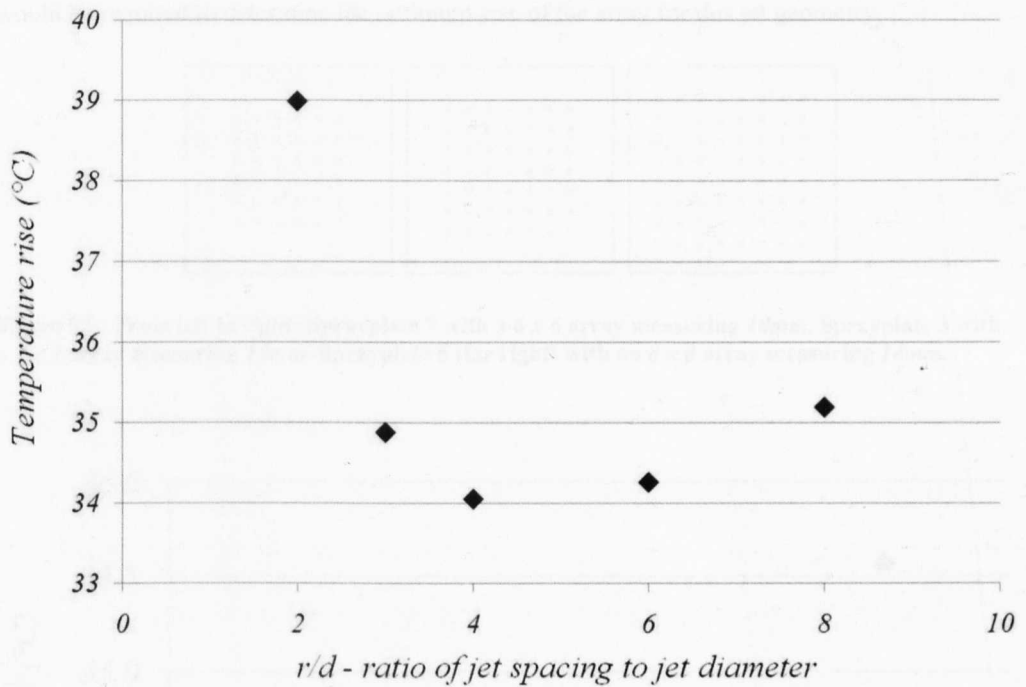


Figure 82 - Ratio of jet spacing to jet diameter versus temperature rise of the electronics at a constant pumping power of 2Watts for sprayplates 1-5.

4.12.5 Size of the array

Sprayplates 3, 6 and 7 each have arrays of jets with diameter 0.5mm and jet spacing of 2mm resulting in a ratio of $r/d = 4$. Sprayplate 7 has a 6×6 array of size 10mm , sprayplate 3 has a 7×7 array of size 12mm and sprayplate 6 has an 8×8 array measuring 14mm . The comparison of the performance of these three sprayplates helps determine how the size of the jet array affects the cooling performance and the effect of heat spreading between the electronic die and the cooled surface on the underside of the substrate tile. Sprayplate 7 with a 10mm array maintained the diodes at a slightly lower temperature than sprayplate 3 with a 12mm array when compared at the same pumping power of 2Watts. Sprayplate 6 which was the largest array tested measuring 14mm produced poorer cooling compared to the other two sprayplates. It is interesting that sprayplate 7 measuring $10\text{mm} \times 10\text{mm}$ which had the smallest array produced the most efficient performance of all of the 12 sprayplates tested, cooling the diodes to 33.55°C above the coolant temperature at a pumping power of 2Watts. When looking at the results plotted in Figure 84 the smaller 10mm array produces more cooling than both the 12mm and 14mm arrays but it is not clear whether the minimum temperature rise has been reached.

The best performance may be produced by an even smaller array with $r/d = 4$. Further tests would be required to determine the optimum size of the array for this jet geometry.

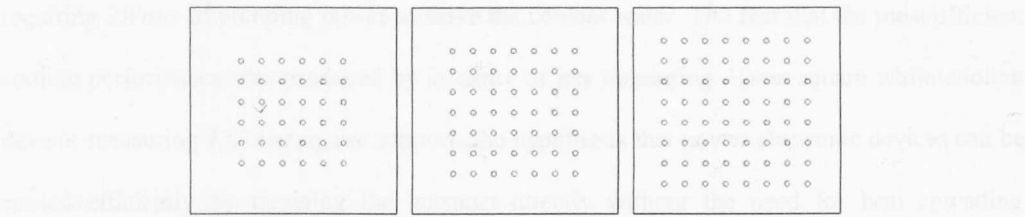


Figure 83 - From left to right: Sprayplate 7 with a 6 x 6 array measuring 10mm. Sprayplate 3 with a 7 x 7 array measuring 12mm. Sprayplate 6 (far right) with an 8 x 8 array measuring 14mm.

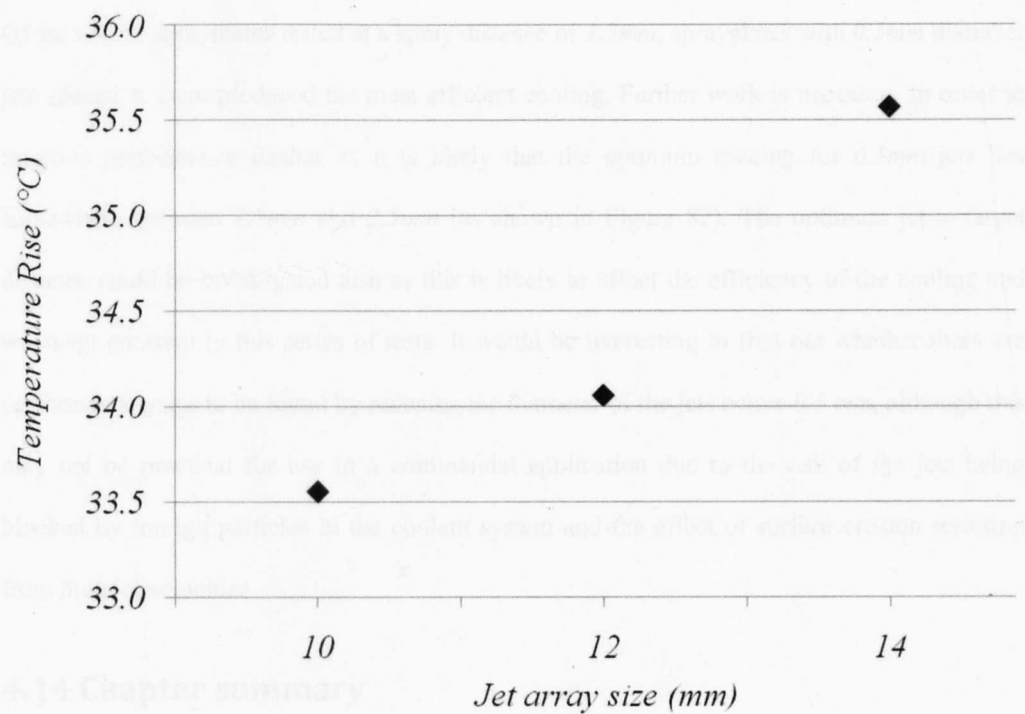


Figure 84 - The effect of the size of the jet array on cooling performance at a pumping power of 2Watts for three jet arrays with $r/d = 4$.

4.13 Experimental testing summary

From the experimental results it is clear that when comparing different jet array geometries it is necessary to take into account the pressure drop across the cooler at a given flow rate. The product of the pressure drop and flow rate determines the amount of pumping power required to pass the coolant fluid through the cooler. It is best to compare the performance of different spray array geometries while they are both operating at the same rate of pumping power. In this way it is possible to determine the most efficient jet impingement array geometries. Sprayplate 7 with a 6 x 6 array of 0.5 mm diameter jets, spaced at 2mm produced the most efficient cooling

performance of all of the 12 sprayplates tested. Sprayplate 7 maintained the two diodes 33.55°C above the water temperature while they were dissipating 300Watts of heat while requiring 2Watts of pumping power to drive the coolant water. The fact that the most efficient cooling performance was produced by an array of jets measuring 10mm square while cooling devices measuring 12.7mm square supports the hypothesis that power electronic devices can be cooled efficiently by targeting the hotspots directly without the need for heat spreading baseplates to be included in the assembly.

4.13.1 Further Work

Of the twelve sprayplates tested at a spray distance of 1.5mm , sprayplates with 0.5mm diameter jets spaced at 2mm produced the most efficient cooling. Further work is necessary in order to improve performance further as it is likely that the optimum spacing for 0.5mm jets lies somewhere between 1.5mm and 2.5mm (as shown in Figure 82). The optimum jet-to-target distance could be investigated also as this is likely to affect the efficiency of the cooling and was kept constant in this series of tests. It would be interesting to find out whether there are performance gains to be found by reducing the diameter of the jets below 0.5mm , although this may not be practical for use in a commercial application due to the risk of the jets being blocked by foreign particles in the coolant system and the effect of surface erosion resulting from high jet velocities.

4.14 Chapter summary

The focus of this chapter was jet impingement cooling and the design of efficient jet array geometries for direct substrate cooling of power electronics. A detailed overview of the parameters affecting the cooling performance of jet arrays is presented. Correlations describing the expected heat transfer performance of impingement arrays were applied to the experimental results from the previous chapter. The existing correlations predicted the heat transfer to the same order of magnitude as the measured results but it was felt that they did not satisfactorily predict the heat transfer performance and further experimental testing was necessary. A test apparatus was constructed where two diodes were used as a heat source. Each diode was cooled by its own jet array located directly beneath it. 12 different array geometries were designed using the findings from the research in order to confirm the hypothesis that it is more

efficient to target the hotspot directly beneath the device rather than cooling a larger surface area with an evenly distributed heat transfer coefficient. The most efficient array geometry of the 12 tested consisted of a 6×6 array of 0.5mm diameter jets spaced at 2mm while the diodes measured 12.7mm square. It is not clear from the results whether this array geometry is the optimum for direct substrate cooling a device of this size. More experimental work will be necessary to determine the optimum jet array design for cooling this device.

Chapter 5

5 Improving the jet impingement array for the cooling of a single power electronic device

5.1 Introduction

The testing of multiple jet impingement array geometries described in the previous chapter produced promising results. The potential heat transfer performance of a jet impingement array in combination with direct substrate cooling resulted in efficient cooling of the electronic devices. A pair of diodes, each measuring $12.7mm$ square, dissipating $300W$ of heat in total, were maintained at $33.55^{\circ}C$ above the coolant temperature while only $2Watts$ of pumping power was required to drive the coolant water. It was decided to perform additional experimental tests of jet impingement arrays designed to directly cool a single power electronic device in order to build on the results from the previous chapter and to determine the optimum jet-to-target distance (H) and jet-to-jet spacing (r) for a 6×6 array of $0.5mm$ diameter jets. A new test apparatus was constructed for the direct substrate cooling of a single $12.7mm$ square diode where the spent fluid exhausts in a single direction. Two series of tests were performed: The first involved varying the jet-to-target distance (H), the second involved varying the jet-to-jet spacing (r). The temperature of the diode was monitored using an infra red thermal imaging camera and the upper surface temperature was used to determine the relative cooling performance of the various jet impingement test pieces. The experimental results were analysed and optimum values of jet-to-target distance (H) and jet-to-jet spacing (r) were determined.

5.1.1 Finding the optimum

For a given combination of coolant fluid, flow rate and allowable pressure drop there is an optimum arrangement of jets which can cool a specific heat source most efficiently. For the experimental tests the heat source is a $12.7mm$ square diode soldered onto an AlN substrate tile as this is representative of a power module assembly suitable for direct substrate cooling. The diode was energised to dissipate $150Watts$ of heat, resulting in a heat flux of $93W/cm^2$ as this is

representative of a typical power electronic heat source. Jet geometries can be optimised for cooling performance by limiting the maximum flow rate, pressure drop or pumping power. In practice, multiple coolers can be cascaded in series with the spent fluid from one cooler passing into the next and so on until the temperature of the coolant is too high thereby maximising the volume of coolant available. It is more important to minimise the pumping power, or to maximise the amount of cooling generated for a given amount of pumping power, as this relates to the ultimate energy cost of operating the cooler. When comparing two coolers at the same rate of pumping power, the more efficient system will maintain the electronic devices at a lower temperature.

5.2 Improving the test rig

In order to characterise the performance of the jet impingement arrays for the cooling of a *12.7mm* square *Si* diode soldered onto the *AlN* substrate tile it was decided to assemble a new test apparatus to improve on the design used in the previous chapter in order to further differentiate between the relative performance of the various array geometries and to allow the spray distance to be modified. In the previous tests two identical jet impingement arrays, laser cut from a single alumina sprayplate cooled two diodes in parallel. The sprayplates were tested over a range of flow rates up to *4 litres/minute*. When the jet arrays were operating at a flow rate requiring *2Watts* of pumping power there was little difference (less than *1°C*) between the cooling performance of the best 3 arrays. In order to improve the resolution of the results it was decided to test the arrays over a wider range of flow rates and to compare the relative performance of the jet arrays at a higher rate of pumping power. This can be achieved by having a single diode as the heat source cooled by a single impingement array (rather than two in parallel), therefore doubling the volumetric flow rate through the single jet array.

5.2.1 Ideal design versus practical layout

Existing heat transfer correlations for the performance of jet impingement arrays tend to assume that the spent fluid after impingement exhausts equally in all directions. In order to implement such a design to cool a typical power module, consisting of multiple devices on a single ceramic substrate, intricate inlet and exit manifolds for the coolant fluid would need to be constructed, greatly increasing the complexity and manufacturing cost of the cooler. One of

the key drivers of this work is to simplify the power module assembly in order to improve its reliability rather than introducing additional complexity to the cooling system. Even if multiple exits are provided around the perimeter of the power module the spent fluid will follow the path of least resistance and this is likely to be in a single direction for each jet array assuming each exit is shared by more than one array. In order for the spent fluid from a single array to exhaust equally in all directions each jet array would require its own concentric exhaust manifold which is carefully constructed to produce a uniform pressure drop along its perimeter as shown in Figure 85. A concentric manifold for each impingement array would only be practical for very expensive or system critical devices and is not a suitable alternative to the commonly used serpentine coldplate. A complex manifold design for each individual device would also negate some of the key advantages of a direct substrate jet impingement cooling system, such as ease of implementation, low cost, low volume and low mass.

Figure 85 – Exit routes around the coldplate. The arrows indicate the direction of the fluid flow after impingement.

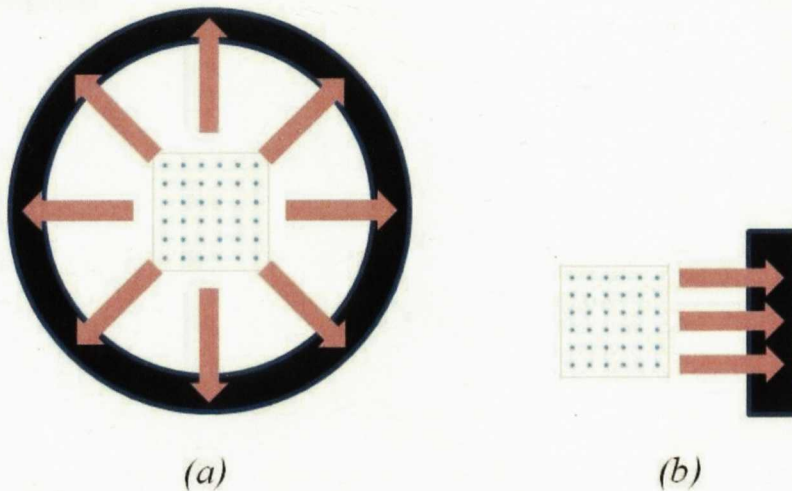


Figure 85 – Exit routes are shown in black, the arrows indicate the direction of flow. (a) In the ideal case after impingement the spent fluid exhausts equally in all directions. (b) In a real situation the spent fluid exhausts towards the nearest exit. Existing heat transfer correlations tend to describe case (a) although this is difficult to implement in practice.

The test apparatus is designed with a single exit route for the spent fluid, 24mm wide, located along the edge of the substrate tile nearest to the device as shown in Figure 86. A more detailed cross-section of the design is shown in Figure 87. The jet array is located directly beneath the diode and the entire underside of the substrate tile is in contact with the coolant water. A stand was constructed to hold the test assembly upright in order to prevent air being trapped in the cooler.

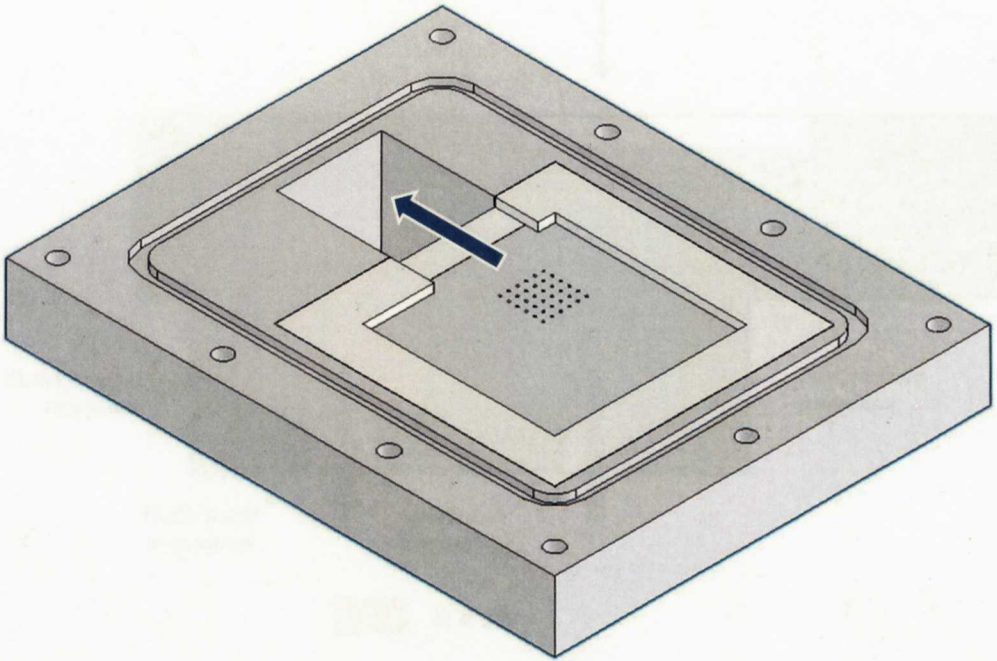


Figure 86 – CAD drawing of the test assembly. The arrow indicates the direction of the water flow after impingement.

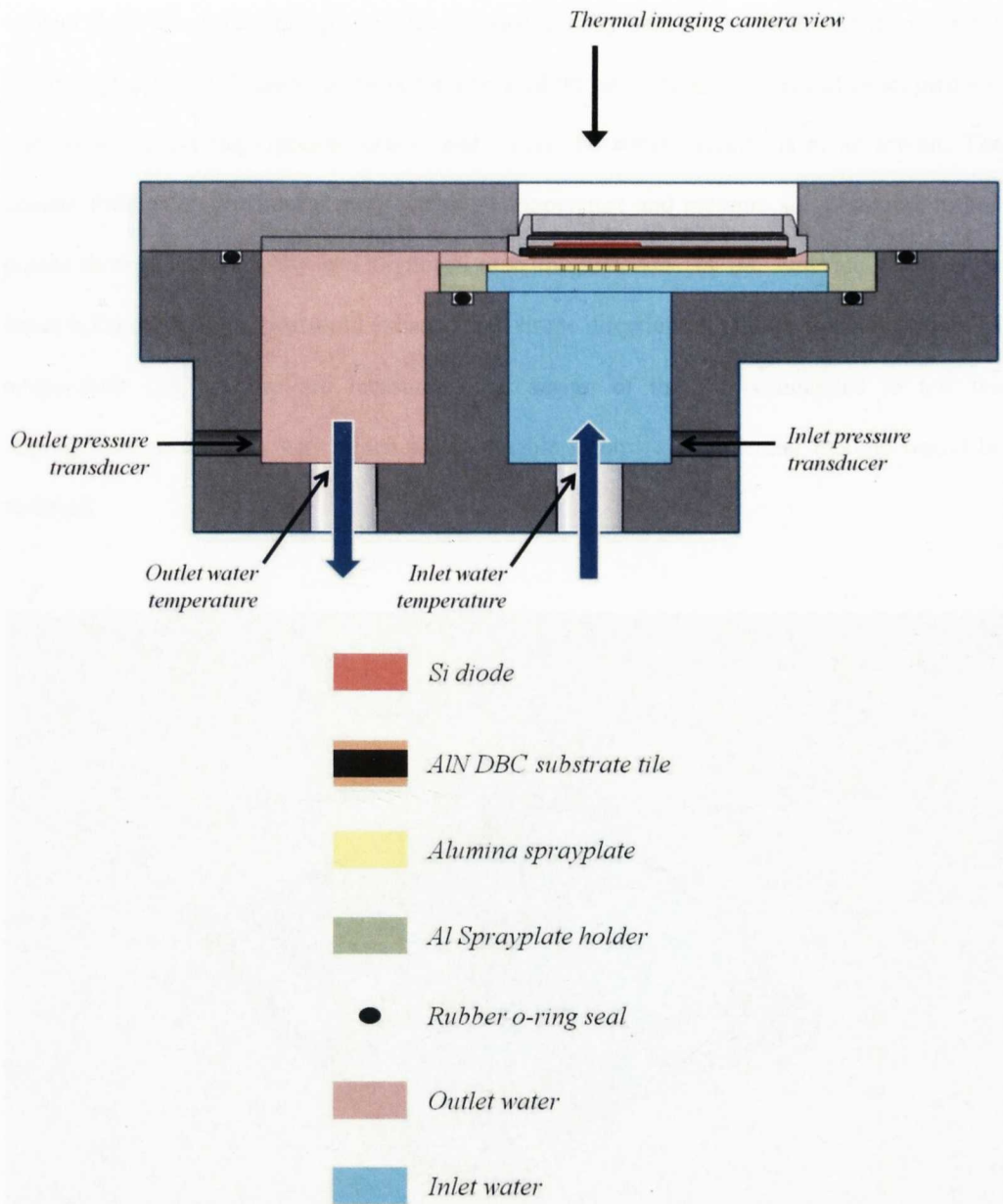


Figure 87 – A cross-sectional view of the test assembly with key parts labelled and colour coded.

5.2.2 Test apparatus design and assembly

A single 12.7mm square diode was soldered onto the *AlN* substrate tile (shown in Figure 88) and aluminium wires were bonded on (as shown in Figure 89). The tile was mounted in a plastic holder which was in turn mounted in the top of a newly built sprayplate test assembly machined from aluminium. The candidate jet arrays, laser cut from from alumina were mounted into aluminium holders (Figure 92). The aluminium sprayplate holders are 6mm thick and can be machined to allow the spray distance to be modified from zero up to a maximum spray distance of 4mm if a 1mm thick sprayplate is used. Deionised water was used as the

coolant fluid. The water inlet plenum was located directly beneath the diode and therefore the jet array (Figure 93). Pressure transducers measured the pressure at the inlet and outlet plenums near to where the impingement occurs and where the water velocity is at its lowest. The coolant fluid enters the inlet plenum where its temperature and pressure are measured, it then passes through the jet array and impinges onto the underside of the substrate tile directly beneath the diode. The spent fluid exhausts in a single direction into the exit plenum where its temperature and pressure are measured. The design of the rig is intended to test the impingement arrays in a way which is comparable to how a commercial module would be arranged.

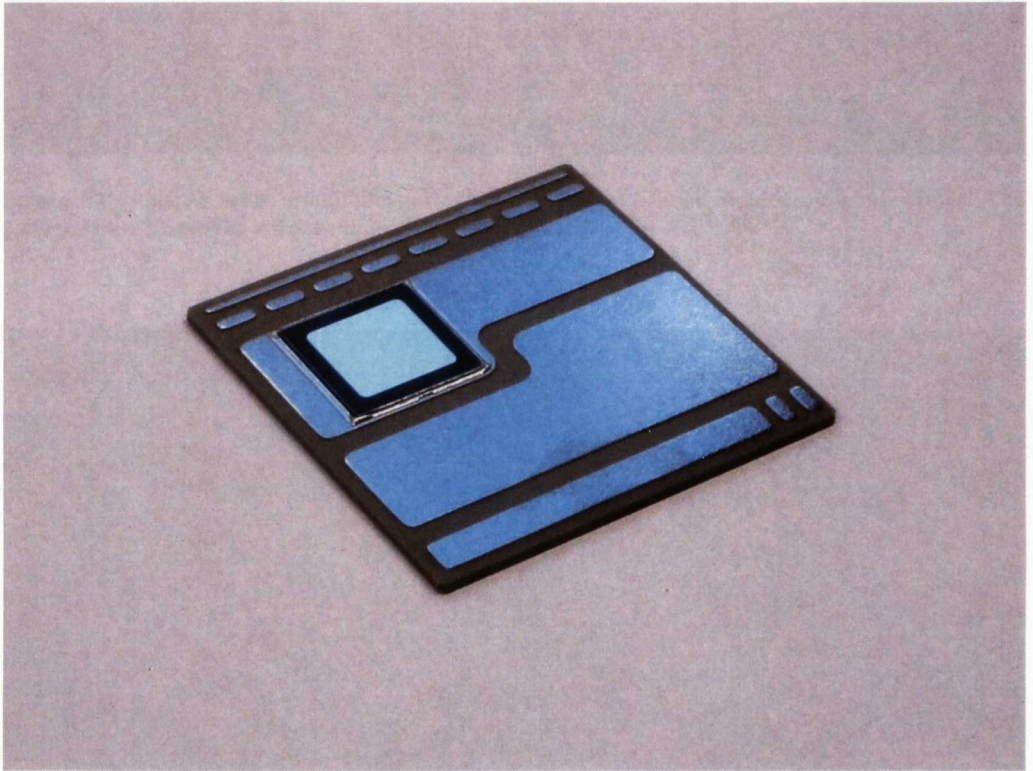


Figure 88 – The Aluminium-Nitride substrate tile with the single test diode soldered on using $100\mu\text{m}$ thick $\text{Sn}3.5\text{Ag}$ solder foil.

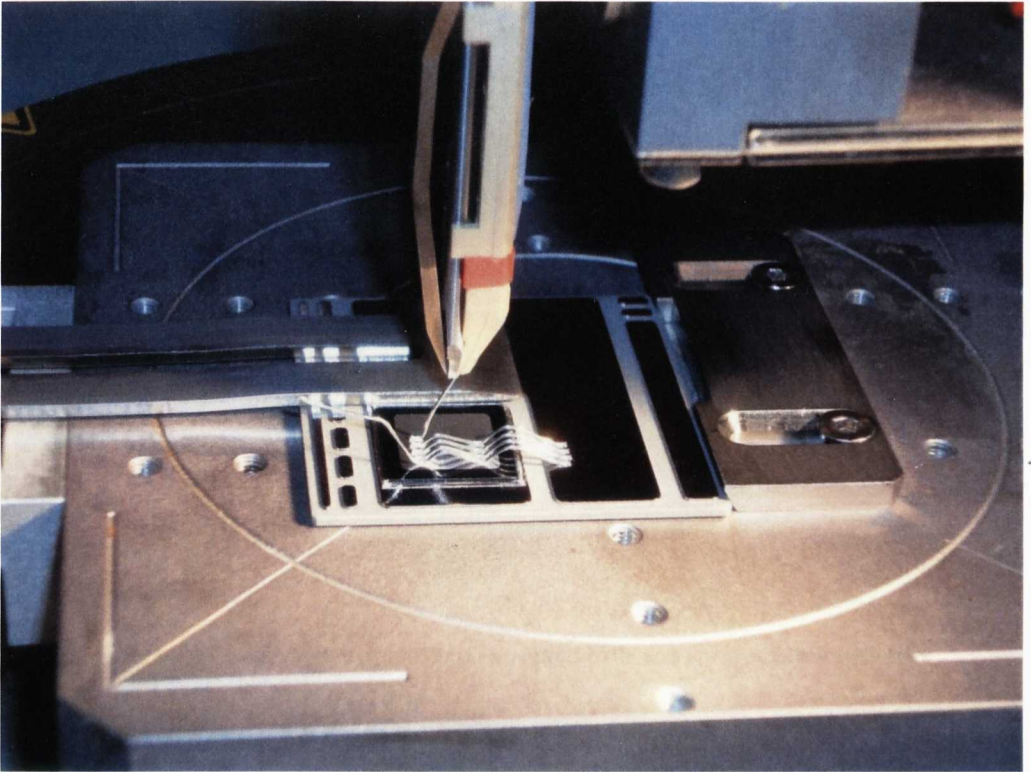


Figure 89 – $500\mu\text{m}$ thick aluminium wires were sonically friction welded onto the device. The picture above shows the wirebonding in progress.

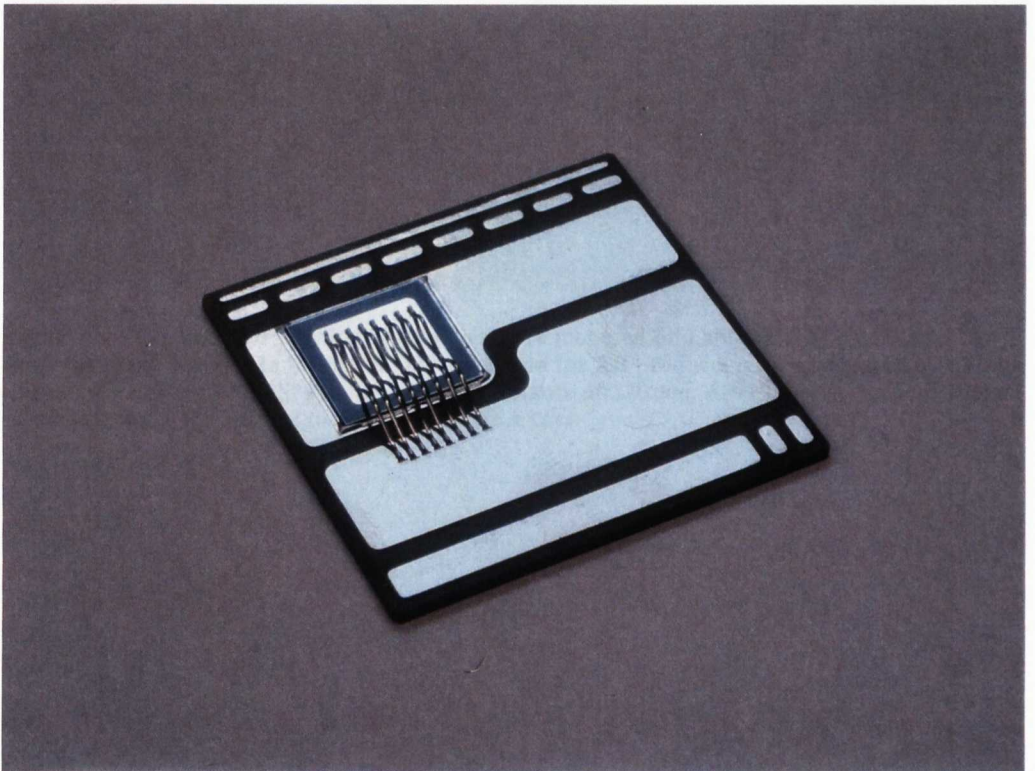


Figure 90 – The tile with 8 wirebonds attached.

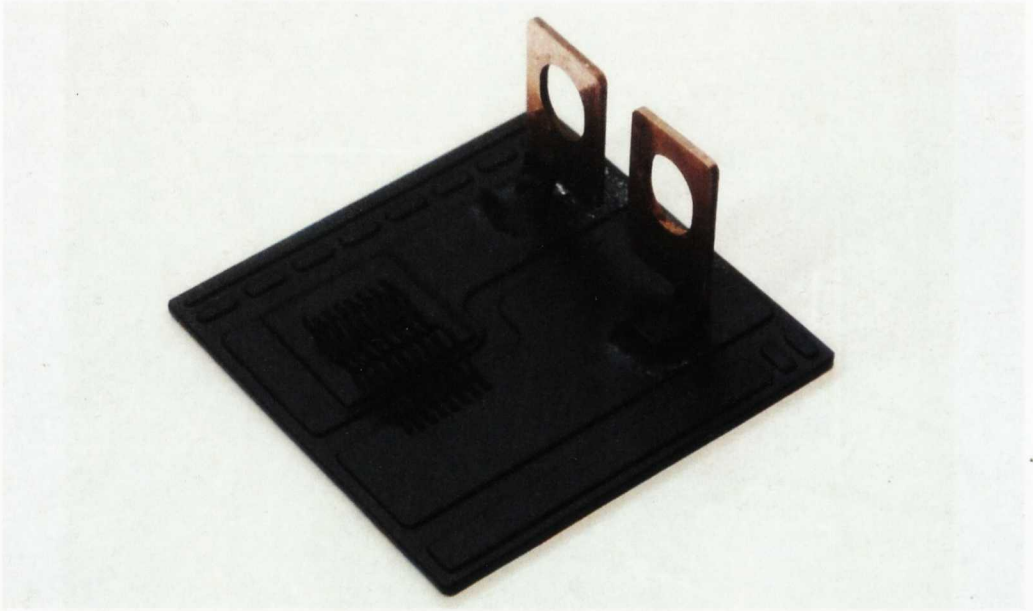


Figure 91 – Electrical connectors were soldered on and the tile was sprayed black with high emissivity paint to aid thermal imaging.

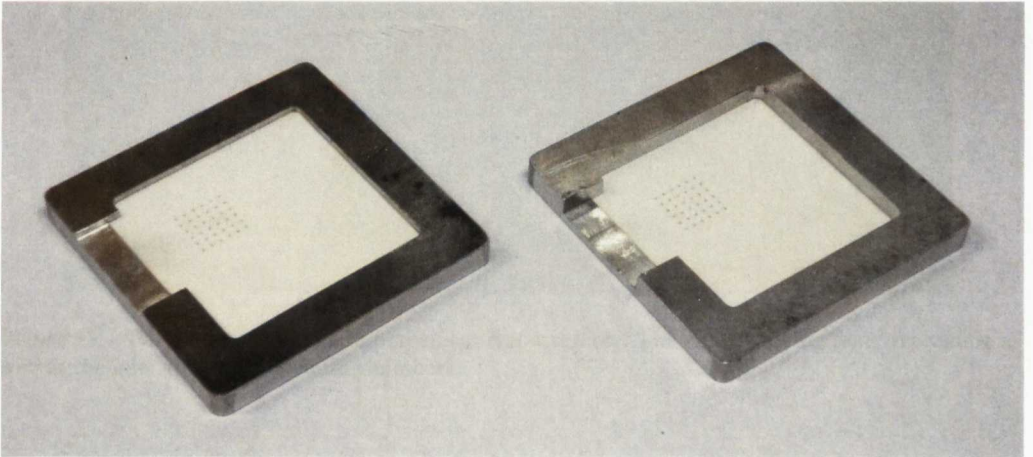


Figure 92 – The laser-cut alumina sprayplates were mounted into aluminium holders in order to allow the spray distance to be varied. The holder on the left produces a spray distance of 0.41mm whereas the one on the right produces a spray distance of 2.93mm . After impingement the coolant exhausts through the channel to the left of the jet arrays.

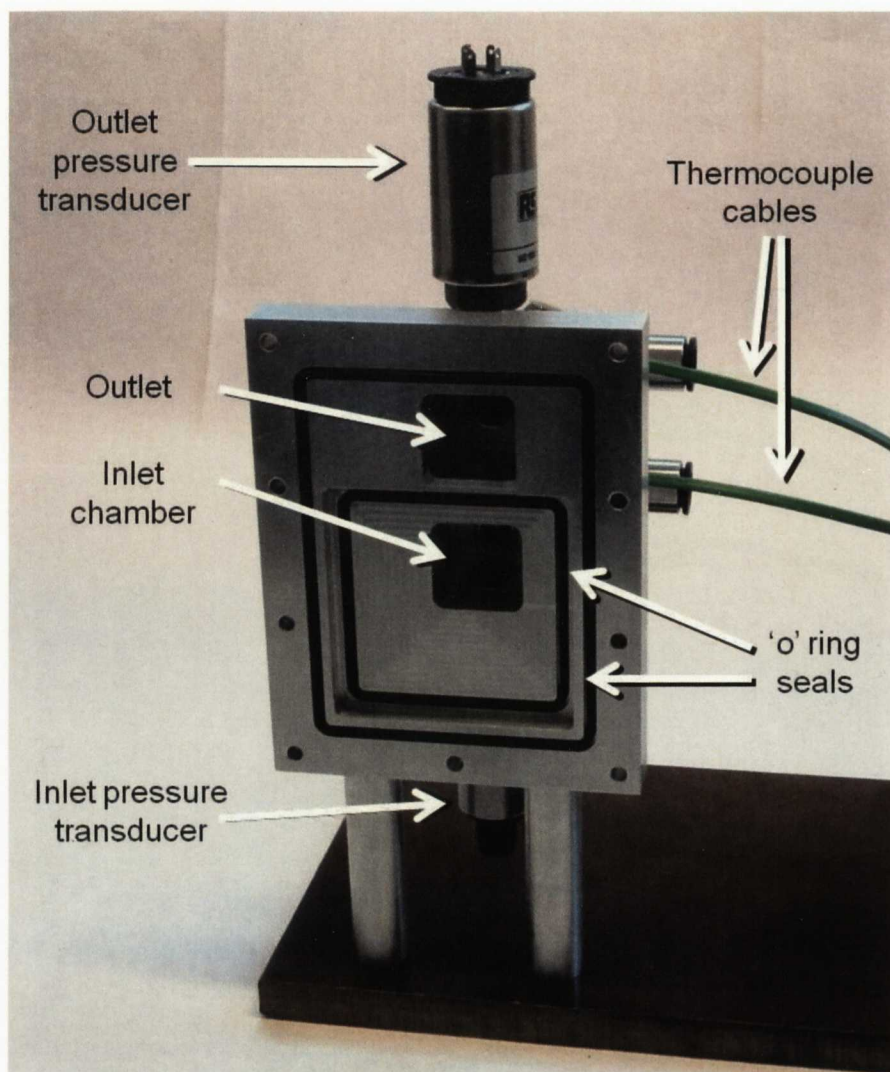


Figure 93 – The main part of the impingement test assembly. The rubber o-ring seals are visible as well as the inlet and outlet plenum chambers.

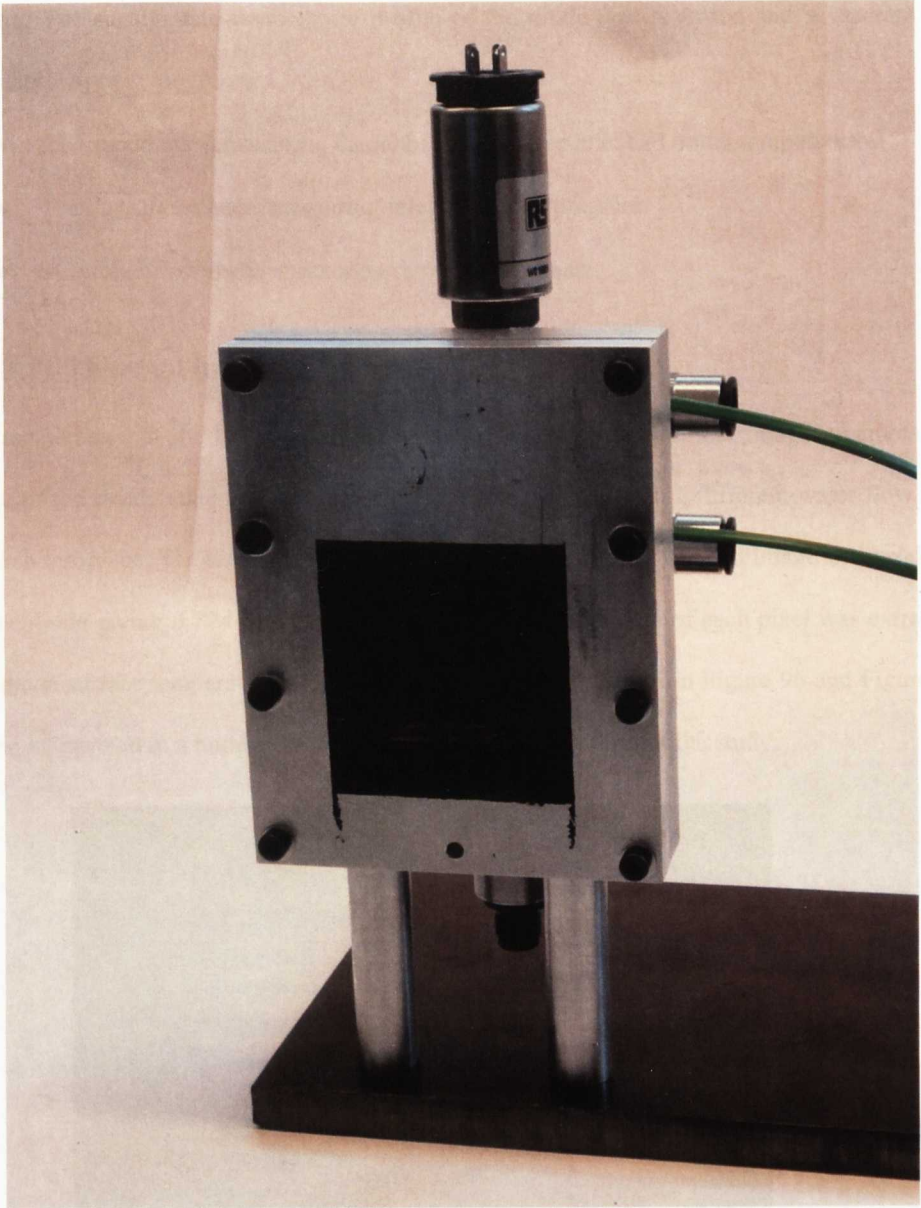


Figure 95 – The second half of the assembly has been mounted, compressing the o-rings and forming a water-tight seal.

5.2.3 Testing regime

The candidate impingement arrays were tested over a range of flow rates up to *5litres/minute*. The flow rate and pressure drop across each sprayplate was recorded and therefore the pumping power required to drive the coolant was calculated. The water was maintained at 40°C by a dedicated chiller unit and the flow rate was varied from 2 to *5litres/minute* in 8 approximately equal steps using a variable speed pump. The diode was energised to dissipate *150Watts* of heat and its surface temperature was monitored using an infra red thermal imaging

camera. The steady state temperature profile of the diode was recorded and a separate data acquisition system logged data from:

- Thermocouples measuring the ambient air, water inlet and outlet temperatures.
- Pressure transducers measuring inlet and outlet pressure.
- A turbine flow meter measuring the water flow rate.

5.2.3.1 Thermal imaging

The temperature of the diode was recorded using an infra red thermal imaging camera. An image of the steady state temperature of the diode was recorded at 8 different water flow rates for each test piece. The lens was centred on the diode and an 82×82 pixel image was produced for the diode giving 6,724 data points from which the temperature of each pixel was extracted. The diode surface temperature plot (examples of which are shown in Figure 96 and Figure 97) can be interpreted in a number of ways depending on the criteria of the study.

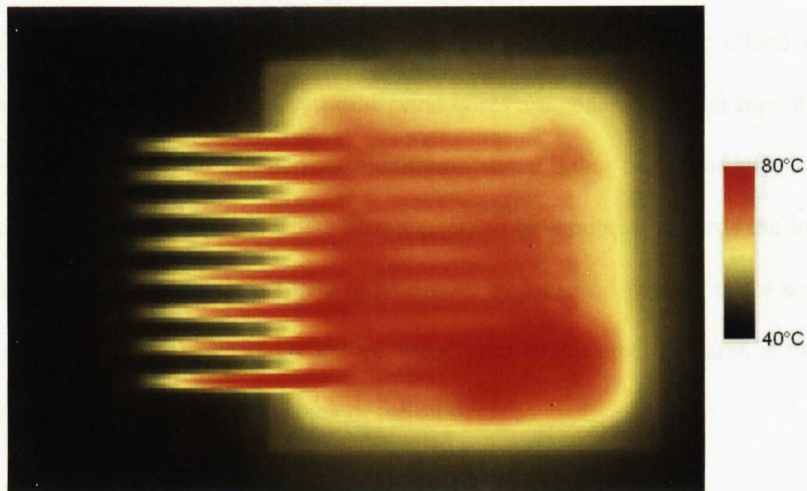


Figure 96 – A thermal image of the diode dissipating 150Watts. Water flow rate 2.13litres/minute, spray distance 1.43mm.

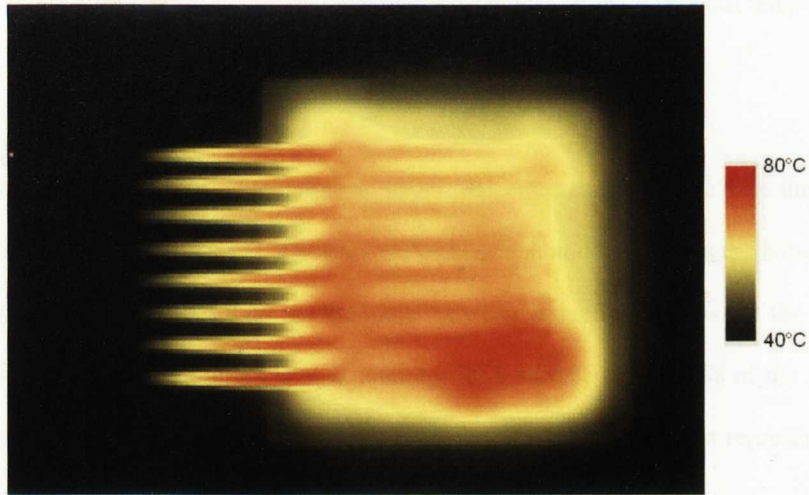


Figure 97 – Diode dissipating 150Watts. Water flow rate 5.11litres/minute, spray distance 1.43mm.

5.2.3.2 Diode temperature plot

In Figure 96 and Figure 97 the thermal image of the diode is shown at two different water flow rates: 2.13litres/minute and 5.11litres/minute respectively. The average and peak temperature of the diode is lower in Figure 97 indicating that it is being cooled more effectively at the higher water flow rate. At both flow rates the bond wires are generally hotter than the surface of the device. This is due to the narrow aluminium wires being heated as they carry over 100Amps of current between them. There also appears to be a hotspot towards the lower right corner of the diode. The hot spot is likely to be caused by localised voiding in the solder layer increasing the thermal resistance and therefore temperature in this area. The area of the hot spot accounts for approximately 5% of the area of the diode.

5.2.3.3 Defining the diode temperature

The reliability of a power electronic device is directly affected by temperature cycling. Hotter parts of the device will experience temperature cycles of larger amplitude. High temperatures amplify the effects of differences in thermal expansion rates between the adjoining layers of the assembly and exacerbate material and bond failure when the device is power cycled. For the assembly under test the long term failure mechanisms are likely to be related to cracking in the solder layer between the device and the substrate tile and failure of the bond wires either by heel crack or lift-off. The ultimate aim of the work is to improve power module reliability in which case the highest temperatures experienced by the device and bond wires should be

minimised rather than simply the overall average temperature or the minimum temperature of the device.

A percentile function can be used to define an upper temperature of the diode from the range of temperatures in the thermal images. The percentile chosen should be towards the hottest end of the temperature range in order to differentiate between the effectiveness of the different cooling assemblies. Due to the hot spot accounting for a surface area of 5% of the diode the 90th percentile of the temperature range was considered to offer a consistent representation of the upper temperature of the device and wirebonds.

The temperature at the centre of the diode can be used as an indication of the average temperature of the silicon device. The peak temperatures in the thermal image plots relate to peak wirebond temperatures. It was found that the average of the diode centre temperature and the peak temperature in the thermal images is linearly proportional with the 90th percentile temperature as shown in Figure 98. In this study the performance of the various jet impingement test pieces is compared using the average of the temperature at the centre of the diode and the peak temperature of the diode surface to describe the temperature of the device.

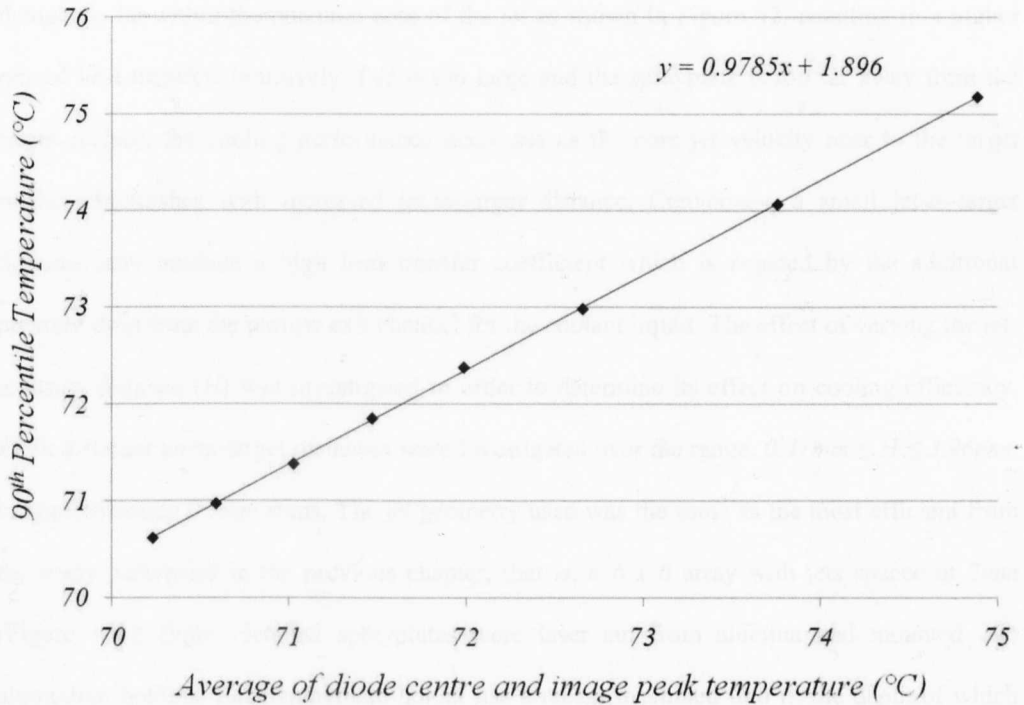


Figure 98 – The temperature of the 90th percentile and the average of the diode centre and peak temperature in the thermal images was found to have a linear relationship.

5.2.4 Variable parameters

The relative cooling performance of the candidate jet impingement arrays are compared using the temperature difference between the diode and the coolant water at a given level of pumping power. From the set of tests performed in the previous chapter, the arrays with 0.5mm diameter jets were found to offer the most efficient cooling performance. For this set of experiments the jet diameter was fixed at 0.5mm . The sprayplate thickness was also fixed at 1mm . The tests involved square arrays with regularly spaced jets. A 6×6 array of jets was used as this was the best performing array from the experiments described in the previous chapter. This leaves two key parameters which can be varied: The jet to target distance, H , and the jet-to-jet spacing, r . The following parameters were varied over two sets of tests in order to more closely define how each parameter individually affects cooling performance and efficiency:

- Jet to target distance – H
- Jet-to-jet spacing – r

5.3 Jet-to-target distance - H

The jet-to-target distance for the tests performed in the previous chapter was kept constant at $H=1.5\text{mm}$. For 0.5mm diameter jets, $H=1.5\text{mm}$ equates to three jet diameters as this was

thought to lie within the potential core of the jet as shown in Figure 62, resulting in a higher rate of heat transfer. Intuitively if H is too large and the sprayplate is too far away from the target surface, the cooling performance decreases as the core jet velocity near to the target surface diminishes with increased jet-to-target distance. Conversely, a small jet-to-target distance may produce a high heat transfer coefficient which is negated by the additional pressure drop from the narrow exit channel for the coolant liquid. The effect of varying the jet-to-target distance (H) was investigated in order to determine its effect on cooling efficiency. Eight different jet-to-target distances were investigated over the range, $0.41\text{mm} \leq H \leq 3.96\text{mm}$; in approximately 0.5mm steps. The jet geometry used was the same as the most efficient from the study performed in the previous chapter, that is, a 6×6 array with jets spaced at 2mm (Figure 100). Eight identical sprayplates were laser cut from alumina and mounted into aluminium holders. Each sprayplate holder has a recess machined into it, the depth of which determines the jet-to-target distance. Figure 99 shows test pieces A and J which represent the smallest and largest jet-to-target distances investigated in this study and each jet-to-target distance tested is listed in Table 17.

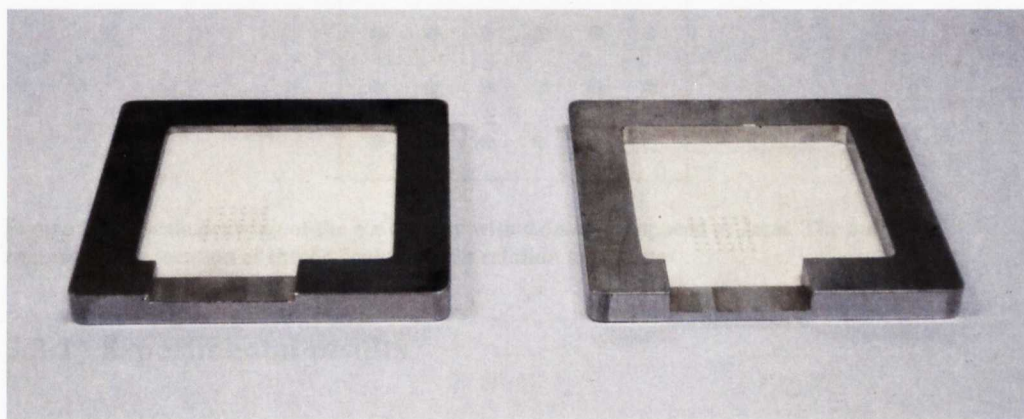


Figure 99 – Test pieces A (left) and J produce a jet-to-target distance of 0.41mm and 3.96mm respectively. Each alumina sprayplate is identical, a recess machined into the aluminium holder determines the jet-to-target spray distance (H). The spent fluid exhausts through the 24mm wide exit channel.

Table 17 – The eight jet-to-target distances which were tested. Each test piece was assigned a letter.

<i>Jet-to-target distance - H (mm)</i>	<i>Assigned letter</i>
0.41	A
0.90	B
1.43	C
1.91	D
2.46	E
2.93	F
3.39	G
3.96	J

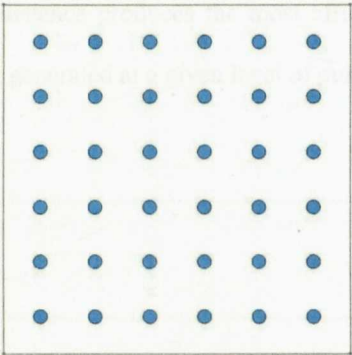


Figure 100 – Scale drawing of the 6 x 6 array with 0.5mm jets spaced at 2mm. The outline represents the location of the 12.7mm diode in relation to the jets

5.3.1 Experimental results

5.3.1.1 Temperature rise at constant water flow rate

In Figure 101 the diode temperature rise is plotted against jet-to-target distance at a constant water flow rate of 4litres/minute. Test piece B with a jet-to-target distance of 0.9mm produces the most effective cooling of the eight test pieces at this flow rate, maintaining the diode at 31.76°C above the coolant temperature. Cooling performance deteriorates as the jet-to-target distance is increased indicating a degradation of the jets before impingement on the target surface. As the jet-to-target distance is increased above 3mm the temperature rise of the diode appears to increase proportionally less indicating that the cooling enhancement of the jets is

having a lesser effect. At a flow rate of *4litres/minute* without an impingement sprayplate in the test assembly the diode was maintained at 54.7°C above the coolant temperature. As the jet-to-target distance is increased further above *4mm* the temperature rise of the diode will follow an asymptote towards 54.7°C . It is interesting that the temperature rise of the diode increased at the small jet-to-target distance of *0.41mm*. This is likely to be due to the jet-to-target distance being so small that the jets are not forming properly reducing the amount of cooling produced.

When the test pieces are compared at a constant water flow rate of *4litres/minute* test pieces *B* and *C* with a jet-to-target distance of *0.9mm* and *1.43mm* respectively, cooled the diode most effectively. The temperature rise of the diode and the amount of pressure drop produced for test pieces *A-E* is listed in Table 18. The pressure drop and therefore the pumping power requirement across the test pieces increases as the jet-to-target distance is decreased. In order to determine which jet-to-target distance produces the most efficient cooling it is necessary to compare the amount of cooling generated at a given level of pumping power.

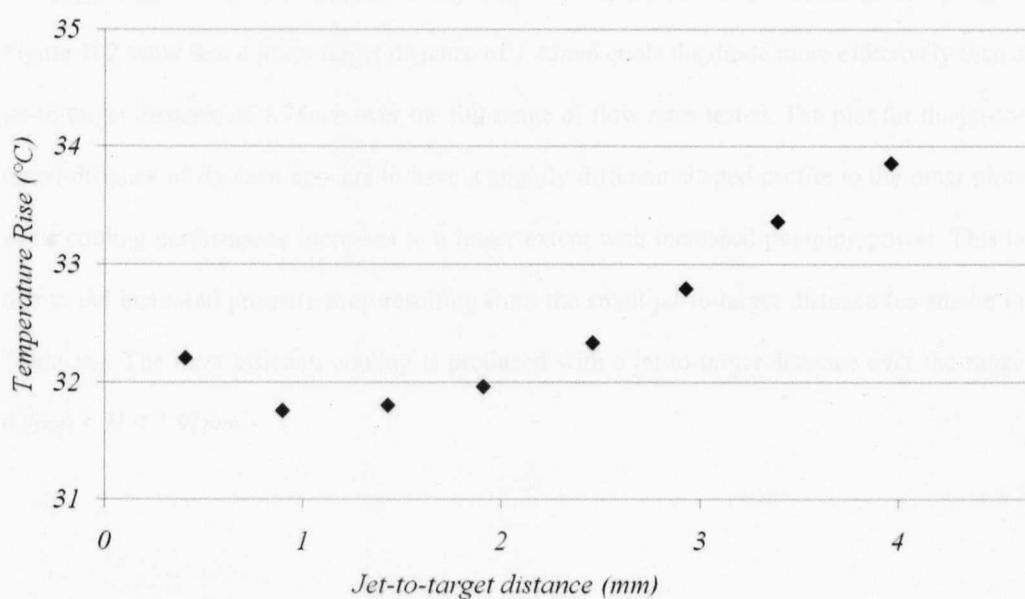


Figure 101 – Diode temperature rise versus jet-to-target distance at a constant water flow rate of *4litres/minute*.

Table 18 – Diode temperature rise, pressure drop and pumping power at a water flow rate of 4litres/minute.

<i>Test piece</i>	<i>Jet-to-target distance (mm)</i>	<i>Temperature rise (°C)</i>	<i>Pressure drop (bar)</i>	<i>Pumping power (Watts)</i>
<i>A</i>	<i>0.41</i>	<i>32.20</i>	<i>0.697</i>	<i>4.65</i>
<i>B</i>	<i>0.9</i>	<i>31.75</i>	<i>0.478</i>	<i>3.19</i>
<i>C</i>	<i>1.43</i>	<i>31.80</i>	<i>0.443</i>	<i>2.95</i>
<i>D</i>	<i>1.91</i>	<i>31.96</i>	<i>0.437</i>	<i>2.92</i>
<i>E</i>	<i>2.46</i>	<i>32.33</i>	<i>0.430</i>	<i>2.87</i>

5.3.2 Diode temperature rise and pumping power

In Figure 102 the diode temperature rise is plotted against pumping power for each of the eight test pieces. From the figure one can see that each jet-to-target distance produces a relatively similarly shaped relationship between temperature rise of the diode and pumping power with the curves appearing to be offset in the y-direction. Each of the eight plots shows an asymptotic relationship of temperature rise with pumping power indicating that the additional amount of cooling generated increases proportionally less as pumping power is increased. The plots in Figure 102 show that a jet-to-target distance of 1.43mm cools the diode more effectively than a jet-to-target distance of 3.96mm over the full range of flow rates tested. The plot for the jet-to-target distance of 0.41mm appears to have a slightly different shaped profile to the other plots as its cooling performance increases to a lesser extent with increased pumping power. This is due to the increased pressure drop resulting from the small jet-to-target distance (as shown in Table 18). The most efficient cooling is produced with a jet-to-target distance over the range $0.9mm < H < 1.91mm$.

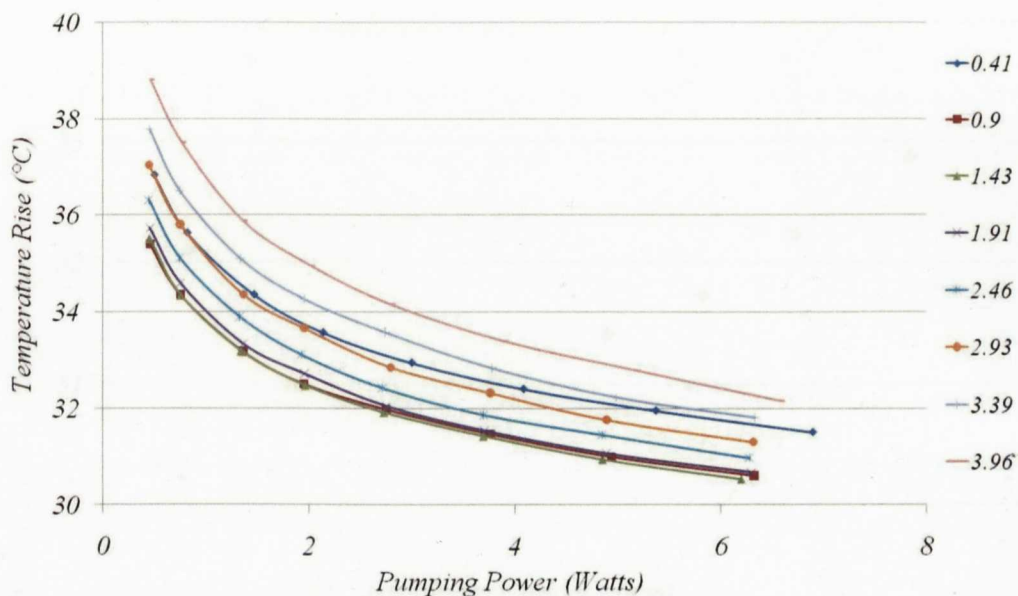


Figure 102 – Diode temperature rise versus pumping power for each of the eight test pieces. The jet-to-target distance in millimetres is listed to the right of the figure.

5.3.3 Diode temperature rise at constant pumping power

In Figure 103 the temperature rise of the diode is plotted against jet-to-target distance at a constant pumping power of 5Watts. Cooling performance appears to deteriorate as the jet-to-target distance is increased above 1.91mm. Cooling performance also deteriorates more strongly as the jet-to-target distance is decreased below 0.9mm. In Figure 103 one can see that the diode was cooled most effectively at a jet-to-target distance of 1.43mm resulting in a temperature rise of 30.89°C, the temperature of the diode varies by a relatively small amount when the jet-to-target distance is increased or decreased from this value by one jet diameter ($d = 0.5mm$). The temperature of the diode is 0.15°C hotter if the spray distance is increased to 1.91mm and 0.1°C hotter if the jet-to-target distance is decreased to 0.9mm. The jet-to-target distance of 1.43mm is approximately 3 jet diameters. The most efficient jet performance is found for a jet-to-target distance over the range $2d \leq H \leq 4d$.

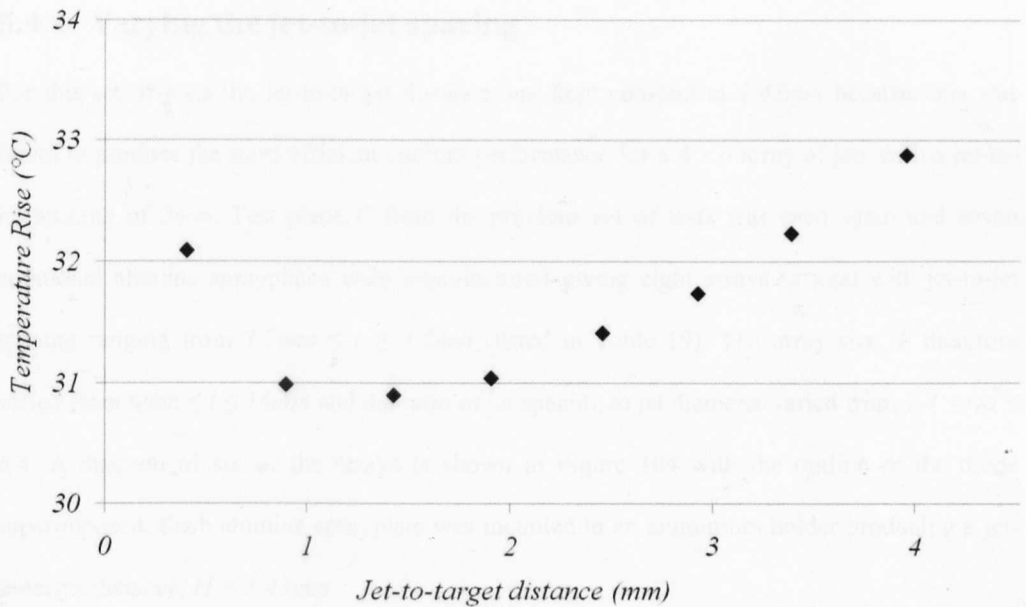


Figure 103 – Diode temperature rise versus jet-to-target distance at a constant pumping power of 5Watts.

5.3.3.1 Summary of jet-to-target distance test

A 6×6 array of jets, with a jet-to-jet spacing of 2mm , operating at a jet-to-target distance of 1.43mm cooled the diode to 30.89°C above the coolant temperature as it dissipated 150Watts of power while requiring 5Watts of pumping power to drive the coolant water. There was little variation in the cooling performance as the jet-to-target distance (H) was varied over the range $2d \leq H \leq 4d$. When the jet-to-target distance was varied outside this range cooling performance deteriorated resulting in an increase in the diode temperature. From Figure 103 the cooling efficiency appears to deteriorate more strongly when the jet-to-target distance is below the optimum value.

5.4 Jet-to-jet spacing and size of the array

A 6×6 ($N=36$) array with jets spaced at 2mm produces an array size $l=10\text{mm}$. For any value of N , there is an optimum value of jet-to-jet spacing and therefore array size which will cool the diode most efficiently. The effect of varying the size of the jet array was investigated for a 6×6 array in order to determine which array size (l) and therefore ratio of jet diameter to jet spacing (r/d) resulted in the most efficient cooling performance.

5.4.1 Varying the jet-to-jet spacing

For this set of tests the jet-to-target distance was kept constant at 1.43mm because this was found to produce the most efficient cooling performance for a 6×6 array of jets with a jet-to-jet spacing of 2mm . Test piece *C* from the previous set of tests was used again and seven additional alumina sprayplates were manufactured giving eight arrays in total with jet-to-jet spacing ranging from $1.2\text{mm} \leq r \leq 3.2\text{mm}$ (listed in Table 19). The array size, l , therefore varied from $6\text{mm} \leq l \leq 16\text{mm}$ and the ratio of jet spacing to jet diameter varied from $2.4 \leq r/d \leq 6.4$. A diagram of six of the arrays is shown in Figure 104 with the outline of the diode superimposed. Each alumina sprayplate was mounted in an aluminium holder producing a jet-to-target distance, $H = 1.43\text{mm}$.

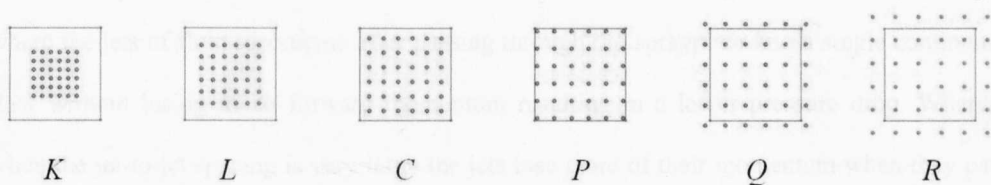


Figure 104 – A diagram of six of the jet arrays with jet-to-jet spacing varying from 1.2mm to 3.2mm with the outline of the 12.7mm diode superimposed.

Table 19 – Jet-to-jet spacing and array size for the eight jet arrays .

<i>Test piece</i>	<i>Jet-to-jet spacing - r (mm)</i>	<i>Array size - l (mm)</i>
<i>K</i>	<i>1.2</i>	<i>6</i>
<i>L</i>	<i>1.6</i>	<i>8</i>
<i>M</i>	<i>1.8</i>	<i>9</i>
<i>C</i>	<i>2</i>	<i>10</i>
<i>N</i>	<i>2.2</i>	<i>11</i>
<i>P</i>	<i>2.4</i>	<i>12</i>
<i>Q</i>	<i>2.8</i>	<i>14</i>
<i>R</i>	<i>3.2</i>	<i>16</i>

5.4.2 Experimental results

5.4.2.1 Pressure drop and flow rate

Despite operating at an identical jet-to-target distance, ($H = 1.43mm$), and containing the same number of jets, ($N = 36$), in a 6×6 array, there is a variation in the pressure drop and therefore pumping power required to drive the coolant fluid through the various arrays. In Figure 105 pressure drop is plotted against jet-to-jet spacing at a flow rate of $4litres/minute$. The measured pressure drop increases with jet-to-jet spacing. There appears to be a change in the pressure drop profile occurring between $2.2mm \leq r \leq 2.4mm$. The range of pressure drop measured across each sprayplate is due to loss of momentum and the way neighbouring jets interact with each other. When the jet-to-jet spacing is very small the jet array behaves like a wire mesh where the jets of fluid recombine after passing through the sprayplate into a single continuous flow without losing much forward momentum resulting in a lower pressure drop. Whereas when the jet-to-jet spacing is very large the jets lose more of their momentum when they pass through the sprayplate and exude into the relatively stationary fluid between the target surface and the sprayplate. There appears to be a transition in the way neighbouring jets interact with each other at a jet-to-jet spacing of approximately $2.3mm$. This is likely to affect which jet-to-jet spacing produces the most efficient cooling at a given level of pumping power.

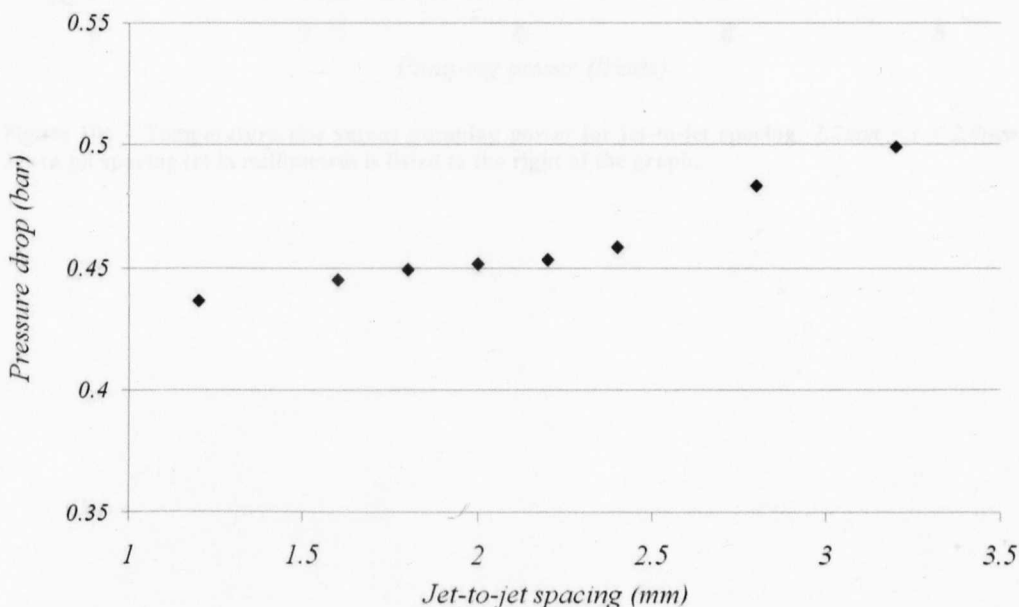


Figure 105 – Pressure drop versus jet-to-jet spacing at a flow rate of $4litres/minute$.

5.4.2.2 Temperature rise and pumping power

In Figure 106 and Figure 107 the temperature rise of the diode is plotted against pumping power for each of the eight test pieces over the range of jet-to-jet spacing: $1.2\text{mm} < r < 3.2\text{mm}$. The data is plotted in two separate figures in order to produce clearer graphs. From the figures it is clear that there is an optimum value of jet-to-jet spacing for a 6×6 array of 0.5mm diameter jets operating at a jet-to-target distance of 1.43mm . In Figure 106 one can see that cooling efficiency deteriorates for $r \leq 1.6\text{mm}$ and in Figure 107 cooling efficiency deteriorates for $r \geq 2.4\text{mm}$. The optimum jet-to-jet spacing is found to lie in the range $1.6\text{mm} < r < 2.4\text{mm}$.

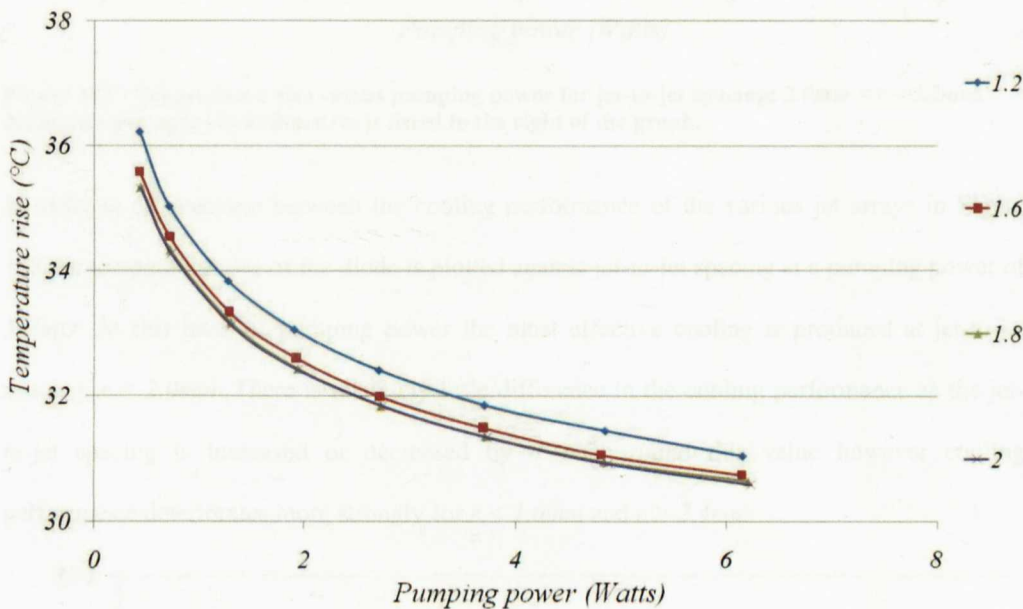


Figure 106 – Temperature rise versus pumping power for jet-to-jet spacing: $1.2\text{mm} < r < 2.0\text{mm}$. Jet-to-jet spacing (r) in millimetres is listed to the right of the graph.

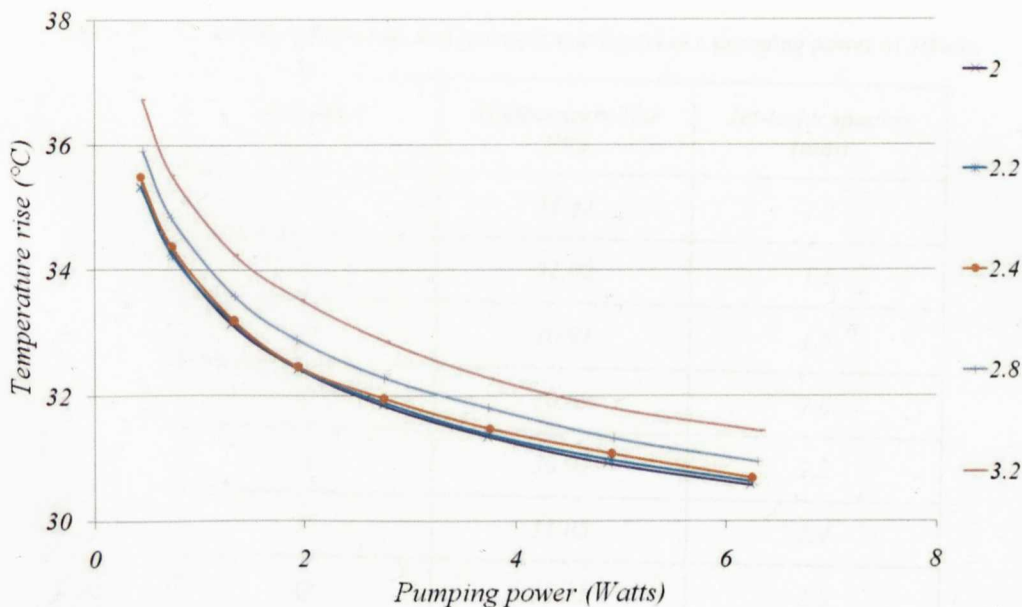


Figure 107 - Temperature rise versus pumping power for jet-to-jet spacing: $2.0\text{mm} < r < 3.2\text{mm}$. Jet-to-jet spacing (r) in millimetres is listed to the right of the graph.

In order to differentiate between the cooling performance of the various jet arrays in Figure 108 the temperature rise of the diode is plotted against jet-to-jet spacing at a pumping power of 5Watts . At this level of pumping power the most effective cooling is produced at jet-to-jet spacing, $r = 2.0\text{mm}$. There is relatively little difference in the cooling performance as the jet-to-jet spacing is increased or decreased by 0.4mm around this value however cooling performance deteriorates more strongly for $r < 1.6\text{mm}$ and $r > 2.4\text{mm}$.

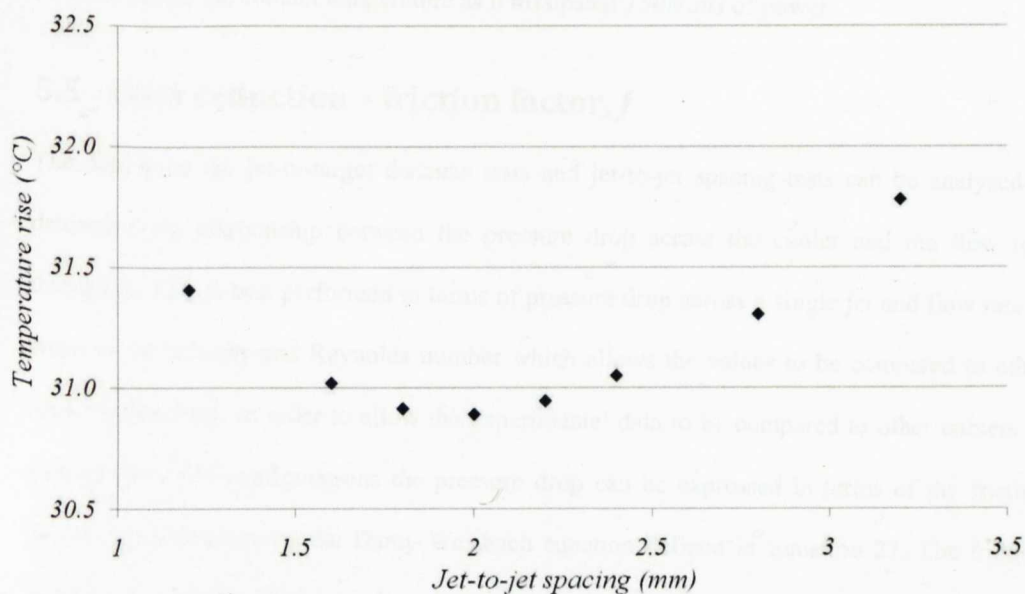


Figure 108 – Temperature rise versus jet-to-jet spacing at a pumping power of 5Watts .

Table 20 – Diode temperature rise and jet-to-jet spacing (r) at a pumping power of 5Watts.

<i>Test piece</i>	<i>Temperature rise (°C)</i>	<i>Jet-to-jet spacing (mm)</i>
<i>K</i>	<i>31.41</i>	<i>1.2</i>
<i>L</i>	<i>31.02</i>	<i>1.6</i>
<i>M</i>	<i>30.91</i>	<i>1.8</i>
<i>C</i>	<i>30.89</i>	<i>2.0</i>
<i>N</i>	<i>30.95</i>	<i>2.2</i>
<i>P</i>	<i>31.05</i>	<i>2.4</i>
<i>Q</i>	<i>31.31</i>	<i>2.8</i>
<i>R</i>	<i>31.78</i>	<i>3.2</i>

5.4.2.3 Summary of jet-to-jet spacing test

Jet-to-jet spacing (r) affects the cooling performance of jet impingement arrays. In Figure 108 it is clear that the effective cooling deteriorates when neighbouring jets are spaced very close together and when they are too far apart. The optimum jet-to-jet spacing to cool this heat source was found to be $2mm$ or $4d$ (where d is the jet diameter). At a pumping power of 5Watts for a 6×6 array of jets, with $H = 1.43mm$ and $r = 2mm$. The temperature rise of the diode was $30.89^{\circ}C$ above the coolant temperature as it dissipated 150Watts of power.

5.5 Data reduction – friction factor, f

The data from the jet-to-target distance tests and jet-to-jet spacing tests can be analysed to determine the relationship between the pressure drop across the cooler and the flow rate through it. This is best performed in terms of pressure drop across a single jet and flow rate in terms of jet velocity and Reynolds number which allows the values to be compared to other cooler geometries. In order to allow the experimental data to be compared to other coolers of various sizes and configurations the pressure drop can be expressed in terms of the friction factor, f , as described by the Darcy-Weisbach equation defined in Equation 27. The friction factor is a property of the cooler and in this case the sprayplate itself, which allows the experimental results to be compared objectively to other cooler geometries.

$$\Delta p = f \cdot \frac{L}{D} \cdot \frac{\rho V^2}{2}$$

Equation 27 – Darcy-Weisbach equation describing pressure drop in terms of friction factor, f .

Where: the pressure loss due to friction Δp (units: Pa or kg/ms^2) is a function of:

- The ratio of the length to diameter of the pipe, L/D ; in this case the length, L , is the thickness of the sprayplate, that is, $1mm$. The diameter of the pipe, D , is $0.5mm$.
- The density of the fluid, ρ (kg/m^3); In this case, for water at $40^\circ C$, $\rho = 992.2kg/m^3$.
- The mean velocity of the flow, for a single jet, V (m/s), as defined above;
- A dimensionless coefficient of laminar, or turbulent flow, f .

5.5.1 Friction factor, f , with variable jet-to-target distance

In Figure 109 the friction factor is plotted against Reynolds number over the full range of flow rates tested. For each jet-to-target distance the friction factor remains relatively constant as the Reynolds number is increased. With the lower and higher jet-to-target distances of $0.9mm$ and $3.96mm$ resulting in a higher friction factor compared to jet-to-target distances between $1.43mm$ and $3.39mm$. The friction factor for this particular array geometry (6×6 array of $0.5mm$ diameter jets) generally produces a friction factor of approximately, $f = 0.5$. There were 36 jets in each array (6×6), a volumetric flow rate of 5.11 litres/minute through the cooler equates to a single jet velocity of $12.043m/s$ and a Reynolds number, $Re = 9151$. The friction factor, $f = 0.5057$, for a jet-to-target distance of $1.43mm$.

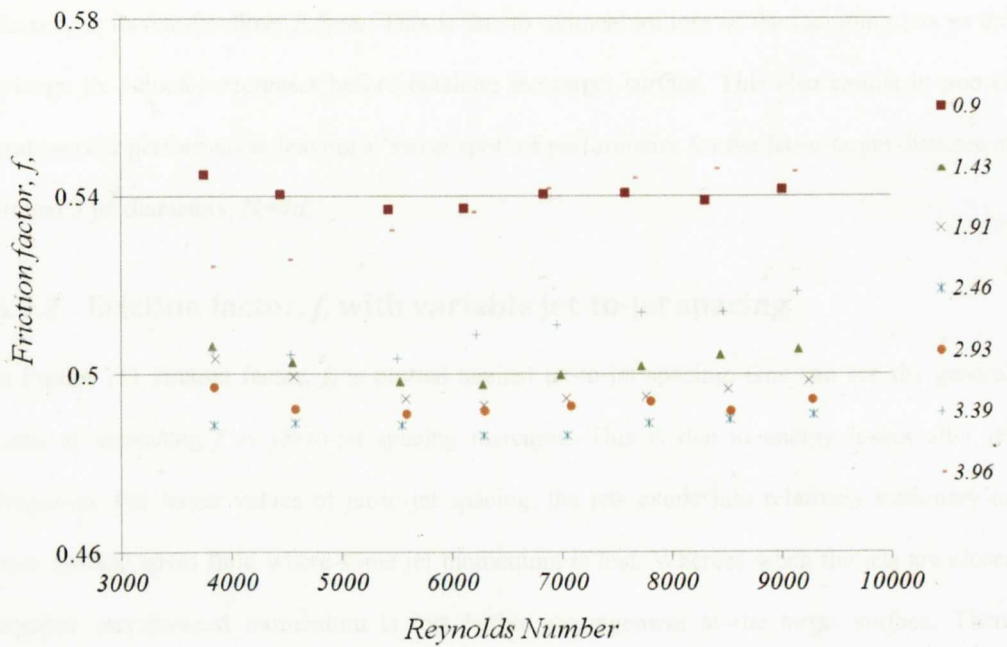


Figure 109 – Friction factor versus Reynolds number for various jet to target distances.

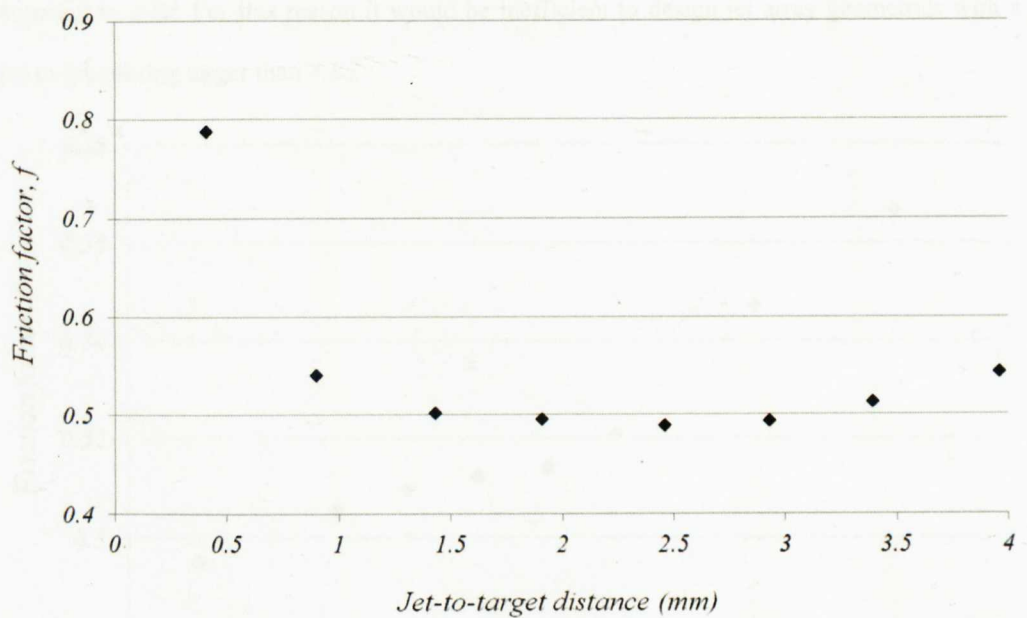


Figure 110 – Friction factor, f , versus jet-to-target distance at a jet velocity of 10m/s ($Re=7599$)

5.5.1.1 Discussion

In Figure 110 the friction factor, f , is plotted against jet-to-target distance at a jet velocity of 10m/s . One can see that as jet-to-target distance is decreased below 1.5mm there is a significant increase in the value of f . As the jet-to-target distance is decreased the coolant water is being forced through an ever thinner channel as it attempts to exit the cooler after impingement. In fact, impingement may not even occur as the velocity of exhausted fluid is high enough to prevent the formation of a jet. Friction factor increases to a lesser extent as the jet-to-target

distance is increased above 2.5mm . This is due to momentum loss of the incoming jets as the average jet velocity decreases before reaching the target surface. This also results in poorer heat transfer performance, leaving a ‘sweet spot’ of performance for the jet-to-target distance at around 3 jet diameters, $H=3d$.

5.5.2 Friction factor, f , with variable jet-to-jet spacing

In Figure 111 friction factor, f , is plotted against jet-to-jet spacing. One can see the general trend of increasing f as jet-to-jet spacing increases. This is due to energy losses after jet formation. For larger values of jet-to-jet spacing, the jets exude into relatively stationery or slow moving spent fluid where some jet momentum is lost. Whereas when the jets are closer together less forward momentum is lost before impingement at the target surface. There appears to be a transition between the two regimes at a jet-to-jet spacing of around 2.4mm equating to $4.8d$. For this reason it would be inefficient to design jet array geometries with a jet-to-jet spacing larger than $4.8d$.

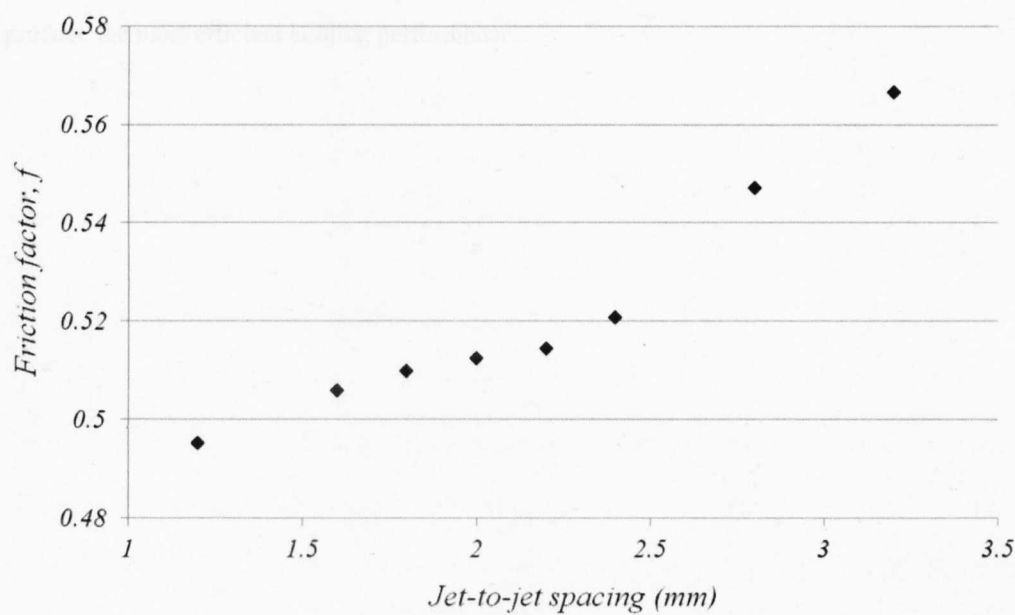


Figure 111 – Friction factor, f , and jet-to-jet spacing at a jet velocity of 10m/s , ($Re=7599$)

5.5.3 Summary of experimental tests

A test rig was constructed to characterise the cooling performance of a 6×6 jet impingement array of 0.5mm diameter jets. The jet-to-target distance (H) and jet-to-jet spacing (r) was varied in two separate series of tests. A 12.7mm square diode soldered onto an AlN substrate tile was powered to dissipate 150Watts and its temperature was monitored using an infra red thermal

imaging camera. The jet array was aligned directly underneath the diode. The spent fluid exhausted to the side via a single slot to the exit plenum.

Jet-to-target distance (H) was investigated over the range: $0.41mm < H < 3.96mm$ relating to: $0.82d < H < 7.92d$. Jet-to-jet spacing (r) was investigated over the range $1.2mm < r < 3.2mm$ relating to $2.4d < r < 6.4d$. Cooling efficiency was determined by comparing the temperature rise of the diode above the coolant temperature at a given level of pumping power. The temperature of the diode was defined as the mean of the diode centre and diode peak temperature as this was found to be proportional to the 90th percentile temperature in order to be representative of the upper device temperature.

Over the range of jet-to-target distance and jet-to-jet spacing investigated, cooling performance varied significantly enough for an optimum value of H and r to be determined for the cooling of the diode. Of the test pieces measured, a value of $H = 1.43mm$ and $r = 2.0mm$ were found to produce the most efficient cooling performance.

Chapter 6

6 Conclusion

The aim of the work presented in this thesis is to improve the operational reliability of a power module and increase the efficiency of its associated cooling system. The initial research indicated that the reliability of a power module is affected by its material structure and the method of cooling employed. Gains in reliability could be achieved by modifying the structure of the module in combination with a reduction of the number of bonded interfaces between the devices and the coolant fluid. Jet impingement was identified as a cooling method which generates a high heat transfer coefficient. The single phase nature of the cooling process enables jet impingement coolers to be used in simple liquid cooling circuits. It was demonstrated that a direct-jet-impingement substrate-cooled power module with an optimised jet array geometry targeting the hotspots beneath the devices would operate more efficiently and reliably than the equivalent power module mounted onto the commonly used coldplate cooler. The gains in power module reliability and the increased efficiency of the cooling system make a direct-jet-impingement substrate-cooled power module assembly an attractive option when designing new power electronic systems.

6.1.1 Initial experimental study

The initial experimental study compared the performance of the commonly used coldplate cooler with the performance of two jet impingement coolers. The first jet impingement cooler, cooled the baseplate of the power module directly with water. The second cooled the DBC substrate tile directly. The devices which were direct-substrate-cooled by jet impingement were cooled most effectively. This initial set of experiments was important in demonstrating that direct-substrate cooling with a high heat transfer coefficient cooling method such as jet impingement can be used to cool a power module more efficiently, without the need for a heatspreader in the assembly. The solder layer between the baseplate and the DBC substrate is prone to crack with thermal cycling inducing thermal failure of the power electronic devices. It is thought that a great improvement in the long term reliability of the module would be

achieved due to the resulting smaller thermal cycles experienced by the devices in combination with the removal of the heatspreading baseplate and its associated solder layer.

6.1.2 Jet impingement optimisation for power electronic devices

A test rig was constructed to investigate how the geometry of the jet arrays affected the efficiency of the cooling produced. Twelve different jet array geometries were tested. The results of the experiments were important because rather than cooling a heat source producing a uniform heat flux, two diodes soldered onto an *AlN* DBC substrate were used as the heat sources which is representative of a real power module. Thermal simulations indicated that there are hot spots on the DBC substrate directly beneath the devices. The jet arrays were aligned directly beneath the devices in order to target the hotspots. In order to determine which jet array geometry was most efficient the performance was characterised by comparing the temperature rise of the diodes at the same level of pumping power. This criteria was chosen as it offered a better representation of the true efficiency of a cooler rather than, for example, choosing the geometry which generated the most cooling at a given flow rate. A 6×6 array of 0.5mm diameter jets was found to cool the diodes most effectively. This was an important result as it showed that only a fraction of the surface area beneath the module corresponding to the hotspots directly beneath the devices required cooling with a high heat transfer coefficient. This is an important step in reducing redundancy, and therefore, increasing the efficiency of the cooling system.

A second test rig was constructed to test 6×6 arrays of 0.5mm diameter jets in more detail by varying the jet-to-target distance and the jet-to-jet spacing in order to determine the optimum values. The test apparatus was carefully designed in order to be representative of how such a cooling system would be implemented in practice, therefore increasing the relevance of the experimental results. A thermal imaging camera was used to monitor the steady state surface temperature of the diode in detail. The tests determined that a 6×6 array of 0.5mm diameter jets spaced at 2mm with a jet-to-target distance of 1.43mm cooled the 12.7mm square diode most effectively.

6.2 The importance of the work

The results from the three sets of experimental tests involving jet impingement are a valuable contribution to the ongoing work in improving the operational reliability of power modules. In the experimental test rigs real power electronic devices were direct-substrate-cooled with jet impingement. The device temperature rise and the amount of pumping power required to drive the coolant water was used to determine the most efficient jet array geometry. The devices were cooled more efficiently with jet impingement compared to a traditional coldplate cooler. Gains in efficiency are achieved by cooling the DBC substrate tile directly with water and by targeting the hotspot directly beneath each device with an optimised jet array geometry. Gains in reliability are potentially achieved by removing the baseplate and associated solder layer from the assembly, which are typically the weakest part of a power module. The experimental apparatus, testing method and data is clearly presented in a way which can be interpreted by others in order to aid the design of efficient jet array geometries for targeting hotspots beneath devices.

6.3 Further work

The experimental work presented has shown that jet impingement arrays can be used to direct substrate cool power modules very efficiently. The operational reliability of the power module has potentially been improved by removing the baseplate and associated solder layer from the assembly which are prone to failure with thermal cycling. It would be of interest to attempt to quantify the reliability gains in some way and to identify the weaknesses or failure mechanisms in the new, simpler assembly. Further work could look at creating simpler empirical relations or design rules to aid with the construction of jet array geometries for new power modules. The experimental results could also be used to aid CFD simulation of jet impingement cooling of power electronic devices. There are a number of different ways which the jets could be arranged rather than regular spacing with square arrays. A hexagonal arrangement or circular arrangement could prove to be more effective for cooling the hotspots beneath devices.

7 Review

Chapter One

In chapter one an overview of the power module is presented. Typical uses and applications of power modules and their specifications are described. The construction of a typical power module is described followed by an overview of alternative design topologies showing how the arrangement of the typical power module assembly can be altered and adapted depending on the criteria of the application. A number of power module cooling methods are presented with advantages and disadvantages listed for each. A problem is identified involving the optimisation of cooling of power modules in order to improve reliability. Jet impingement cooling is identified as a cooling method with great potential to be investigated further in the context of power electronic cooling. The approach to finding a solution is outlined and the structure of the thesis is described with a brief summary of each chapter.

Chapter Two

In chapter two the issues relating to the long term operational reliability of power modules are explored with a focus on the material layers constituting the module. The properties of the material layers and interfaces making up the thermal path from heat source to heat sink are defined. Reliability issues and weak points in the power module stack which are prone to failure are identified. The necessity or in some cases the redundancy of a heat spreader depending on the heat transfer coefficient produced by the cooler is analysed.

Chapter Three

In this chapter liquid cooling of power modules is investigated in combination with reducing the number of layers in the power module stack. Jet impingement is identified as a cooling method which can produce very high heat transfer coefficients. It is postulated that a power module can be cooled more efficiently if the number of layers in the thermal stack between the heat source and coolant fluid are reduced and the underside of the substrate tile is cooled directly by jet impingement. Two jet impingement coolers were designed and constructed to directly cool a power module with and without a baseplate as part of the assembly. The power module was also cooled by a traditional coldplate as a comparison. The tests demonstrated the

improvement found by removing thermal layers in the package and cooling the baseplate and substrate tile of a power module directly with liquid jet impingement. When the substrate tile was cooled directly the electronic devices operated with a lower peak temperature and exhibited a smaller amplitude of thermal cycling compared to the baseplate cooled and coldplate cooled methods.

Chapter Four

The work in chapter four builds on the experimental results described in chapter three by looking into direct substrate cooling with jet impingement in more detail. This chapter aims to build on the experimental results from the previous chapter and focuses on direct substrate cooling with jet impingement. The parameters affecting the performance of jet arrays are covered in detail. Existing heat transfer correlations for jet impingement predicted the heat transfer to the same order of magnitude as the measured results but it was felt that they did not satisfactorily predict the heat transfer performance and further experimental testing was necessary. Rather than cooling the entire surface area of the substrate tile it is postulated that more efficient cooling of the electronic devices could be achieved by targeting the hot spot beneath each device individually with a carefully designed array of impinging jets. An apparatus allowing various jet array geometries to be tested was constructed. The performance of each jet array was characterised in order to determine which array geometry produced the most efficient cooling. 12 different array geometries were tested in order to confirm the hypothesis that it is more efficient to target the hotspot directly beneath the device rather than cooling a larger surface area with an evenly distributed heat transfer coefficient. The most efficient array geometry of the 12 tested consisted of a 6×6 array of 0.5mm diameter jets spaced at 2mm while the diodes measured 12.7mm square.

Chapter Five

The testing of multiple jet impingement array geometries described in the previous chapter produced promising results. The potential heat transfer performance of a jet impingement array in combination with direct substrate cooling resulted in efficient cooling of the electronic devices. It was decided to perform additional experimental tests of jet impingement arrays designed to directly cool a single power electronic device in order to build on the results from

the previous chapter. A new test apparatus was constructed for the direct substrate cooling of a single 12.7mm square diode where the spent fluid exhausts in a single direction. Two series of tests were performed with a 6×6 array of 0.5mm diameter jets: The first involved varying the jet-to-target distance (H), the second involved varying the jet-to-jet spacing (r). The temperature of the diode was monitored using an infra red thermal imaging camera and the upper surface temperature was used to determine the relative cooling performance of the various jet impingement test pieces. Over the range of jet-to-target distance and jet-to-jet spacing investigated, cooling performance varied significantly enough for an optimum value of H and r to be determined. Of the test pieces measured, a value of $H = 1.43\text{mm}$ and $r = 2.0\text{mm}$ were found to produce the most efficient cooling performance.

References

1. CIA, C.I.A. *World Factbook*. 2011; Available from: <https://www.cia.gov>.
2. REN21, R.E.P.N.f.t.s.C., *Renewables 2010: Global Status Report*. 2010.
3. Contributors, W., *Power Electronics*, in *Wikipedia*. 2011.
4. Laboratory, P.E., *Applications of Power Electronics*. 2011.
5. Adams, C. *A380: 'More Electric' Aircraft*. 2001 October 1, 2001; Available from: <http://www.aviationtoday.com/av/issue/feature/12874.html>.
6. Fleuriat, J.P., et al. *Thermoelectric microcoolers for thermal management applications*. in *Thermoelectrics, 1997. Proceedings ICT '97. XVI International Conference on*. 1997.
7. Drofenik, U., Laimer, G., Kolar, J. W., *Theoretical Converter Power Density Limits for Forced Convection Cooling*, in *Proceedings of the International PCIM Europe 2005 Conference*. 2005: Nuremberg, Germany. p. pp. 608 - 619.
8. Advanced Thermal Solutions, I.N., MA, *Direct Cooling of Power Modules Using Microchannel Structures*, in *Power Electronics Technology*. 2010.
9. Jasperson, B.A., et al., *Comparison of Micro-Pin-Fin and Microchannel Heat Sinks Considering Thermal-Hydraulic Performance and Manufacturability*. *Components and Packaging Technologies*, IEEE Transactions on. **33**(1): p. 148-160.
10. Calame, J.P., et al., *Experimental investigation of microchannel coolers for the high heat flux thermal management of GaN-on-SiC semiconductor devices*. *International Journal of Heat and Mass Transfer*, 2007. **50**(23-24): p. 4767-4779.
11. CPS-Technologies. *CPS AlSiC IGBT Pin Fin Coolers data sheet*. 2010; Available from: <http://www.alsic.com/pdf/CPS%20AlSiC%20IGBT%20Coolers.pdf>.
12. Lang, F. and U. Scheuermann, *Long Term Reliability of Spring Pin Pressure Contacts in an Industrial Environment*. *Integrated Power Systems (CIPS)*, 2006 4th International Conference on, 2006: p. 1-6.
13. Charboneau, B.C., et al., *Double-Sided Liquid Cooling for Power Semiconductor Devices Using Embedded Power Packaging*. *Industry Applications*, IEEE Transactions on, 2008. **44**(5): p. 1645-1655.
14. Powerex, *General Considerations for IGBT and Intelligent Power Modules*. 2011.
15. Bouarroudj, M., et al., *Degradation behavior of 600 V-200 A IGBT modules under power cycling and high temperature environment conditions*. *Microelectronics Reliability*. **47**(9-11): p. 1719-1724.
16. Leslie, S.G., *Cooling Options and Challenges of High Power Semiconductor Modules*. *ElectronicsCooling*, 2006. **12**(4).
17. AMD. *Processor Thermal Resistance*. *Processor Thermal Resistance*]. Available from: http://www.amd.com/us-en/Processors/ComputingSolutions/0,,30_288_13265_13295%5E13332,00.html.

18. Lightstream, *Wick Heat Pipe Schematic Cutaway*. p. Wick Heat Pipe Schematic Cutaway.
19. Metku, *Heat Pipe*. p. Heat Pipe.
20. Metku, *Heat Pipe, Fan & Finned Heat Sink*. p. Heat Pipe, Fan & Finned Heat Sink.
21. TS-Heatronics, *Closed Loop Pulsating Heat Pipe Schematic*. p. Closed Loop Pulsating Heat Pipe Schematic.
22. Guide, X.R., *Finned Heat Sink - Natural Convection*
p. Finned Heat Sink - Natural Convection.
23. PACS, *Heat Sink with Fan*. p. Heat Sink with Fan.
24. Lytron, *Lytron Cold Plate*. p. Lytron Cold Plate.
25. Lytron, *Lytron Pin Fin Coldplate*. p. Lytron Pin Fin Coldplate.
26. Powerelectronics.com, *Spray Cooling Schematic*
p. Spray Cooling Schematic.
27. Efirdcor, *Jet Impingement Flow Types*. p. Jet Impingement Flow Types.
28. Oliphant, K., B.W. Webb, and M.Q. McQuay, *An experimental comparison of liquid jet array and spray impingement cooling in the non-boiling regime*. *Experimental Thermal and Fluid Science*, 1998. **18**(1): p. 1-10.
29. Electronics-Cooling, *Spray Cooling Schematic*
p. Spray Cooling Schematic.
30. SCS, *Spray Cooling with droplets schematic*
p. Spray Cooling with droplets schematic.
31. Turek, L.J., et al. *Evaporative spray cooling of power electronics using high temperature coolant*. in *Thermal and Thermomechanical Phenomena in Electronic Systems, 2008. IThERM 2008. 11th Intersociety Conference on*. 2008.
32. Angioletti, M., E. Nino, and G. Ruocco, *CFD turbulent modelling of jet impingement and its validation by particle image velocimetry and mass transfer measurements*. *International Journal of Thermal Sciences*, 2005. **44**(4): p. 349-356.
33. Ciappa, M. and W. Fichtner. *Lifetime prediction of IGBT modules for traction applications*. in *Reliability Physics Symposium, 2000. Proceedings. 38th Annual 2000 IEEE International*. 2000.
34. Marckx, D.A., *Breakthrough in power electronics from SiC*. 2005, *Subcontractor Report*.
35. Schulz-Harder, J., *Efficient Cooling of Power Electronics*, in *Proceedings of the Power Conversion and Intelligent Motion Conference — China (PCIM - China)*. 2006: Shanghai, China.
36. Schulz-Harder, J., Exel, K. and Meyer, A., *Direct Electronic Cooling of Power Electronics Devices*, in *CIPS 2006*. 2006: Naples, Italy.
37. Silver, A. *Arctic Alumina Thermal Compound*. 2011; Available from: http://www.arcticsilver.com/arctic_alumina.htm.
38. Junji Yamada, T.S., Muneyosi Kawaguchi, Mitsuhiko Nakamura, Masao Kikuchi, Eckhard Thal, , *The latest High Performance and High Reliability IGBT*

- Technology in New Packages with Conventional Pin Layout*. 2004, Mitsubishi.
39. Tsao, B.-H.L., J.; Scofield, J.; Laing, C.; Brown, J., *3D Thermal Stress Model for SiC Power Modules*, in *International Conference on SiC and Related Materials*. 2007.
 40. Johnson, C.M., *Lecture Course: Thermal Management in Power Electronics*. 2010: University of Nottingham, School of EEE.
 41. Garimella, S.V. and B. Nenaydykh, *Nozzle-geometry effects in liquid jet impingement heat transfer*. *International Journal of Heat and Mass Transfer*, 1996. **39**(14): p. 2915-2923.
 42. Florschuetz, L.W., D.E. Metzger, and C.C. Su, *Heat Transfer Characteristics for Jet Array Impingement With Initial Crossflow*. *Journal of Heat Transfer*, 1984. **106**(1): p. 34-41.
 43. Whelan, B.P. and A.J. Robinson, *Nozzle geometry effects in liquid jet array impingement*. *Applied Thermal Engineering*, 2009. **29**(11-12): p. 2211-2221.
 44. Li, C.-Y. and S.V. Garimella, *Prandtl-number effects and generalized correlations for confined and submerged jet impingement*. *International Journal of Heat and Mass Transfer*, 2001. **44**(18): p. 3471-3480.
 45. Pan, Y. and B.W. Webb, *Heat Transfer Characteristics of Arrays of Free-Surface Liquid Jets*. *Journal of Heat Transfer*, 1995. **117**(4): p. 878-883.
 46. Robinson, A.J. and E. Schnitzler, *An experimental investigation of free and submerged miniature liquid jet array impingement heat transfer*. *Experimental Thermal and Fluid Science*, 2007. **32**(1): p. 1-13.
 47. Garimella, S.V. and R.A. Rice, *Confined and Submerged Liquid Jet Impingement Heat Transfer*. *Journal of Heat Transfer*, 1995. **117**(4): p. 871-877.
 48. Glynn, C., O'Donovan, T. S., and Murray, D. B., *Jet Impingement Cooling*, in *9th UK National Heat Transfer Conference*. 2005: Manchester.
 49. Womac, D.J., F.P. Incropera, and S. Ramadhyani, *Correlating Equations for Impingement Cooling of Small Heat Sources With Multiple Circular Liquid Jets*. *Journal of Heat Transfer*, 1994. **116**(2): p. 482-486.
 50. Rao, P.V. and D.H. Buckley, *Unified empirical relations for cavitation and liquid impingement erosion processes*. *Wear*, 1987. **120**(3): p. 253-288.
 51. Janakiram, K.S., *Erosion studies due to liquid jet impingement with plain and cavitating jets*. *Journal of the Indian Institute of Science*, 1981. **63**: p. 183-211.
 52. Lienhard, J.V.H. and A.M. Khoumsary, *Liquid jet impingement cooling with diamond substrates for extremely high heat flux applications*. 1993: SPIE.
 53. Fabbri, M. and V.K. Dhir, *Optimized Heat Transfer for High Power Electronic Cooling Using Arrays of Microjets*. *Journal of Heat Transfer*, 2005. **127**(7): p. 760-769.
 54. Martin, H., *Heat and mass transfer between impinging gas jets and solid surfaces*. *Advances in Heat Transfer*, 1977. **13**: p. 1-60.